CROSSTALK BETWEEN CALCIUM SIGNALING AND LIPID METABOLISM AT ENDOPLASMIC RETICULUM-PLASMA MEMBRANE JUNCTIONS

APPROVED BY SUPERVISORY COMMITTEE

Jen Liou, Ph.D. (Mentor)

Orson Moe, M.D. (Chair)

Michael Roth, Ph.D.

Helen Yin, Ph.D.

DEDICATION

To my parents and my grandparents, who taught me what persistence is.

ACKNOWLEDGEMENTS

Scientific research is the love of my life and it has brought me a lot of joys. Pursuing the truths behind the fascinating and mysterious cellular processes requires a deep mind, two careful hands, and timeless hardworking. Without the help and supports from many others, this work wouldn't have been possible.

I thank my mentor, Dr. Jen Liou. She is an educator. She provides a supporting and encouraging environment that allows me to grow into a better scientist. She is also a visionary. Her insights and open-mindedness have broadened my views, and propelled me to think creatively. Discussion with her becomes my daily entertainment in the lab. She has set the standard of a true scientist for me. It is my great honor to work with her.

I would like to thank my thesis committee, Drs. Orson Moe, Michael Roth, and Helen Yin, for being genuinely interested in science. Discussion with them is always pure and satisfactory. I am also grateful to Drs. Yi Liu and Ilya Bezprozvanny for providing straightforward feedbacks during my presentations.

I am sincerely thankful to my friends Yi-Chieh Peng, Chia-Li Kao, Ting-En Su, Joshua Chang, Maria Carreira, Lindsay Whitman, Wan-Jin Lu, Yao-Chang Tsan, and Ling-Yun Chu. Although they are not always around, they've been the greatest cheerleaders for me. I also thank every member of Taiwanese student association at UTSW. Special thanks to Sarah Cadwell, Brittany Harper, and Kelly Stoeppel for meticulously proofreading this dissertation.

Finally, I thank to my grandparents, parents, and my brother for their never-ending love, support, and encouragement.

CROSSTALK BETWEEN CALCIUM SIGNALING AND LIPID METABOLISM AT ENDOPLASMIC RETICULUM-PLASMA MEMBRANE JUNCTIONS

by

CHI-LUN CHANG

DISSERTATION

Presented to the Faculty of the Graduate School of Biomedical Sciences

The University of Texas Southwestern Medical Center at Dallas

In Partial Fulfillment of the Requirements

For the Degree of

DOCTOR OF PHILOSOPHY

The University of Texas Southwestern Medical Center

Dallas, Texas

May, 2014

CROSSTALK BETWEEN CALCIUM SIGNALING AND LIPID METABOLISM AT ENDOPLASMIC RETICULUM-PLASMA MEMBRANE JUNCTIONS

CHI-LUN CHANG, Ph.D.

The University of Texas Southwestern Medical Center at Dallas, 2014

Supervising Professor: JEN LIOU, Ph.D.

Receptor-induced Ca^{2+} signaling is the key to many cellular functions, such as secretion, migration, differentiation, and proliferation. The increase in cytosolic Ca^{2+} signals is dependent on the hydrolysis of phosphatidylinositol 4,5-bisphosphate (PIP_2) at the plasma membrane (PM). To enable subsequent signaling activation and maintain cellular homeostasis, it is necessary to replenish the consumed PIP_2. However, the molecular mechanisms underlying PM PIP_2 replenishment after hydrolysis remain elusive. PIP_2 is generated at the PM by sequential phosphorylation of phosphatidylinositol (PI) originating from the endoplasmic reticulum (ER). Delivering PI from the ER to the PM by PI transfer proteins (PITPs) is therefore postulated to support PM PIP_2 replenishment. Such transfer is more likely to take place at

ER-PM junctions, since the close apposition of the ER and the PM enables PITPs to efficiently interact with two heterologous membranes.

To study ER-PM junctions and their roles in PM PIP_2 replenishment, I generated a genetically-encoded fluorescent marker to selectively label ER-PM junctions. With this marker, minute ER-PM junctions were easily observed in live cells using multiple imaging techniques. At the resting state, approximately two hundred stable ER-PM junctions were detected at the adhesion surface of a single HeLa cell. Photo-activated localization microscopy (PALM) super-resolution imaging further demonstrate that ER-PM junctions labeled by this marker were remarkably uniform in size and slightly elongated in shape with a long axis of 255.5 nm and a short axis of 157.7 nm. Furthermore, analysis of the distance to nearest neighbor of individual ER-PM junctions show that these junctions are distributed uniformly in the cells.

Following the activation of Ca^{2+} signaling, I observed an enhanced ER-to-PM connection resulting from new junction formation and a decrease in the gap distance of ER-PM junctions. The enhanced ER-to-PM connection depends on cytosolic Ca^{2+} levels and extended synaptotagmin-like protein 1 (E-Syt1), a C2 domain-containing ER membrane protein. E-Syt1 detects the increase in cytosolic Ca^{2+} via its C2C domain and translocates from the bulk of ER to ER-PM junctions to enhance ER-to-PM connection. This in turn facilitates the recruitment of Nir2, an ER-associated PITP, to ER-PM junctions to promote PM PIP_2 replenishment. In summary, these results indicate a feedback loop for PM PIP_2 replenishment via E-Syt1 and Nir2 at ER-PM junctions. Disruption of this feedback mechanism by knockdown of E-Syt1 or Nir2 abolished PM PIP_2 replenishment and therefore, impaired receptor-induced Ca^{2+} signaling. This work reveals the long-sought mechanism of PM PIP_2 replenishment following hydrolysis and sheds light on the functional roles of poorly characterized ER-PM junctions. Furthermore, given the fact that PIP_2 and Ca^{2+} are pivotal signaling molecules for many cellular functions, these findings are of significance for providing new mechanistic insights into the signaling crosstalk and may have a broader impact on fields beyond cell signaling, organelle dynamics, and lipid trafficking.

TABLE OF CONTENTS

PRIOR PUBLICATIONS

1. Yuan-Li Huang, **Chi-Lun Chang**, Chih-Hsin Tang, Yueh-Chien Lin, Tsai-Kai Ju, Wei-Pang Huang, Hsinyu Lee. Extrinsic Sphingosine 1-Phosphate Activates $S1P_5$ and Induces Autophagy through Generating Endoplasmic Reticulum Stress in Human Prostate Cancer PC-3 Cells. Cell Signaling. 26(3): 611-618. 2014.

2. **Chi-Lun Chang**, Ting-Sung Hsieh, T. Tony Yang, Karen G. Rothberg, Dicle Berfin Azizoglu, Elzibeth Volk, Jung-Chi Liao, Jen Liou. Feedback Regulation of Receptor-Induced Ca^{2+} Signaling Mediated by E-Syt1 and Nir2 at ER-PM Junctions. Cell Reports. 5(3): 813-825. 2013.

3. Shanna A. Arnold, Lee B. Rivera, Juliet G. Carbon, Jason E. Toombs, **Chi-Lun Chang**, Amy D. Bradshaw, Rolf A. Brekken. Losartan Slows Pancreatic Tumor Progression and Extends Survival of SPARC-Null Mice by Abrogating Aberrant TGFβ Activation. PLoS ONE. 7(2): e31384. 2012.

4. **Chi-Lun Chang**, Ming-Chih Ho, Po-Huang Lee, Chi-Yen Hsu, Wei-Pang Huang, Hsinyu Lee. $S1P_5$ is Required for Sphingosine 1-Phosphate-induced Autophagy in Human Prostate Cancer PC-3 Cells. American Journal of Physiology-Cell Physiology. 297(2): C451-C458. 2009.

5. **Chi-Lun Chang**, Hsien-Yeh Hsu, Hong-Yu Lin, Wenchang Chiang, Hsinyu Lee. Lysophosphatidic Acid-induced Oxidized Low-density Lipoprotein Uptake is Class A Scavenger Receptor-dependent in Macrophages. Prostaglandins & Other Lipid Mediators. 87(1-4): 20-25. 2008.

6. **Chi-Lun Chang**, Mu-En Lin, Hsien-Yeh Hsu, Chao-Ling Yao, Shiaw-Min Hwang, Chien-Yuan Pan, Chi-Yen Hsu, Hsinyu Lee. Lysophosphatidic Acid-induced Interleukin-1β Expression is mediated through G_i/Rho and Generation of Reactive Oxygen Species in Macrophages. Journal of Biomedical Science. 15(3): 357-363. 2008.

7. **Chi-Lun Chang***, Jia-Jun Liao*, Wei-Pang Huang, Hsinyu Lee. Lysophosphatidic Acid Inhibits Serum Deprivation-induced Autophagy in Human Prostate Cancer PC-3 Cells. Autophagy. 3(3): 268-270. 2007. (*Equal contribution)

8. Ming-Chih Ho, Chiung-Nien Chen, Hsinyu Lee, Fon-Jou Hsieh, Chia-Tung Shun, **Chi-Lun Chang**, Yeun-Tyng Lai, Po-Huang Lee. Placenta Growth Factor not Vascular Endothelial Growth Factor A or C Can Predict the Early Recurrence after Radical Resection of Hepatocellular Carcinoma. Cancer Letters. 250(2): 237-249. 2007.

LIST OF FIGURES

Chapter 1

Chapter 2

Chapter 3

Chapter 4

Chapter 5

Chapter 6

Chapter 7

LIST OF TABLES

LIST OF ABBREVIATIONS

°C	degree Celsius
α-SNAP	alpha-synaptosomal-associated protein
μM	micromolar
μs	microsecond
BAPTA-AM	1,2-Bis(2-aminophenoxy)ethane-N,N,N′,N′-tetraacetic acid tetrakis(acetoxymethyl **ester)**
BHQ	1,4-Dihydroxy-2,5-di-*tert*-butylbenzene
Ca^{2+}	calcium
COPI	coat protein complex I
COPII	coat protein complex II
EGTA	ethylene-bis(oxyethylenenitrilo)tetraacetic acid
mCherry	monomeric Cherry fluorescence protein
ms	millisecond
Nir	PYK2 N-terminal domain-interacting receptor
nM	nanomolar
nm	nanometer
NP-EGTA	o-Nitrophenyl EGTA
PH	pleckstrin homology
PITPNC	phosphatidylinositol transfer protein, cytoplasmic
PITPNM	phosphatidylinositol transfer protein, membrane-associated
POST	partner of STIM1
Rdg	retinal degeneration
REEP	receptor expression enhancing protein
SARAF	SOCE-associated regulatory factor
Surf4	surfeit locus protein4

Chapter 1

Introduction

Ca^{2+} and phosphatidylinositol 4,5-bisphosphate (PIP_2) are small signaling molecules that govern tremendous cellular functions in animal cells. Therefore, regulation of the levels and subcellular distribution of Ca^{2+} and PIP_2 has profound physiological impacts. Intriguingly, PIP_2 at the plasma membrane (PM) is the linchpin to trigger Ca^{2+} signaling cascades streaming in different subcellular compartments in most non-excitable cells. During receptor-induced Ca^{2+} signaling, the event of PIP_2 hydrolysis at the PM transduces a signal to release the Ca^{2+} from the endoplasmic reticulum (ER), leading to the activation of Ca^{2+} effectors in the cytosol. Meanwhile, this signaling cascade diverges en route to ER-PM junctions, where the ER and PM membranes form close appositions, to activate a Ca^{2+} influx pathway called store-operated Ca^{2+} entry (SOCE) that refills the ER Ca^{2+} store and maintains high cytosolic Ca^{2+} levels. One obvious missing link in this elaborate signal network is how to replenish the consumed PIP_2 following receptor activation at PM. The answer to this question has long remained a mystery. In this dissertation, I will provide evidence to support a feedback mechanism elicited by cytosolic Ca^{2+} levels that leads to PIP_2 replenishment at ER-PM junctions following its hydrolysis.

1.1 Endoplasmic Reticulum (ER)

The ER is a membrane-bound organelle in eukaryotic cells, which performs key cellular functions. The ER is responsible for membrane and secretory protein biogenesis, and *de novo* biosynthesis of lipids, including phospholipids and cholesterol (Baumann and Walz, 2001). In addition, ER is the main intracellular Ca^{2+} store. The release of ER Ca^{2+} via inositol 1,4,5-triphosphate (IP_3) receptor leads to the activation of Ca^{2+} signaling in animal cells (Berridge et al., 2000). The ER is the largest membrane system in animal cells and constitutes a continuous extensive network extending from the nuclear envelop (NE) to the cell periphery (Baumann and Walz, 2001). When examined under a fluorescence microscope

in live cells, the ER network undergoes constant remodeling, and can be easily divided into morphological distinct subdomains including the NE, the cisternae (or sheet), and the tubules (Figure 1-1) (West et al., 2011). The mechanisms of shaping ER into different subdomains have been revealed, but are not fully understood. Two protein families, reticulons (Rtns) and DP1/Yop1, have been reported to shape ER membrane into tubules in yeast and animal cells (Voeltz et al., 2006). These proteins preferentially localize to the ER membrane with high curvature, including tubular ER and the edges of ER cisternae (Shibata et al., 2010; Voeltz et al., 2006). Overexpression of Rtns in cells resulted in long and unbranched tubular ER. Addition of purified Rtn1 or Yop1 was sufficient to generate membrane tubules from proteoliposomes *in vitro* (Hu et al., 2008). Rtns and DP1/Yop1 generate ER tubules though their hydrophobic segments that have been proposed to form short hairpin domains. These hairpin structures are not long enough to form transmembrane domains. Instead, they preferentially span the outer leaflet of the ER membrane. This uneven insertion of hairpin domains likely bends the ER membrane by hydrophobic wedging leading to tubule formation (Park and Blackstone, 2010; Voeltz et al., 2006; Zurek et al., 2011). To further generate a continuous network, ER tubules need to be connected by membrane fusion to form three-way junctions. The atlastin (ALT) family of dynamin-like GTPase has been demonstrated to localize to three-way junctions and mediate ER membrane fusion (Hu et al., 2009; Orso et al., 2009; Park et al., 2010). Knockdown of ALTs led to the accumulation of long, unbranched ER tubules in cells, and antibodies against ATLs inhibited network formation in *Xenopus* egg membrane extracts (Hu et al., 2009). In summary, these studies revealed how ER tubules are generated and then fuse with each other to form the ER network. In contrast, the mechanisms underlying the formation of ER cisternae remain less understood. One hypothesis is that the levels of Rtns and /DP1/Yop1 may determine the abundance of cisternae because cells lacking these proteins displayed extensive ER cisternae (Voeltz et al., 2006). Interestingly, distribution of tubule-generating proteins to the edges of ER cisterna suggests a supportive role for these proteins in cisternae formation by stabilizing the high curvature edges (Shibata et al., 2010). In addition, Climp63 has been reported to function as a spacer via its luminal coiled-coil domain to set the luminal width of ER cisternae. Knockdown of Climp63 led to a marked decrease of

luminal width in animal cells (Shibata et al., 2010). Nonetheless, the molecular components for the formation of ER cisternae remain unclear. The arrangement of ER architecture may have functional impacts to the cells. For example, ER structure undergoes remarkable reorganization during mitosis. As NE rapidly partitions into vesicles, the bulk of the ER converts into extended cisternae interconnected by ER tubules (Lu et al., 2009). A more recent *in vitro* study using *Xenopus* egg mitotic extracts showed that small cisternae formed along the tubules and eventually merged at three way junctions to generate large cisternae (Wang et al., 2013). Moreover, mutations in ER shaping protein ALT-1 and REEP1 (structurally related to DP1/Yop1 family) have been linked to inherited neurological disorders characterized by lower extremity spastic weakness. Further work indicated that defects in ER shaping seemed to be the prominent cause of these disorders (Park et al., 2010). A recent study revealed that stacked ER cisternae are connected by helicoidal membrane motifs that resemble a parking garage. These unique connections implicated an optimal arrangement of ER cisternae in the restricted cytosolic space (Terasaki et al., 2013). These studies showed that the morphological organization of the ER is important for cell functions, although detailed mechanisms involved in regulation of this elaborate ER network remain to be determined.

How does this morphological organization of ER network correlate to its functions? In general, ER cisternae are considered ribosome-bound rough ER as exemplified by electron microscopy (EM) images showing massive cisternae studded with ribosomes in secretory cells. In contrast, smooth ER with a low density of ribosomes often adopts the tubule morphology as demonstrated by expanded tubular ER in muscle cells (Shibata et al., 2010; Shibata et al., 2006; West et al., 2011). Thus, it is reasonable to postulate that ER cisternae are likely to participate in protein secretion, and tubular ER is preferentially responsible for Ca^{2+} regulation and lipid synthesis. In addition, ER cisternae in yeast have an average volume-to-surface area ratio of 9.2, which is greater than that of ER tubules with a value of 7.0. This observation suggested that ER cisternae may be suitable for functions that require larger luminal space, while membrane-associated processes, such as lipid synthesis, may occur in tubular ER (West et al.,

2011). In summary, organizing ER into distinct subdomains may be important for optimizing different functions.

Since the ER is the primary organelle for the synthesis of membrane proteins and lipids, other organelles with limited *de novo* biogenesis ability have to rely on ER for these materials. Thus, communication between the ER and other organelles is an important issue to orchestrate cellular functions. The vesicular transport pathway was considered the main mechanism for inter-organelle communication. This type of transport delivers proteins and lipids in membrane-bound vesicles to their designated compartments with high specificity (Cai et al., 2007). However, the fact that there is lipid exchange between the ER and the other organelles that are not connected to the vesicular transport pathway argues for the presence of other mechanisms for inter-organelle communication (Lev, 2010). In parallel, the ER forms membrane junctions, where two heterologous membranes closely appose to each other, with other organelles suggesting that these contacts may provide a direct inter-organelle communication (Levine and Loewen, 2006). Multiple lines of evidence indicated that these membrane junctions participate in many cellular processes. For example, ER-mitochondria junctions are required for mitochondrial Ca^{2+} uptake. Disruption of these junctions by deleting mitofusin 2 (MFN2), an ER-mitochondria tether, resulted in reduced mitochondrial Ca^{2+} levels following ER Ca^{2+} release. By contrast, tightened connection between the ER and mitochondria led to mitochondrial Ca^{2+} overloading (Csordas et al., 2006; de Brito and Scorrano, 2008). ER-PM junctions are significant because they directly connect the ER, the largest membrane system important for many cellular functions, to the PM, an active interface between the cells and extracellular environment. Therefore, ER-PM junctions not only provide a spatial platform for inter-organelle communication, but also serve as direct conduits for inside-out and outside-in signal transduction. ER-PM junctions have been reported to participate in many cellular functions including store-operated Ca^{2+} entry (SOCE), a universal mechanism in maintaining Ca^{2+} homeostasis and regulating Ca^{2+} signaling.

1.2 Ca^{2+} Signaling and Store-Operated Ca^{2+} Entry (SOCE)

Ca^{2+} is a universal second messenger that governs many important cellular functions. Elevation of cytosolic Ca^{2+} is the key to regulating diverse processes from relatively rapid events, such as muscle contraction and neurotransmitter release, to slower responses including cell migration and differentiation, and eventual apoptosis (Berridge et al., 2000; Dupont et al., 2011; Lewis, 2011). Aberrant Ca^{2+} regulation leads to several pathological conditions or diseases. For example, changes in basal Ca^{2+} homeostasis are often associated with neurodegenerative diseases and cardiac dysfunctions (Ter Keurs and Boyden, 2007; Treves et al., 2005). Therefore, intracellular Ca^{2+} level must be tightly regulated for the cells to execute the diverse functions precisely. During the resting state, cytosolic Ca^{2+} level is maintained at a low level of approximately 50 to 100 nM by the activities of sarco/endoplasmic reticulum Ca^{2+}-ATPase (SERCA) and plasma membrane Ca^{2+}-ATPase (PMCA) in the ER and the PM, respectively. With the consumption of energy, SERCA and PMCA are able to constitutively pump Ca^{2+} from the cytosol, against the steep chemical gradient, back to the ER with an estimated luminal Ca^{2+} concentration of 400 to 600 μM, and the extracellular space usually with a Ca^{2+} concentration over 1 mM, respectively (Figure 1-2A) (Carrasco and Meyer, 2011; Hogan et al., 2010). During Ca^{2+} signaling, stimulation of many cell surface receptors mediates activation of phospholipase C (PLC). G protein-coupled receptors activate PLCβ while tyrosine kinase-coupled receptors activate PLCγ. Activated PLC hydrolyzes phosphatidylinositol 4,5-bisphosphate (PIP_2) at the PM to generate IP_3, which binds to and opens IP_3 receptor Ca^{2+} channel in the ER. The opening of the IP_3 receptor releases ER Ca^{2+} leading to the increase in cytosolic Ca^{2+} levels and subsequent activation of Ca^{2+} effectors (Figure 1-2B) (Berridge et al., 2000). Because the ER only contains a limited Ca^{2+} store, animal cells develop an elaborate mechanism called store-operated Ca^{2+} entry (SOCE) to refill the ER store and to maintain sustained cytosolic Ca^{2+} levels. SOCE mechanism was first proposed by James Putney in 1986 based on the observation that the level of the ER Ca^{2+} pool negatively operated a Ca^{2+} influx from the extracellular space (Putney, 1986). Subsequent studies using thapsigargin (TG), a SERCA inhibitor that empties the ER Ca^{2+} store without opening the IP_3 receptor (Thastrup et al., 1989), demonstrated that ER Ca^{2+} depletion is sufficient to activate SOCE (Parekh and

Penner, 1997; Putney and Bird, 1993). Together, these observations raised the hypothesis that there must be a Ca^{2+} sensor that detects the reduction of ER Ca^{2+} levels, and then initiates a signaling cascade to open a Ca^{2+} channel at PM leading Ca^{2+} to influx. The first evidence to support this idea was the detection of the Ca^{2+} current elicited by SOCE in mast cells and T cells (Lewis and Cahalan, 1989; Penner et al., 1988). This current, with characteristics of high Ca^{2+}-selectivity over monovalent cations and extreme low conductance, was named Ca^{2+} release-activated Ca^{2+} (CRAC) current (I_{CRAC})(Hoth and Penner, 1992). Although these characteristics or fingerprint of I_{CRAC} explicitly defined the rules for identifying the potential candidates for SOCE, the mechanisms that link ER Ca^{2+} store depletion to SOCE across the PM remained unclear for decades due to the lack of a molecular component. In 2005, the discovery of stromal interaction molecule-1 (STIM1) as the ER Ca^{2+} sensor, and a year later, the identification of Orai1 as the PM SOC channel, provided the first two clues to reveal the mechanisms of SOCE (Feske et al., 2006; Liou et al., 2005; Roos et al., 2005; Vig et al., 2006; Zhang et al., 2006).

STIM1 was identified by RNAi screens for SOC regulator from two independent groups in 2005 (Liou et al., 2005; Roos et al., 2005). STIM1 is an ER transmembrane protein with an N-terminal Ca^{2+}-sensing EF hand-SAM (EF-SAM) domain in the ER lumen, coiled-coil domains, a serine and proline rich region, and a polybasic tail in the cytosol (Figure 1-3A). During the resting state, STIM1 binds to Ca^{2+} via its luminal EF hand motif and localizes diffusely throughout the ER. This Ca^{2+}-bound STIM1 is inactive give the evidence that disruption of STIM1 Ca^{2+} binding by mutation of a key residue in the EF hand motif resulted in constitutive SOCE (Liou et al., 2005). Following ER Ca^{2+} depletion, STIM1 rapidly forms oligomers, likely resulting from the partial unfolding and aggregation of the EF-SAM domain when Ca^{2+} is released (Liou et al., 2007; Stathopulos et al., 2008). Oligomerization of STIM1 is the key step to activate SOCE. This is supported by the observation that rapamycin analogs-induced oligomerization of STIM1 fusion proteins, which with the Ca^{2+}-sensing domain replaced by a FKBP12 motif or a FKBP12-rapamycin binding (FRB) motif, was sufficient to trigger SOCE without ER Ca^{2+} depletion (Luik et al., 2008; Putyrski and Schultz, 2012). STIM1 oligomers translocate to ER-PM junctions via a polybasic tail

binding to PIP_2 and phosphatidylinositol 3,4,5-triphosphate (PIP_3) at the PM (Ercan et al., 2009; Korzeniowski et al., 2009; Liou et al., 2007; Walsh et al., 2010). This translocation of STIM1 to ER-PM junctions is also called puncta formation based on the initial finding that cells overexpressing YFP-tagged STIM1 showed bright fluorescence signals in puncta near the cell periphery following ER Ca^{2+} depletion (Liou et al., 2005). The absence of STIM1 at ER-PM junctions in resting cells suggests that the PM targeting motif is not accessible. It is likely that the positive-charged residues in the STIM1 polybasic tail were structurally hindered or their binding affinity to PM was too weak to retain STIM1 at ER-PM junctions. Thus, oligomerization likely mediates the exposure of the positive-charged residues and/or creates a stronger PM binding that enables STIM1 oligomers to localize at ER-PM junctions. The close apposition between the ER and the PM allows STIM1 in the ER to directly interact with the PM localized SOC channel, Orai1. The minimal domain of STIM1 binding to and activating Orai1 has been identified by several groups. This domain is called CAD (CRAC activation domain, amino acid 342 to 448) (Park et al., 2009), SOAR (STIM1-Orai activating region, amino acid 344 to 442) (Yuan et al., 2009), or Ccb9 (amino acid 339 to 444) (Kawasaki et al., 2009). I will refer to this minimal domain as CAD in my dissertation. CAD has been shown to bind to Orai1 directly, and overexpression of CAD alone led to constitutive activation of I_{CARC} in the absence of ER Ca^{2+} depletion (Park et al., 2009). This data indicated that STIM1 is a direct SOC channel activator. It is postulated that Orai1 diffuses passively into ER-PM junctions, and is then trapped and activated by prior translocated STIM1 to elicit SOCE. This hypothesis is supported by the facts that Orai1 is highly mobile in the PM and the I_{CRAC} activation is delayed following STIM1 translocation to ER-PM junctions (Luik et al., 2006; Madl et al., 2010; Park et al., 2009). Intriguing, a recent report showed that distribution of Orai1 at PM may affect its recruitment to ER-PM junctions. Defective PIP_2 rearrangement at PM by septin4 knockdown only abolished Orai1 but not STIM1 accumulation at ER-PM junctions following ER Ca^{2+} depletion. These results implicated that Orai1 might be pre-localized in certain PM microdomains that facilitate STIM1-Orai1 interactions (Sharma et al., 2013). Further studies are required to understand how septin4 further modulates STIM1

interaction with Orai1 at ER-PM junctions. Based on the current knowledge, the molecular mechanism that STIM1 activates Orai1 at ER-PM junctions during SOCE is summarized in Figure 1-3B.

The importance of SOCE has been demonstrated in mouse genetics studies as well as in human patients lacking functional STIM1 or Orai1. Mice lacking STIM1 showed perinatal lethality (Baba et al., 2008; Oh-Hora et al., 2008; Stiber et al., 2008; Varga-Szabo et al., 2008). STIM1-deficient mice that managed to survive also exhibited severe growth retardation and muscle fatigue (Stiber et al., 2008; Varga-Szabo et al., 2008). Loss of Orai1 in mice displayed phenotypes similar to those in STIM1-deficient animals, and mostly abolished the functions of immune cells because their activation is highly dependent on SOCE. Mast cells lacking STIM1 or Orai1 showed impaired activation of nuclear factor of activated T-cells (NFAT), reduced degranulation, and defective cytokine production (Baba et al., 2008; Vig et al., 2008). Similarly, T cells from STIM1- and Orai1-defecient mice displayed reduction in SOCE and cytokine production (Gwack et al., 2008; Oh-Hora et al., 2008). T cell-specific ablation of STIM1 also resulted in a lymphoproliferative phenotype and a selective decrease in regulatory T cell numbers (Oh-Hora et al., 2008). The phenotypes in immune cells acquired from mouse genetic studies were consistent with the severe combined immunodeficiency (SCID) symptoms in human patients lacking normal STIM1 and Orai1 functions (Feske et al., 2010). Of notice, STIM1-deficient mice displayed skeletal myopathy, and STIM1 haploinsufficient mice also exhibited increased susceptibility to fatigue (Stiber et al., 2008). Similar muscle phenotypes of muscle myopathy and reduced strength also presented in human patients lacking functional STIM1 or Orai1 (Feske et al., 2010). In addition, STIM1 and Orai1 were shown to be highly expressed in human and mouse skeletal muscle (Gwack et al., 2008; Stiber et al., 2008; Vig et al., 2008; Williams et al., 2001). These observations indicated the requirement of SOCE in wild-type muscle cells. Interestingly, SOCE in muscle cells occurs remarkably faster than in non-excitable cells (Launikonis and Rios, 2007). STIM1-L, a muscle specific variant of STIM1, is pre-localized at ER-PM junctions and thus may provide an explanation for faster SOCE activation in muscle cells (Darbellay et al., 2011). In summary, these genetic studies and clinical observations indicated the

importance of SOCE in development, immune cell activation, as well as maintaining muscle cell functions.

The discovery of STIM1 as an ER Ca^{2+} sensor for SOCE resulted in a series of studies in deciphering the molecular mechanisms underlying this pivotal yet not-fully-understood cellular process. Concurrently, the fact that STIM1 interaction with Orai1 absolutely requires the presence of ER-PM junctions also generated new research interests in the inter-organelle signaling at these membrane microdomains that have long been overlooked.

1.3 Definition of ER-PM Junctions

ER-PM junctions are ER regions that form close appositions with the PM. In general, ER-PM junctions in different cell types share several common features. First, the distance between the ER and the PM at ER-PM junctions is in the range of 10 to 20 nm. This variation could reflect the real difference in ER-PM junctions or may simply be the result of experimental artifacts. Because of the narrow distance, the presence of ribosomes in this space has never been reported. Instead, electron-dense cytosol is often observed in the gap suggesting a concentration of proteins, lipids or ions. Second, the ER and PM membranes are aligned in parallel often with a length of approximately 200 nm in many cells types. No membrane fusion between these two compartments has been observed, though the narrowest gap distance reported was 1.3 nm in STIM1 overexpressing cells (Orci et al., 2009).

A variety of nomenclatures throughout the literature have been used to describe ER-PM junctions in different cell types or organisms. These terms include dyad and triad junctions (or dyads and triads), excitation-contraction (E-C) units, and peripheral couplings in muscle cells (Franzini-Armstrong and Jorgensen, 1994); subsurface cisterns (SSC's) in neurons (Rosenbluth, 1962); PM-associated ER and cortical ER in yeast (Loewen et al., 2007; West et al., 2011); subrhabdomeric cisternae (SRC) in *Drosophila* photoreceptor cells (Vihtelic et al., 1993). I will use the term junctions to emphasize that these are the loci at which the ER and the PM are joined in both physical proximity and functional coupling.

Some literature misinterpreted the translocation or accumulation of proteins at ER-PM junctions as the formation of these junctions. The lack of signals of proteins only indicates their absence at ER-PM junctions, but does not reflect the absence of junctions. ER-PM junctions should be visualized independently and examined carefully to avoid confusion and misunderstanding.

1.4 ER-PM Junctions in Muscle Cells

ER-PM junctions were first described in 1957 in studies using EM in muscle cells (Porter and Palade, 1957). Similar structures were reported in neurons a few years later (Henkart et al., 1976; Rosenbluth, 1962). In skeletal and cardiac muscles, these junctions are called triad and dyad junctions, respectively. These junctions are formed by the sarcoplasmic reticulum (SR, equivalent to ER in non-excitable cells) making extensive contacts with the tubular invaginations or transvers tubules (T tubules) of sarcolemma (PM in muscle cells). The gap distance was measured to be 9 to 12 nm between the two membranes, and electron-dense materials were observed in the gap implicating the enrichment of proteins (Flucher, 1992; Henkart et al., 1976; Rossi and Dirksen, 2006). The gap distance often correlates with different contractile functions. Triad junctions with smaller gap distance were observed in fast contraction skeletal muscle fibers, while relaxed junctions were present in slow twitch or cardiac fibers (Franzini-Armstrong, 1972). In addition, the periodic distribution of triad and dyad junctions, along with T tubules, ensures the even proximity to contractile fibers in muscle cells to maximize the contraction strength (Carrasco and Meyer, 2011; Flucher, 1992). These junctions are required for contractile functions in muscles by serving as a platform for excitation-contraction (E-C) coupling. During muscle contraction, the PM localized voltage-gated Ca^{2+} channel, dihydropyridine receptor (DHPR), is first activated by membrane depolarization to mediate a Ca^{2+} influx. The increase in Ca^{2+} levels at the junctional area subsequently opens the Ca^{2+}-releasing ryanodine receptor (RyR) in SR leading to a further increase in cytosolic Ca^{2+} levels and muscle contraction. This amplification process is called Ca^{2+}-induced Ca^{2+} release (Endo, 2009). Both RyRs and DPHRs are localized in triad and dyad junctions. The cytosolic portion of RyRs displayed feet structures that span the gap of triad junctions and appeared to tether the

two membranes under EM (Loesser et al., 1992). Immunostaining of RyRs also demonstrated their localization at triad junctions (Airey et al., 1990). DHPRs were first shown to localize in T tubules (Fosset et al., 1983). Later studies further confirmed the apposition of DHPRs and RyRs at triad and dyad junctions (Flucher et al., 1991; Yuan et al., 1991). Despite the presence of DHPRs and RyRs and their functions at triad and dyad junctions, multiple lines of evidence suggested that they are not required for the formation of these junctions. First, triad junctions still existed in muscle cells lacking either DHPRs or RyRs (Franzini-Armstrong et al., 1991; Ikemoto et al., 1997; Takekura et al., 1995a). Moreover, coexpression of DHPR and RyR was unable to generate close membrane appositions between the ER and PM in Chinese hamster ovarian (CHO) cells (Takekura et al., 1995b). These studies indicated that other structural components are required for formation of ER-PM junctions in muscle cells. In addition, no E-C coupling was observed in the latter study even though the overexpressed DHPR and RyR were demonstrated to be functional, indicating the requirement of these junctions for physiological coupling between DHPR and RyR.

To identify the components required for the formation of triad and dyad junctions, Takeshima and colleagues generated monoclonal antibodies from mice immunized with membrane vesicles of rabbit skeletal muscle. By antibody screening, they identified a protein family called junctophilin (JPH) (Takeshima et al., 2000). Four JPHs have been reported and they are expressed exclusively in excitable tissues: JPH-1 and JPH-2 are expressed in both heart and skeletal muscle, and JPH-3 and JPH-4 is highly expressed in brain tissue. A low amount of JPH-2 was also detected in tissues containing smooth muscle, such as stomach and lung (Nishi et al., 2003; Takeshima et al., 2000). JPHs are ER transmembrane proteins with eight N-terminal membrane occupation and recognition nexus (MORN) motifs that mediate JPHs PM targeting, likely via phospholipid binding (Garbino et al., 2009; Ma et al., 2006). The ER transmembrane domain and MORN motifs constitute the dual targeting mechanism for both the ER and PM. Thus, one can postulate that JPHs might be able to bridge the ER and the PM to form junctions. Indeed, *Cynops pyrrhogaster* (amphibian) embryos expressing exogenous full-length JPH-1 exhibited

extensive ER-PM junctions with structural similarities to those in muscle cells. In contrast, cardiac myocytes isolated from JPH-2 null embryos exhibited a 90% reduction of functional dyad junctions. The average length of the remaining junctions in JPH-2 null myocytes was also significantly reduced to 170 ± 60 nm, while in wild-type cells the length was 370 ± 160 nm. The defective dyad junctions led to impaired Ca^{2+} transients in cardiac myocytes, which likely caused the phenotypes of weak heartbeats, cardiac arrest, and eventual embryonic lethality in mice lacking JPH-2. This data demonstrated that JPHs are required for the formation ER-PM junctions in muscle cells. Notably, JPH-1 overexpression in amphibian embryos generated ER-PM junctions with an average gap distance of 7.6 ± 0.6 nm. This was similar to the gap distance of triad junctions in muscle cells lacking RyR, but not that distance found in wild-type muscles (Takekura et al., 1995a; Takeshima et al., 2000). These results raised the question whether JHP-1 is flexible enough to extend up to 12 nm to interact with PM in the presence of RyRs, or if there are other junctional components together with JPH-1 to bridge triad or dyad junctions. In addition, myotubes lacking JPH-1 displayed a severe reduction of SOCE, low basal cytosolic Ca^{2+} levels, and low SR Ca^{2+} store (Hirata et al., 2006; Li et al., 2010). These results provided the first structural components to bridge the SR and the PM in triad and dyad junctions. Genetic ablation of JPHs further showed that ER-PM junctions are important for Ca^{2+} signaling consisting of E-C coupling and SOCE in muscle cells.

1.5 ER-PM Junctions in Non-Excitable Cells

Muscle cells are highly specialized cells that adopt extensive triad and dyad junctions to perform contractile functions. Non-excitable cells that execute diverse functions have ER-PM junctions of negligible abundance. Therefore, it is difficult to link a particular cellular process to ER-PM junctions despite their structural similarity to triad and dyad junctions. Lacking a molecular component and a functional relevance, ER-PM junctions were difficult to study in non-excitable cells. The discovery of STIM1 revealed a functional significance of ER-PM junctions, which prompted the field to re-evaluate these minute subcellular structures.

1.5.1 EM Characterization of ER-PM Junctions

In non-excitable cells, ER-PM junctions were initially observed in mouse fibroblasts in 1979 by EM (Henkart and Nelson, 1979). These junctions displayed typical characteristics including electron-dense materials in the gap and a gap distance of 16-20 nm. In 1983, Gardiner and Grey described ER-PM junctions of *Xenopus* eggs in detail. In matured, unfertilized eggs, pre-existing ER-PM junctions with the length of 100 to 700 nm were observed. The gap distance of these junctions was at the range of 8 to 13 nm, and periodic electron-dense material was also observed in the gap. Notably, the abundance of ER-PM junctions seemed to correlate with Ca^{2+} signaling events during oocyte maturation including the alteration of PM Ca^{2+} permeability and an increase in cytosolic Ca^{2+} levels (Gardiner and Grey, 1983). These initial observations demonstrated that ER-PM junctions in non-excitable cells were structurally and functionally similar to triad and dyad junctions. However, because of the low abundance of ER-PM junctions in non-excitable cells, the importance of these junctions was often overlooked.

After the discovery of STIM1, ER-PM junctions were re-examined using EM by many groups. In 2006, Wu and colleagues revealed ER-PM junctions in details in Jurkat T cells using EM. Because of the lack of a specific marker for ER-PM junctions, a horseradish peroxidase (HRP)-tagged ER luminal marker was applied to label ER, and the ER tubules in close apposition of PM within 50 nm were defined as ER-PM junctions. By examining hundreds of individual ER-PM junctions, they showed that the average length of a single ER-PM junction was approximately 150 nm, and the gap distance was in the range of 10 to 25 nm. By measuring the total length of ER-PM junctions and circumference of the entire cells, they further demonstrated that only 4% of the PM was covered by ER-PM junctions in resting cells. This coverage was up-regulated to 6% following ER Ca^{2+} depletion by TG due to an increase in number but not in size of ER-PM junctions. Overexpression of HRP-tagged STIM1 did not change the number of ER-PM junctions. However, overexpressed STIM1 translocation to ER-PM junctions after TG stimulus resulted in a significant increase in the length of individual junctions to almost 300 nm (Wu et al., 2006). Together, these results indicated that ER-PM junctions are dynamically regulated during ER Ca^{2+}

depletion and STIM1 translocation may generate bigger junctions. This was the first EM study that systematically investigated ER-PM junctions in one cell type. The details provided in this report also became the standard for future studies.

ER-PM junctions in HeLa cells were also examined by Orci and colleagues in 2009. They applied conventional post-staining EM to label all membrane compartments. Similar to Jurkat T cells, TG treatment resulted in an increase of PM coverage of ER-PM junctions from 0.23% to 1.24%. Overexpression of STIM1 led to a marked induction of PM coverage to 1.40% and to 5.44% in unstimulated and in TG-treated HeLa cells, respectively. In STIM1 expressing cells, the average length of single ER-PM junctions was 200 to 400 nm, and the average gap distance was 8.3 ± 0.3 nm with huge variation ranging from 1.3 to 14.7 nm. A similar gap distance of 11.3 ± 2.9 was observed in cryosections. Interestingly, ER-PM junctions were more often distributed to the basal-lateral membranes of the cells indicating the specific membrane features in determining the formation of ER-PM junctions even in poorly polarized HeLa cells (Orci et al., 2009). The uneven distribution of ER-PM junctions was also demonstrated in pancreatic acinar cells, a cell type specialized in secretion. In these cells, ER-PM junctions were mostly found in the basal-lateral regions of the cells, but not in the regions with secretory granules, suggesting that the spatial organization of ER-PM junctions and other functional domains are regulated (Lur et al., 2009). In addition, STIM1 overexpression resulted in a 2-fold increase in density of ER-PM junctions, while the gross appearance of these junctions was not affected. Unexpectedly, TG treatment failed to trigger any change in the density of ER-PM junctions in both the control and STIM1 overexpressing acinar cells (Lur et al., 2009). The ER in pancreatic acinar cells is mostly organized into ribosome-bound cisternae to maximize the protein-producing activity, and thus the ability to generate new ribosome-free ER-PM junctions in these cells may be limited to coordinate secretory functions.

In summary, these EM studies revealed the structure of ER-PM junctions in great detail, and demonstrated that the regulation of these junctions is dependent on Ca^{2+} signaling and STIM1 overexpression. In general, an increase in the contacts between the ER and PM was observed in most cell

types during Ca^{2+} signaling. No change in gap distance was reported. Nonetheless, it is difficult to derive the dynamic properties of ER-PM junctions during cellular processes using EM.

1.5.2 Visualization of ER-PM Junctions in Live Cells

In 2007, Varnai and colleagues first attempted to label ER-PM junctions in live cells by applying a chemically inducible molecular bridge formation approach. In this method, a FKBP12 protein was targeted to the inner leaflet of the PM, and a FRB protein was targeted to the cytosolic surface of the ER. Both constructs contain a fluorescence protein. They reasoned that the molecule bridges triggered by the addition of rapamycin could only occur at regions where the ER and PM are in close proximity. As expected, both proteins rapidly translocated to the same puncta from their original localizations following rapamycin treatment. These puncta eventually expanded into stable patches with the size at a lower micrometer range and were confirmed to be ER-PM junctions by colocalizating with STIM1 following TG treatment. Moreover, by manipulating the length of these two proteins, they found that Orai1 might be in complex with other bulky proteins and the size of this complex was estimated to be larger than 9 nm but smaller than 14 nm. Interestingly, STIM1 containing a long cytosolic region seemed to fit well into the 9-nm ER-PM junctions suggesting that STIM1 has a flexible cytosolic region (Varnai et al., 2007).

A similar rapamycin-induced crosslink approach was used to label ER-PM junctions by Lavieu and colleagues in 2010 (Lavieu et al., 2010). They generated FKBP12 and FRB chimeric proteins containing a fluorescence protein, and the last ER transmembrane domain and a PM targeting motif from the yeast protein Ist2. Overexpression of Ist2 in mammalian cells resulted in puncta or patch-like localization at cell periphery, which was interpreted as recruitment of the ER to the PM (Ercan et al., 2009). A more recent study showed that Ist2 is involved in ER-to-PM tethering in yeast cells (Manford et al., 2012). These Ist2 domain-containing synthetic FKBP12 and FRB constructs showed diffuse ER localization at basal. Following rapamycin analog treatment, these two proteins first concentrated in intracellular puncta, and then accumulated to the cell periphery. The authors argued that the peripheral accumulation of these

proteins was a "trafficking or transportation" event that eventually led to the formation of ER-PM junctions. Disruption of microtubule dynamics using nocodazole (NocZ) or siRNA against end binding protein 1 (EB1) abolished the peripheral accumulation. Based on the observation that the localization of Ist2 to ER-PM junctions required a COPI coatomer βCOP, they concluded that Ist2 anchoring the ER to the PM was mediated through COPI- and microtubule-dependent mechanisms (Lavieu et al., 2010). Further studies are needed to understand the detailed mechanisms of the formation of ER-PM junctions.

1.5.3 Identification of Tethers of ER-PM Junctions

Another obstacle of studying ER-PM junctions is the lack of a structural component and its underlying mechanisms. Prior studies using EM showed the correlation of STIM1 overexpression and the formation of ER-PM junctions (Lur et al., 2009; Orci et al., 2009; Wu et al., 2006). Indeed, STIM1 contains both ER and PM targeting motifs that are capable of tethering the ER to the PM. Nonetheless, ER-PM junctions have never been examined in cells with STIM1 knockdown or lacking STIM1. Thus, the requirement of STIM1 in the formation of ER-PM junctions remains inconclusive due to the lack of this key evidence. Also, STIM1 is only present at ER-PM junction after ER Ca^{2+} depletion, indicating that other tethering components must exist to maintain ER-PM junctions during the resting state. Junctate appeared to be a promising candidate for the formation of ER-PM junctions. It was identified as an ER membrane Ca^{2+} binding protein that is expressed in a variety of tissues (Treves et al., 2000). Overexpression of junctate in HEK293 cells displayed a significant increase in the number and the size of ER-PM junctions. Notably, knockdown of junctate dramatically reduced the average size of ER-PM junctions from 218 ± 94 nm to 139 ± 51 nm, and the number of ER-PM junctions (Treves et al., 2004). However, junctate only contains 23 amino acids in the cytosolic region, which is too short for tethering the ER to the PM, and overexpression of junctate showed diffuse ER localization, but not enriched at ER-PM junctions (Srikanth et al., 2012; Treves et al., 2010). Junctate has been reported to interact with IP_3 receptor and STIM1-Orai1 complex to modulate Ca^{2+} signaling (Srikanth et al., 2012; Treves et al., 2004; Treves et al., 2010). Thus, it is likely that junctate interacts with other components at ER-PM junctions to

provide ER-to-PM tethering. Recently, several proteins including α-SNAP, SARAF, Surf4, and POST, have been shown to interact with STIM1 at ER-PM junctions and to modulate SOCE (Fujii et al., 2012; Krapivinsky et al., 2011; Miao et al., 2013; Palty et al., 2012). These proteins may also contribute to the tethering of ER-PM junctions.

A family of proteins named extended synaptotagmin-like proteins (E-Syts), which includes E-Syt1, E-Syt2, and E-Syt3, has recently been identified as tethers for ER-PM junctions in mammalian cells (Figure 1-4A) (Giordano et al., 2013). E-Syts are named after synaptotagmin because of the domain similarity. E-Syts contain N-terminal hydrophobic segments for their ER membrane targeting, followed by cytosolic synaptotagmin-like mitochondrial lipid binding protein (SMP) domain and three to five C2 domains (Figure 1-4A) (Min et al., 2007). SMP domains were identified by protein sequence alignment (Lee and Hong, 2006) and were proposed to have a role in phospholipid transfer (Kopec et al., 2010). Studies in yeast showed that all SMP domain containing proteins localize to ER-organelle junctions implicating their common functions at these membrane junctions (Toulmay and Prinz, 2012). Many C2 domains are capable of Ca^{2+} or phospholipid binding and they comprise the second largest Ca^{2+} binding motif in the proteome (Min et al., 2007). When fluorescence protein tagged-E-Syts were overexpressed in cells, E-Syt1 displayed diffuse ER localization, while E-Syt2 and E-Syt3 appeared to localize at PM but with very dim intracellular signals (Giordano et al., 2013; Min et al., 2007). Further examination of HRP tagged-E-Syt2 and E-Syt3 by EM revealed that both proteins were enriched at ER-PM junctions. The PM localization observed by fluorescence microscopy reflected the expansion of ER-PM junctions due to overexpression of E-Syt2 and E-Syt3 (Giordano et al., 2013). This piece of data suggested that E-Syt2 and E-Syt3 were capable of PM binding to mediate tethering between the ER and PM. As expected, the very C-terminal C2C domains from both E-Syt2 and E-Syt3 were sufficient for their PM targeting via PIP_2 binding (Giordano et al., 2013; Min et al., 2007). Remarkably, knockdown of all three E-Syts resulted in a significant reduction in the number of ER-PM junctions up to 50% as detected by ER luminal marker and TIRF microscopy. When these triple knockdown cells were examined by EM, a 75%

decrease in the PM coverage by ER-PM junctions was observed. Reconstitutions of E-Syt1 and E-Syt2 in triple knockdown cells were sufficient to restore the abundance of ER-PM junctions to control level, indicting the redundancy of E-Syts in ER-to-PM tethering (Giordano et al., 2013). These results showed that E-Syts function as direct tethers for ER-PM junctions via PIP_2 binding at the PM. However, triple knockdown of E-Syts only resulted in a 50% decrease in the number of ER-PM junctions, indicating that additional unknown components also provide tethering to maintain ER-PM junctions.

1.5.4 Additional Cellular Functions Occurring at ER-PM Junctions

In addition to SOCE, ER-PM junctions have been reported as the spatial platform for other cellular functions. Protein tyrosine phosphatase 1B (PTP1B) is an ER localized enzyme with its catalytic domain facing the cytosol (Frangioni et al., 1992). PTP1B has been shown to directly interact with many cell surface receptors including insulin receptor (IR), epidermal growth factor receptor (EGFR), and platelet-derived growth factor receptor (PDGFR), to regulate their activities (Boute et al., 2003; Eden et al., 2010; Haj et al., 2002). The PTP1B-substrate interaction is shown to be very transient and dynamic in live cells. Thus, a PTP1B mutant (D118A, PTP1B-DA) that forms stable interaction with substrates became a useful tool to reveal the loci of PIP1B-substrate interaction. Overexpression of a fluorescence protein-tagged PIP1B-DA displayed a punctate distribution. These puncta have been shown to colocalize with focal adhesion kinase (FAK) as well as to define the distal tips of adhesion sites (Hernandez et al., 2006). In addition, PTP1B-DA also interacts with the protein tyrosine kinase Src at PM (Monteleone et al., 2012). Defective PTP1B signaling in fibroblasts resulted in impaired cell spreading and low Src activity (Arregui et al., 1998; Cheng et al., 2001). This data indicated that PITP1B regulates cell motility and adhesion in *trans* at ER-PM junctions.

Furthermore, ER-PM junctions have recently been suggested to function as membrane protein trafficking hubs. Recycling of both the fluorescence protein-labeled transferrin receptor (TfR) and voltage-gated potassium channel Kv1.4 occurred juxtaposed to ER-PM junctions labeled by ER Tracker

(fluorescence dye for ER). Thin-section EM imaging also revealed that some vesicular structures that are likely in the process of exocytosis or endocytosis were present in close proximity to ER-PM junctions within 200 nm (Fox et al., 2013). Although these observations indicated the spatial correlation of ER-PM junctions and protein trafficking events, a thorough study is needed to provide further mechanistic insights. In summary, these studies suggested that ER-PM junctions are involved in multiple cellular processes. Regulation of ER-PM junctions may have greater impacts on cell functions in addition to SOCE.

1.6 ER-PM Junctions in Yeast

Yeast cells have a very different organization of ER-PM junctions than those in mammalian cells. The ER forms extensive contacts with the PM covering 40% to 70% of the PM. In yeast cells expressing a fluorescence ER luminal marker, these contacts appear as sheet-like structures that run in parallel with the PM and are referred to cortical ER (Loewen et al., 2007; Manford et al., 2012). I will use the term cortical ER to refer to ER-PM junctions in yeast since this term better describes the morphology of this ER subdomain. If examined under 3D EM tomography in detail, cortical ER actually consisted of ER tubules and highly fenestrated cisternae with an average gap distance of 33 nm (West et al., 2011). Yeast cells lacking Rtn1/Rtn2 and Yop1 exhibited extensive cortical ER sheets devoid of tubules and fenestrated cisternae. These observations indicated that tubule-generating proteins are involved in determining the distinct shape of cortical ER (West et al., 2011). In addition, the mechanisms underlying the formation of cortical ER have been revealed in several genetic studies. Scs2 and Scs22, the yeast orthologs of mammalian VAMP-associated proteins (VAPs), have been shown to support cortical ER formation. VAPs are conserved ER membrane proteins known to interact with FFAT (two phenylalanine in an acidic track) motif-containing proteins including, many lipid transfer proteins (Lev et al., 2008). Deletion of Scs2 resulted in a significant decrease in the PM coverage by cortical ER up to 50% (Loewen et al., 2007). The reduction, but not complete depletion in cortical ER in Scs2-deficient yeast cells suggested the existence of other tethering proteins. By using quantitative proteomics approaches in

searching for Scs2 interacting proteins, Manford and colleagues identified additional tethering components for the formation of cortical ER: Ist2 and tricalbins. Ist2 is a multi-transmembrane ER protein with a C-terminal polybasic tail that binds to PIP_2 at the PM, and has been shown to localize to ER-PM junctions (Ercan et al., 2009). Tricalbins (Tcb), including Tcb1, Tcb2, and Tcb3, are the yeast orthologs of E-Syts. Yeast cells lacking all six tethering proteins (Δtether cells), including Scs2/Scs22, Ist2, and Tcb1/Tcb2/Tcb3, displayed a dramatic, nearly complete reduction of cortical ER, and an accumulation of cytoplasmic ER structures under fluorescence microscopy. Further ultrastructural analysis in the Δtether cells using EM showed a nearly 90% decrease in the PM coverage by cortical ER. Unlike the knockdown of E-Syts, which significantly decreased ER-PM junctions in mammalian cells, deletion of Tbcs alone seemed to have the least effect. It appeared that Tcbs mediate synergistic effects with Scs2/Sce22 to support the formation of cortical ER through unknown mechanisms. Moreover, C2 domains in Tcbs do not contain conserved Ca^{2+} binding residues, suggesting that Ca^{2+}-independent mechanisms may be involved in Tcbs ER-to-PM tethering (Min et al., 2007). It is noteworthy that constitutive unfolded protein response (UPR) was observed in the Δtether cells. This up-regulated UPR was not due to the defects in protein trafficking. Instead, it is required for the viability in the Δtether cells. Therefore, cortical ER may participate in crucial, yet unidentified, ER functions that suppress UPR in wild-type yeast cells (Manford et al., 2012).

The best documented function of cortical ER in yeast is lipid biogenesis or metabolism. PM-associated ER isolated by biochemical methods showed high capacity of phosphatidylinositol (PI) and phosphatidylserine (PS) synthesis *in vitro* (Pichler et al., 2001). A recent genetics study also demonstrated that cortical ER participates in phosphatidylcholine (PC) synthesis (Tavassoli et al., 2013). In parallel, several sterol sensing proteins and lipid binding proteins have been shown to localize in cortical ER (Loewen et al., 2003; Schulz et al., 2009). In addition, cortical ER is the spatial loci for PI4P metabolism. PI4P level at PM is regulated by an ER localized phosphatase called Sac1, and is important for many cellular functions. Yeast lacking Sac1 displayed elevated PM PI4P levels leading to defects in membrane

trafficking, lipid metabolism, and growth (Foti et al., 2001; Guo et al., 1999; Rivas et al., 1999). Sac1 in the ER regulates PM PI4P levels in *trans* at cortical ER in a protein complex containing oxysterol-binding homology protein 3 (Osh3) and Scs2/Scs22. When the PM PI4P level is high, Osh3 is recruited to the cortical ER via its PH domain binding to PI4P at PM and FFAT motif interaction with Scs2/Scs22 in the ER. This retention of Osh3 subsequently activates Sac1 to dephosphorylate PI4P in cortical ER (Stefan et al., 2011). Given that the cortical ER is the spatial platform for Sac1 functions, a significant elevation of PI4P levels at PM was indeed observed in the Δtether cells (Manford et al., 2012). The functional significance of Sac1 in higher organisms has been demonstrated by embryonic lethality in mice and in *Drosophila* lacking Sac1 (Liu et al., 2008; Wei et al., 2003). Nonetheless, a recent study showed that Sac1 functions at ER-trans Golgi network (TGN) junctions and dephosphorylates PI4P in the ER in *cis* (Mesmin et al., 2013). Further research is required for understanding the mechanisms behind the functions of Sac1 at different ER-organelle junctions.

1.7 Non-Vesicular Phosphatidylinositol (PI) Transfer at ER-PM Junctions

Eukaryotic cells are organized into membrane-bound organelles with unique protein and lipid compositions. The accurate distribution of proteins is often determined by the intrinsic trafficking signals recognized by the sorting machinery in the vesicular transport pathway. By contrast, the mechanisms underlying the distinct distribution of lipid molecules, which are too small to carry "address codes", are not fully understood. The fact that eukaryotic cells contain more than a thousand lipid species makes it more difficult to reveal the detailed lipid delivery machinery (Sleight, 1987). Intuitively, lipid trafficking was thought to be mediated primarily by vesicular transport given that lipids are the major constituents of vesicles. However, perturbations in vesicular transport pathway by ATP depletion, reduction in temperature, and by brefeldin A treatment to disrupt the Golgi network, were unable to completely block lipid transport (Kaplan and Simoni, 1985; Vance et al., 1991). Several lines of evidence support the non-vesicular lipid transport mechanism. The best documented example is the lipid exchange between the ER and mitochondria that are not connected to the vesicular transport pathway. This lipid transport is

bidirectional, in which mitochondria acquire sterols, PI, PS, and PC from the ER, and phosphatidylethanolamine (PE) synthesized in mitochondria is transported to the ER to support PC synthesis (Levine, 2004; Voelker, 1989). In addition, ER-TGN junctions have been shown to participate in lipid transport, including ceramide, glucosylceramide, PI4P and, sterol (De Matteis and D'Angelo, 2007; Hanada et al., 2003; Mesmin et al., 2013).

Non-vesicular lipid transport is mainly mediated by monomeric lipid exchange. This mechanism involves extraction of one lipid molecule from the outer leaflet of a donor membrane, diffusion across the aqueous cytosol, and then delivery to the outer leaflet of an acceptor membrane (Holthuis and Levine, 2005; Lev, 2010). Given that most lipid molecules are highly insoluble in water, this process is extremely slow, and usually takes hours or days to complete. In general, lipid molecules with higher hydrophobicity take longer to be transferred *in vitro* (Bai and Pagano, 1997). Lipid transfer proteins (LTPs) have been shown to facilitate this process. LTPs were first discovered as soluble factors that accelerate the transfer of lipid molecules between isolated mitochondria and microsome membranes (Wirtz and Zilversmit, 1968). To date, many LTPs have been identified in bacteria, in plants, and in eukaryotes. According to their lipid specificity, LTPs have been subdivided into different families, such as PITP (PI transport protein), Sec14 (functional homologs of PITP in yeast), and OSBP (oxysterol-binding protein)/ORP (OSBP-related protein) (D'Angelo et al., 2008). The ability of LTPs to accelerate lipid transport has been demonstrated in numerous studies *in vitro* using radiolabeled or fluorescent lipids (Lev, 2010). LTPs greatly facilitate lipid transfer up to several orders of magnitude possibly by increasing the rates of lipid desorption from donor membrane (Lalanne and Ponsin, 2000). This transfer could be further enhanced by decreasing the diffusion time if LTPs function at membranes in apposition or membrane junctions (Lev, 2010; Levine, 2004). This tempting hypothesis likely explains how lipids are distributed selectively and efficiently among different membrane compartments. However, the mechanisms of how LTPs mediate lipid transfer in the context of membrane junctions in intact cells remain to be determined.

Non-vesicular PI transport from the ER to the PM has been postulated for a long time. This PI transport is thought to encompass an important step for a recycling mechanism called PI cycle to support PIP_2 levels at the PM (Cockcroft and Garner, 2013; Michell, 1975). The PI cycle is initiated by receptor-induced PIP_2 hydrolysis at PM and the subsequent production of a lipid second messenger, diacylglycerol (DAG). DAG is rapidly phosphorylated and converted to phosphatidic acid (PA) by DAG kinase at PM. Next, PA at the PM is transferred to the ER through undetermined mechanisms to support PI synthesis. Although ER is capable of *de novo* synthesis of PA from glycerol-3-phosphate, inhibition of PA production at PM resulted in a reduced rate of PI resynthesis implying that PA transferred from the PM is required for PI cycle (Cockcroft and Garner, 2013). This idea is also supported by a recent report showing that a PITP called RdgBβ (PITPNC1) binds to PA, and is likely to facilitate PA transfer *in vitro* (Garner et al., 2012). Subsequently, PA in the ER is converted into CDP-DAG, the substrate of PI-synthase (PIS) for the synthesis of PI. This raised an obvious question of how the precursor lipid, PI, in the ER was being delivered to the PM to support PIP_2 levels. Therefore, non-vesicular PI transfer at ER-PM junctions was proposed to fill this elusive step of PI cycle. The only evidence that supports this idea was derived from the genetics studies of a protein called RdgBα in *Drosophila* photoreceptor. During photo-transduction, PIP_2 is hydrolyzed by light-activated PLC to generate IP_3 leading Ca^{2+} signaling. This activation cascade is similar to the receptor-induced Ca^{2+} signaling in mammalian cells. The replenishment of PIP_2 at PM is important to support further photo-transduction, since light stimuli constantly drive PIP_2 hydrolysis in photoreceptor cells. Flies lacking RdgBα, named after the phenotype, showed retinal degeneration and defective photo-transduction (Hotta and Benzer, 1970). RdgBα encodes a PITP that localized to subrhabdomeric cisternae (SRC), a specialized ER domain juxtaposed to the PM in photoreceptor cells (Trivedi and Padinjat, 2007). Therefore, SRC is considered to be ER-PM junctions in these cells. Further electrophysiological studies using Kir channels as a PIP_2 biosensor demonstrated defective PIP_2 replenishment following light exposure in the mutant photoreceptor cells (Harris and Stark, 1977). The defects in PIP_2 replenishment likely caused the phenotypes, because reconstitution of the N-terminal PTIP domain of RdgBα alone was sufficient to rescue the retinal degeneration and defects in light response in

mutant flies. This genetic data suggested that PI transfer via RdgBα at ER-PM junctions is important for PM PIP_2 levels to support photo-transduction.

The human genome contains five PITPs and can be grouped into two classes. PITPα and PITPβ are Class I PITPs that contain a single conserved PITP domain. The crystal structures of these proteins showed that PITPα and PITPβ contain a hydrophobic cavity that often is occupied by either PI or PC (Tilley et al., 2004; Vordtriede et al., 2005). This cavity is closed by a lid-like α-helix, and the phospholipid is completely buried in this cavity with the polar headgroup located at the far end of the lid. Four residues, T59, K61, E86, and N90, in the cavity make hydrogen bonds with the inositol headgroup of PI. These residues are conserved and are found in many, if not all, PITPs in animal cells (Tilley et al., 2004). Mutation of any one of these residues lead to defective PI binding and transfer (Cockcroft, 2012; de Brouwer et al., 2002). Class II PITPs contain RdgBβ (PITPNC1) and a Nir protein family, the mammalian orthologs of *Drosophila* RdgBα. RdgBβ only contains a PITP domain and has been recently reported to transfer PI and PA *in vitro* (Garner et al., 2012). Nirs are multi-domain containing proteins (Figure 1-4B). Nir2 and Nir3 (also PITPNM1 and PITPNM2, respectively) contain an N-terminal conserved PITP domain, a FFAT motif for VAPs binding (Amarilio et al., 2005), and C-terminal DDHD and LNS2 domains, while Nir1 (PITPNM3) lacks the N-terminal PITP domain. Ablation of Nir2 in mice exhibited embryonic lethality, indicating it is essential during development, whereas Nir3 knockout animals appeared completely normal (Lu et al., 2001). Nir2 has been reported to localize to the ER and the Golgi, and siRNA targeting Nir2 resulted in decreased DAG level and disorganized Golgi (Litvak et al., 2005). Reconstitution of Nir2 in flies lacking RdgBα fully rescued the retinal degeneration phenotype and defective photo-transduction (Chang et al., 1997). In addition, Nir2 can be targeted to PM via its LNS2 binding to PA, and positively regulates PIP_2 signaling at PM (Kim et al., 2013). In summary, Nir2 is essential for development and for many cellular functions. In addition, Nir2 harbors both ER and PM targeting motifs and is able to restore the phenotypes due to RdgBα deficiency. These observations implied a tempting hypothesis that Nir2 promotes PI transfer at ER-PM junctions. Given that the key

evidence of non-vesicular PI transfer remains undetermined, it would be of significance to investigate the cellular functions elicited by Nir2 and their underlying molecular mechanisms.

1.8 Dissertation Objectives

ER-PM junctions are membrane microdomains that have been shown to participate in many cellular processes, and thus the spatial-temporal regulation of ER-PM junctions will lead to prominent functional consequences. My dissertation work is dedicated to understand the dynamic regulation of ER-PM junctions in live cells. To achieve this, I first design and generate MAPPER, a genetically-encoded fluorescence marker for ER-PM junctions as illustrated in Chapter 2. MAPPER selectively labels ER-PM junctions in live cells without perturbing cellular functions. In Chapter 3, I describe the size, shape, and distribution of ER-PM junctions labeled by MAPPER. In Chapter 4 and Chapter 5, I demonstrate an enhanced ER-to-PM connection triggered by cytosolic Ca^{2+} levels and E-Syt1. This enhanced ER-to-PM connection facilitates Nir2 translocation to ER-PM junctions and subsequent PIP_2 replenishment at the PM as shown in Chapter 6. This work elucidates the mechanism of enhanced ER-to-PM connection during Ca^{2+} signaling, and further reveals the key evidence to support the idea of non-vesicular PI transfer at ER-PM junctions.

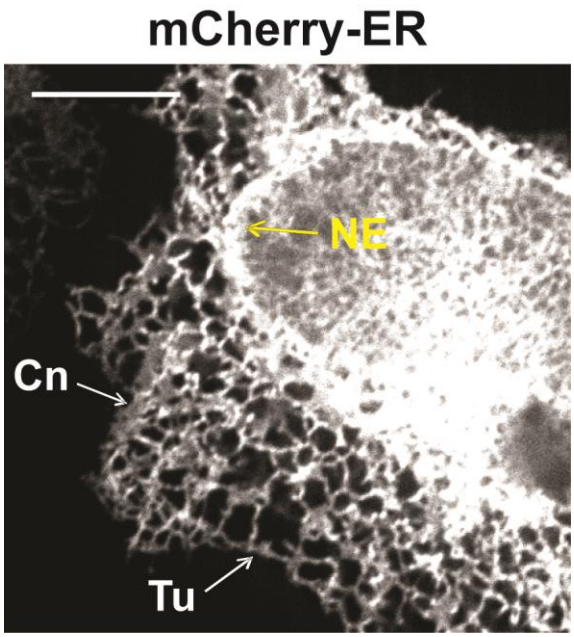

Figure 1-1. ER Subdomains in a HeLa cell.

A confocal image of a HeLa cell expressing mCherry tagged-ER luminal marker. NE: nuclear envelop; Cn: ER cisternae; Tu: ER tubules. Scale bar: 10 μm.

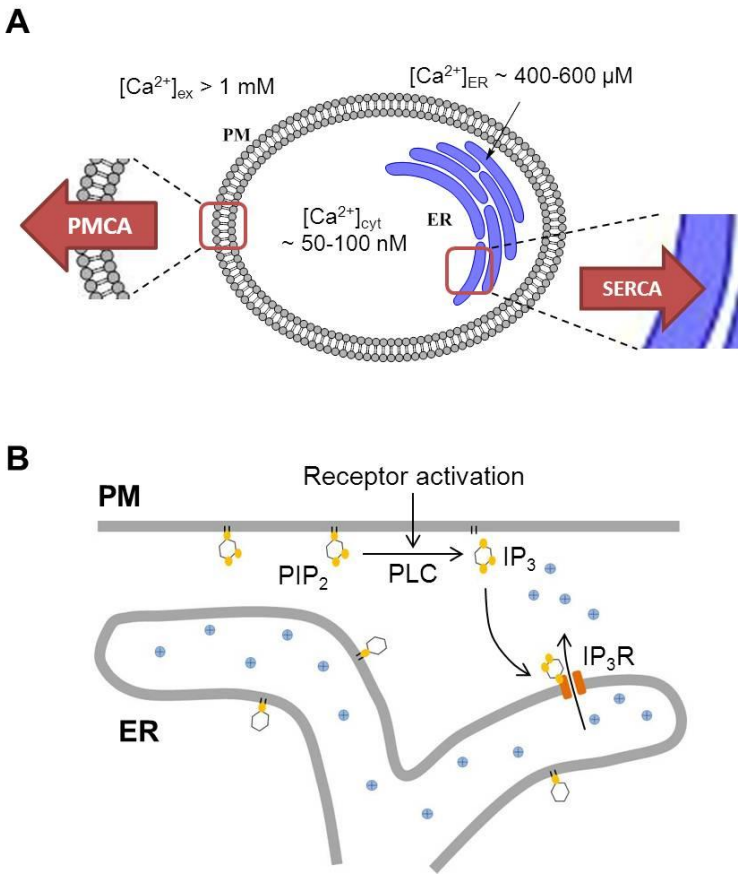

Figure 1-2. Regulation of Ca^{2+} Signaling.

(A) A diagram that depicts Ca^{2+} homeostasis in a cell during the resting state. SERCA, sarco/endoplasmic reticulum Ca^{2+}-ATPase; PMCA, plasma membrane Ca^{2+}-ATPase. Ca^{2+} concentration at different compartments is indicated,

(B) A diagram that depicts receptor-induced Ca^{2+} signaling. PIP_2, phosphatidylinositol 4,5-bisphosphate; PLC, phospholipase C; IP_3, inositol 1,4,5-triphosphate; IP_3R, IP_3 receptor.

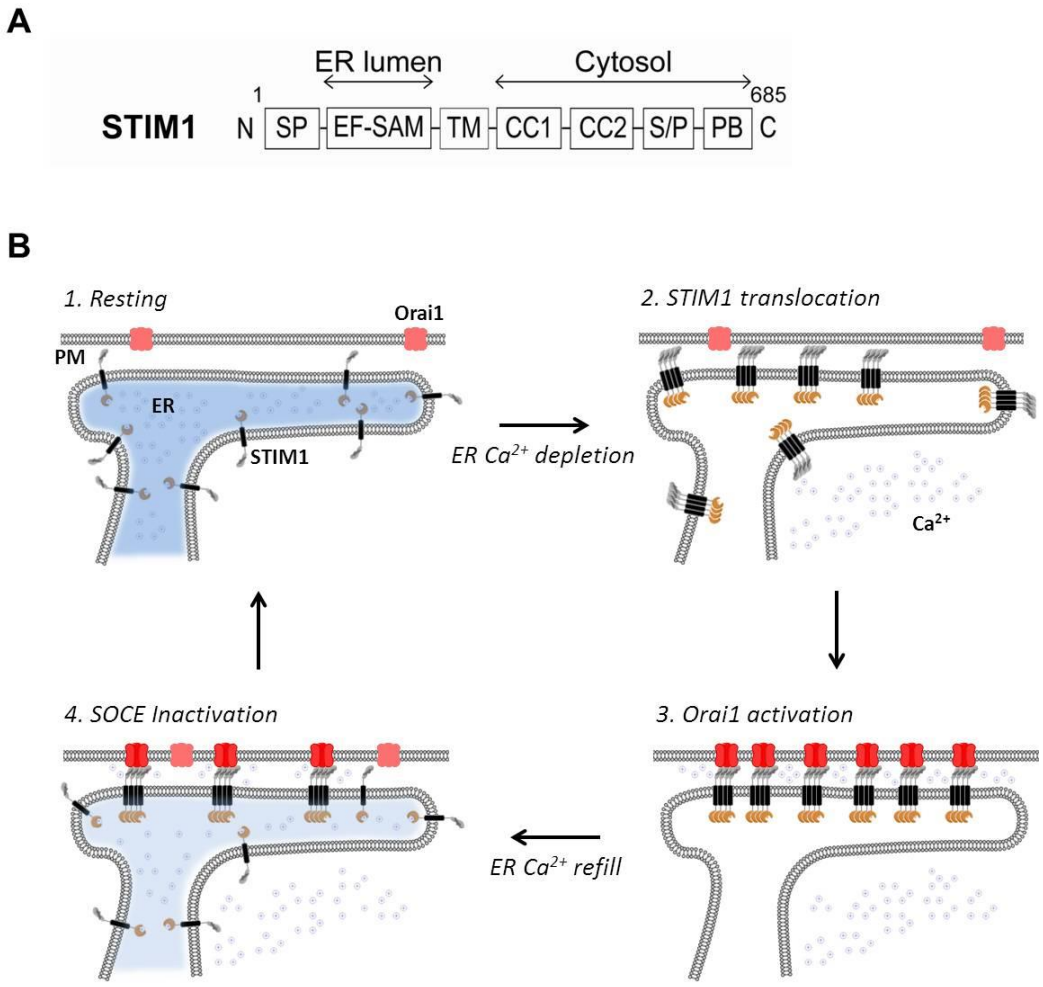

Figure 1-3. Activation of SOCE at ER-PM Junctions.

(A) Diagrams of STIM1. Amino acid numbers are indicated. SP, signal peptide; EF-SAM, EF hand and sterile alpha motif; TM, transmembrane; CC1 and CC2, coiled coil domain 1 and 2; S/P, serine and proline rich region; PB, polybasic.

(B) Summary of STIM1 activation Orai1 during SOCE at an ER-PM junction. ER Ca^{2+} levels are color coded in blue.

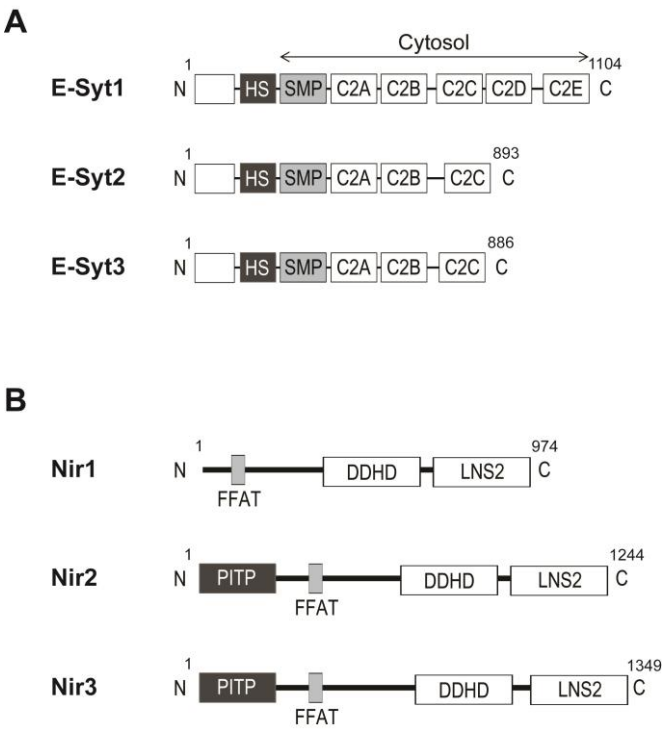

Figure 1-4. Structure of E-Syts and Nirs.

(A) Diagram of E-Syts. Amino acid numbers are indicated. HS, hydrophobic segment; SMP, synaptotagmin-like-mitochondrial-lipid binding protein; C2, C2 doamin.

(B) Diagram of Nirs. Amino acid numbers are indicated. FFAT, two phenylalanine in an acidic track; PITP, DDHD, and LNS2 domains are indicated.

Chapter 2

Visualization of ER-PM Junctions in Live Cells

2.1 Stable ER-PM Junctions Monitored by a Fluorescent ER Luminal Marker

The ER is an extensive and dynamic membrane network throughout the cytosol in animal cells. Statistically, the ER would be able to make random contacts with the PM in a giving period of time. Combined with the fact of low abundance of ER-PM junctions in animal cells, previous studies suggested that ER-PM junctions occur transiently in the resting state. The abundance of ER-PM junctions can be up-regulated by STIM1 or COPI dependent mechanisms in cells overexpressing STIM1 or an artificial ER-PM tether (Lavieu et al., 2010; Orci et al., 2009; Wu et al., 2006). However, the dynamic properties of endogenous ER-PM junctions have never been examined in live cells. I first tested whether stable ER-PM junctions can be observed by detecting ER regions closely associated to the PM in live, unstimulated cells. HeLa cells transfected with a YFP-tagged ER luminal marker (YFP-ER) were examined using total internal reflection fluorescence (TIRF) microscopy. TIRF microscopy technique selectively generates an evanescent field that only penetrates from the PM to the cytosol for approximate 100 nm (Steyer and Almers, 2001), and thus it is suitable to specifically detect the ER signals very close to the PM. As shown in the top panels of Figure 2-1, some bright punctate structures, in contrast to dim ER background, detected by the YFP-ER remained stable for more than 10 minutes (as indicated by arrows). To confirm that these stable ER puncta correspond to ER-PM junctions, a reversible translocation of STIM1 was induced by BHQ treatment, a reversible ER Ca^{2+} depleting agent (Liou et al., 2005). STIM1 translocated into puncta pre-labeled by YFP-ER when ER Ca^{2+} is depleted by BHQ (Figure 2-1, bottom panel). Notably, the same ER puncta remained stable after BHQ washout that reverted STIM1 translocation. These results demonstrate that stable ER-PM junctions indeed exist and could be tracked in live cells using YFP-ER in resting cells. In addition, the absence of STIM1 at ER-PM junctions before ER Ca^{2+} depletion and after BHQ washout suggested that these junctions are maintained by STIM1-independent

mechanisms. Nonetheless, detection of ER-PM junctions using YFP-ER requires taking a series of TIRF images to identify stable junctions, and signal at ER-PM junctions is obstructed by the background signal from the bulk of the ER. STIM1 translocation provides better signal at ER-PM junctions with minimal ER background, but this enrichment of STIM1 only occurs when ER Ca^{2+} is depleted, which activates Ca^{2+} signaling and eventually perturb cellular functions. Therefore, a neutral marker that selectively labels ER-PM junctions with minimal manipulation to cells is in need to study ER-PM junctions.

2.2 Generation of MAPPER

To selectively label and investigate the dynamic regulation of ER-PM junctions, a genetically encoded marker based on the subcellular targeting mechanisms of STIM1 was designed since it is the best understood protein that translocates to ER-PM junctions. In principle, both ER and PM targeting motifs are required for a protein to localize at ER-PM junctions. The targeting motif can be an integral transmembrane domain, a protein-protein interaction motif, or a protein-lipid binding motif. For example, STIM1 is an ER transmembrane protein and it translocates to ER-PM junctions is dependent on the C-terminal polybasic tail for inducible binding to PM (Figure 2-2A). Absence of the PM targeting polybasic tail abolished STIM1 translocation to ER-PM junctions (Liou et al., 2007). Based on this rationale, I first generated a construct containing the signal peptide (SP) and the transmembrane domain of STIM1 at the N and C termini, respectively, of a GFP. This SP-GFP-TM fusion protein containing only ER targeting motifs was localized to the ER (Figure 2-2B). Next, FRB domain was added after the transmembrane domain. The addition of FRB domain did not alter the ER localization (Figure 2-2C). The FRB domain may be used to recruit FKBP-fusion proteins using rapamycin or its analogs (Putyrski and Schultz, 2012). STIM1 targeting to ER-PM junctions requires ER Ca^{2+}-depletion to trigger oligomerization and a subsequent binding of the C-terminal polybasic motif to PIP_2 and PIP_3 at the PM (Ercan et al., 2009; Korzeniowski et al., 2009; Liou et al., 2007; Walsh et al., 2010). To enable a constitutive localization to ER-PM junctions, a stronger polybasic motif of the small G protein Rit, which binds to phosphoinositides in the PM (Heo et al., 2006), was added to the C terminus of the marker. In addition, several flexible and

helical linkers were engineered into the cytosolic portion of the marker to ensure that expression of the marker did not alter the gap distance of ER-PM junctions, which range from 10 to 25 nm based on EM studies of mammalian cells (Wu et al., 2006). This genetically encoded marker is named "MAPPER" for "*m*embrane-*a*ttached *p*eri*p*heral *ER*" (Figure 2-2A).

When MAPPER-transfected HeLa cells were examined using confocal microscopy, hundreds of bright puncta were observed near the adhesion surface of each cell (Figures 2-2D and 2-3A). Confocal midsections of MAPPER-transfected cells showed weak signals in the bulk of the ER and nuclear membrane and strong signals in puncta along the cell periphery (Figures 2-2E). When the localization of MAPPER and an ER luminal marker were examined at the bottom of the cells by confocal micorscopy, they appeared dramatically different (Figure 2-3A). Nonetheless, all puncta detected by MAPPER were overlaid with the ER marker indicating that MAPPER puncta are part of the ER. The overlay of MAPPER and the ER marker was better illustrated using TIRF microscopy (Figure 2-3B), in which MAPPER signals only colocalized with ER puncta but not the tubules at the background. These results indicate that MAPPER is an ER protein highly concentrated at ER-PM junctions similar to activated STIM1. Compared with the ER marker, MAPPER greatly enhanced the identification of ER-PM junctions with minimal background signal from the rest of the ER. EM was further applied to confirm the subcellular localization of MAPPER. Immunogold labeling using an antibody against GFP showed that MAPPER was highly enriched in regions closely apposed to the PM (Figure 2-3C). Moreover, a direct labeling of MAPPER by miniSOG, a genetically encoded tag for EM (Shu et al., 2011), resulted in moderate electron-dense signals in the ER network and strong signals in the ER regions juxtaposed to the PM (Figure 2-3D, top panel). In some huge ER-PM junctions generated by MAPPER, the strong electron-dense signals were only observed in the gap between the ER and PM but not in the ER membrane facing cytosol (Figure 2-2D, bottom panel). Together, these results demonstrate that MAPPER selectively labels ER-PM junctions in live and fixed cells as detected by various imaging approaches.

I further tested if MAPPER expression affects the functions of ER-PM junctions, such as STIM1 translocation and SOCE. Following ER Ca^{2+} depletion by TG, STIM1 was able to translocate into ER-PM junctions labeled by MAPPER (Figure 2-3E). Consistently, SOCE as measured by Ca^{2+} influx following ER Ca^{2+} depletion by TG and histamine was similar in MAPPER-transfected and in control-transfected cells (Figure 2-3F). This data demonstrated that MAPPER does not perturb the functions of ER-PM junctions. I also found that the density of ER-PM junctions detected by MAPPER was approximate 0.2 junctions per μm^2, similar to that detected by YFP-ER (Figure 2-3G) indicating that MAPPER does not create ER-PM junctions. Because the average adherent surface area of HeLa cells is approximate 1000 μm^2, the density of 0.2 means that there are 200 ER-PM junctions at the bottom of a HeLa cell. In summary, these results indicate that MAPPER selectively labels ER-PM junctions with minimal perturbations to cells. Therefore, MAPPER is suitable for investigating the regulation and functions of ER-PM junctions in live cells.

The EM work presented in this chapter was performed in collaboration with Karen Rothberg, Ph.D. in the Live Cell Imaging Core Facility, UTSW.

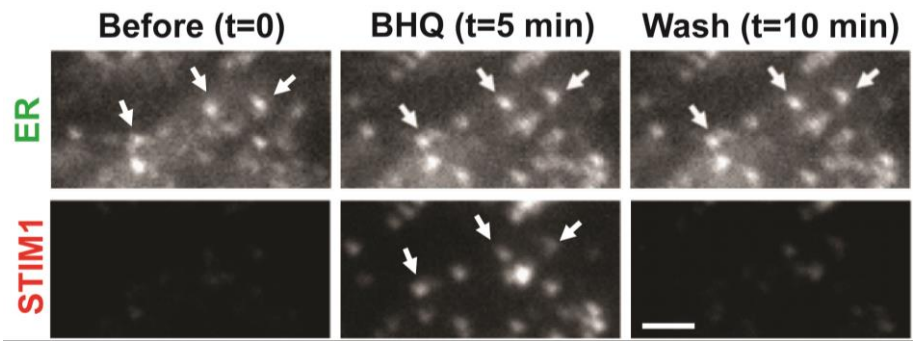

Figure 2-1. Stable ER-PM Junctions Labeled by an ER Marker.

TIRF images of a HeLa cell coexpression with YFP-ER (top) and mCherry-STIM1 (bottom). Arrows indicate stable ER-PM junctions that STIM1 reversibly translocated into during 5 μM BHQ treatment and washout. Scale bar: 2 μm.

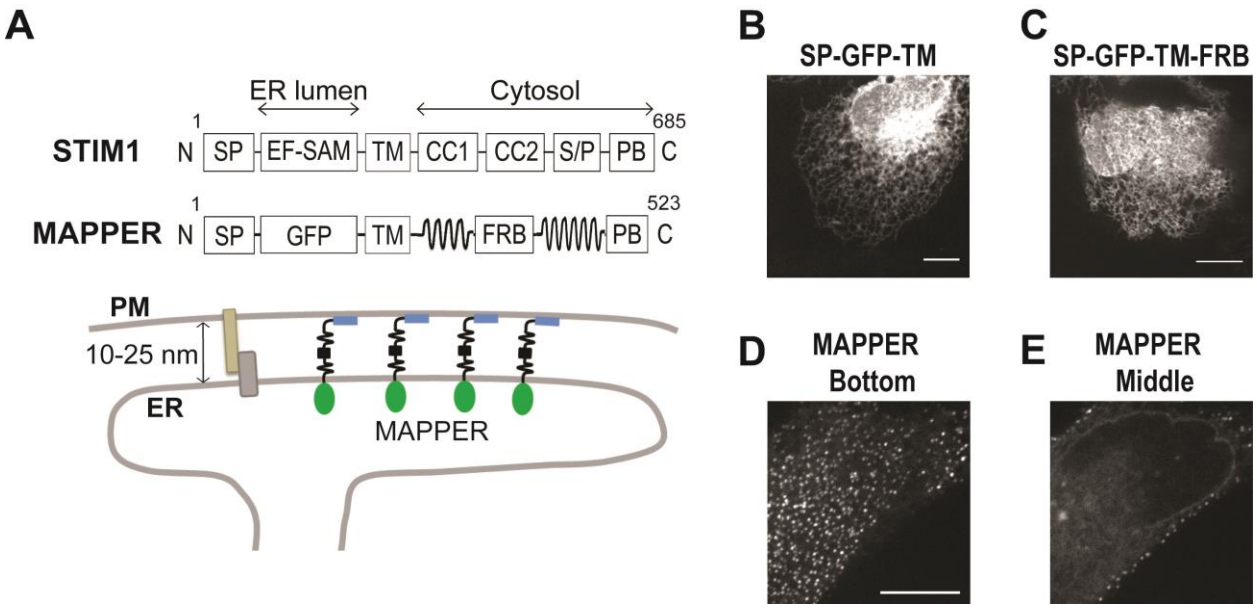

Figure 2-2. Localization of SP-GFP-TM, SP-GFP-TM-FRB, and MAPPER.

(A) Diagrams of STIM1 (top) and MAPPER (middle) and a schematic depicting the expected localization of MAPPER at ER-PM junctions maintained by unknown structural components (bottom). Amino acid numbers are indicated. SP, signal peptide; EF-SAM, EF hand and sterile alpha motif; TM, transmembrane; CC1 and CC2, coiled coil domain 1 and 2; S/P, serine and proline rich region; PB, polybasic; FRB, FKBP12-rapamycin binding.

(B and C) Confocal images of HeLa cells transfected with SP-GFP-TM (B) or SP-GFP-TM-FRB (C). Scale bar, 10 μm.

(D and E) Confocal images of the bottom (D) and middle (E) sections of a MAPPER-expressing HeLa cell. Scale bar: 10 μm.

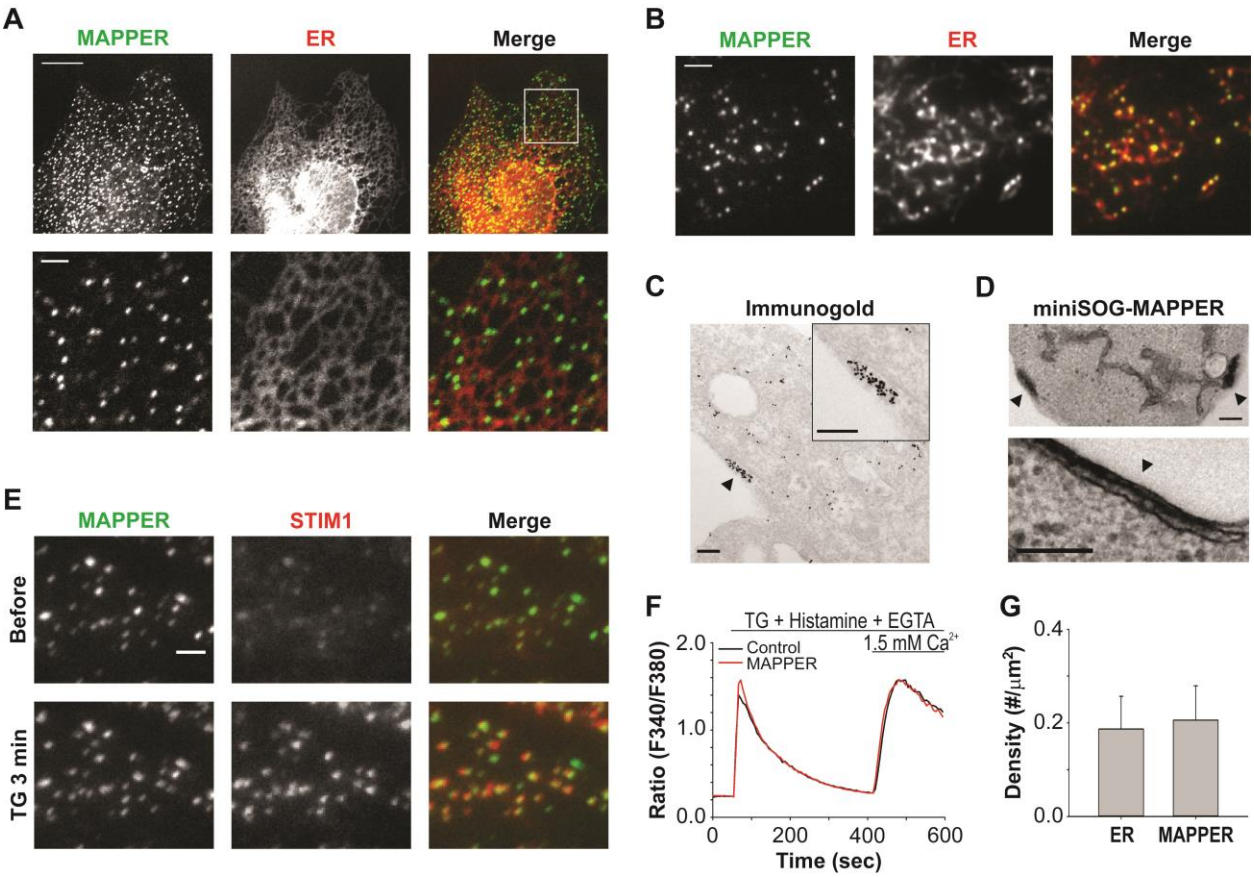

Figure 2-3. MAPPER Selectively Labels ER-PM Junctions.

(A) (Top panels) Bottom-section confocal images of a HeLa cell coexpressing MAPPER and mCherry-ER. The scale bar represents 10 μm. (Bottom panels) Magnified images. The scale bar represents 2 μm.

(B) TIRF images of a HeLa cell coexpressing MAPPER and mCherry-ER. The scale bar represents 2 μm.

(C and D) Ultrastructural analysis of MAPPER localization by EM. (C) Immunogold staining of a MAPPER-transfected cell. The scale bar represents 200 nm. (D) EM image of a HeLa cell transfected with miniSOG-tagged MAPPER. Arrowheads indicate ER-PM junctions. The scale bar represents 200 nm.

(E) STIM1 translocation induced by 1 μM TG monitored by TIRF microscopy in a HeLa cell coexpressing MAPPER and mCherry-STIM1. The scale bar represents 2 μm.

(F) SOC entry triggered by 1 μM TG and 100 μM histamine in control (SP-GFP-TM) or MAPPER-transfected HeLa cells. Shown are average traces derived from more than 90 cells.

(G) Density of ER-PM junctions labeled by the ER marker or MAPPER in HeLa cells monitored by TIRF microscopy. Mean ± SD is shown (26 cells from three independent experiments).

Chapter 3

Characterization of ER-PM Junctions by MAPPER

3.1 Characterization of ER-PM Junctions Labeled by MAPPER using Super-Resolution Imaging

The structural details of ER-PM junctions were mostly examined using EM in previous studies. Although EM provided the ultimate resolution in measuring the length and the gap distance of ER-PM junctions, it is difficult to reconstruct the membrane contact area and shape of ER-PM junctions in two dimensions. Based on the EM studies, the length of ER-PM junctions is in the range of 200 nm, which is slightly under the resolution of TIRF microscopy of ~250 nm as determined by the diffraction limit of light. Therefore, I applied super-resolution imaging technique to determine the area and shape of single ER-PM junctions labeled by MAPPER. The high labeling density of MAPPER at ER-PM junctions makes it ideal for photo-activated localization microscopy (PALM). During PALM imaging process, only a sparse subset of fluorophores are activated and imaged at a given time; therefore, the high-precision localizations of these fluorophores can be determined under the resolution of diffraction limit. After sufficient number of fluorophores being imaged, a super-resolution image can be reconstructed from the localizations (Betzig et al., 2006; Rust et al., 2006). For PALM imaging, the GFP tag in MAPPER was replaced with mEos4h, a photo-convertible fluorescent protein that was developed recently based on mEos2 (McKinney et al., 2009). When mEos4h-MAPPER-transfected cells were examined using TIRF microscopy, individual ER-PM junctions were observed with moderate variations in area and in intensity (Figure 3-1A, TIRFM). Strikingly, when the same region of the cell was imaged using PALM, single ER-PM junctions appeared very similar in area (Figure 3-1A, PALM). The boundary of single ER-PM junctions became clearly visible and adjacent junctions were separated (Figure 3-1A, inset 2). Analysis of the PALM images showed that the average area of single ER-PM junctions was 31,718 ± 115 nm^2 (Figure 3-1B). Single ER-PM junctions appeared to have slightly elongated shape (Figure 3-1A, zoom images). To further define ER-PM junctions, the length of their long and short axes was measured. The average

length of the long axis of single ER-PM junctions is 255.5 ± 79.8 nm (Figure 3-1C). Intriguingly, the short axis of ER-PM junctions is remarkably uniform at 157.7 nm ± 26.1 nm (Figure 3-1D). The average aspect ratio of single ER-PM junctions is 1.659 ± 0.625 (Figure 3-1E), consistent with the slightly elongated shape of single junctions observed in Figure 3-1A. The length of both axes was consistent to the length measured by EM in previous studies. With the precise area of ER-PM junctions measured by PALM microscopy (Figure 3-1B) combined with the density shown in Figure 2-3G, the PM area covered by ER-PM junctions was estimated to be 0.65%. This coverage is consistent with other reports which demonstrated the low abundance of ER-PM junctions in HeLa cells (Giordano et al., 2013; Orci et al., 2009). Together, PALM super-resolution imaging results revealed the area and shape of ER-PM junctions.

3.2 Distribution of ER-PM Junctions

ER-PM junctions were preferentially distributed in the animal hemisphere in *Xenopus* eggs and basal-lateral membranes of other animal cells suggested that occurrence of ER-PM junctions is not random (Gardiner and Grey, 1983; Lur et al., 2009; Orci et al., 2009). If a bigger region of MAPPER-expressing cells was examined by TIRF or PALM imaging, streaks of ER-PM junctions were often observed (Figure 3-2A). Notably, the distance between the ER-PM junctions in streaks seemed to be uniform. To understand the distribution of ER-PM junctions labeled by MAPPER, the distance to nearest neighbor of individual junctions was first determined using PALM super-resolution imaging. More accurate positions of individual ER-PM junctions can be obtained with this imaging technique. Remarkably, the distance to nearest neighbor derived from one PALM image of total 95 ER-PM junctions showed a multi-modal distribution. The smallest mode center is approximate 600 nm, and adjacent centers are separate by about 300 nm (Figure 3-2B). Further modal analysis of the distance to nearest neighbor from total 956 ER-PM junctions pooled from eight PALM images decomposed the population into four modes and each mode center represented multiplied minimal distance of 319 nm (Table 1). The smallest center of 619 nm (2X) and the second smallest center of 925 nm (3X) comprised most of the population, while the two largest centers of 1325 (4X) and 2218 (7X) combined only occupied 30%.

These findings suggest that individual ER-PM junctions are separate periodically by set distances of multiplied of approximate 300 nm. To further obtain the distribution of ER-PM junctions from the distance to nearest neighbor, an algorithm described by Clark and Evans population distribution was applied (Clark and Evans, 1954). This algorithm outputs the distribution as an R value, which measures the degree deviating from random distribution with an R = 1. R values derived from nearest distance to neighbor were greater than 1 from all eight PALM images (Table 2), indicating a more uniform distribution of ER-PM junctions rather than random scattering. This result also implicated the undetermined regulatory mechanisms contributing to the distribution of ER-PM junctions.

Multi-modal distribution of the distance to nearest neighbor and uniform area of individual ER-PM junctions served as a reminder of the organization of the cortical actin network underneath the PM. This network is often arranged as mesh-like structures with relatively uniform area and shape (Morone et al., 2006). To test the hypothesis of whether cortical cytoskeleton defines the organization ER-PM junctions, cytochalasin D (CytD) that abolishes the dynamic properties of actin was applied to MAPPER-expressing cells (Fenteany and Zhu, 2003). Disruption of actin by 10 μM CytD treatment led to a drastic lateral movement of several ER-PM junctions (Figure 3-3A, as indicated by numbers). In contrast, ER-PM junctions remained stable in cells treated with 10 μM nocadazole (NocZ) to disassemble microtubules, which is less involved in the formation of cortical cytoskeletal network (Figure 3-3B). These results suggest that cortical actin network may provide physical barriers contributing to the distribution and stability of ER-PM junctions.

The work presented in this chapter was performed in collaboration with a current graduate student in the Liou lab, Ting-Sung Hsieh.

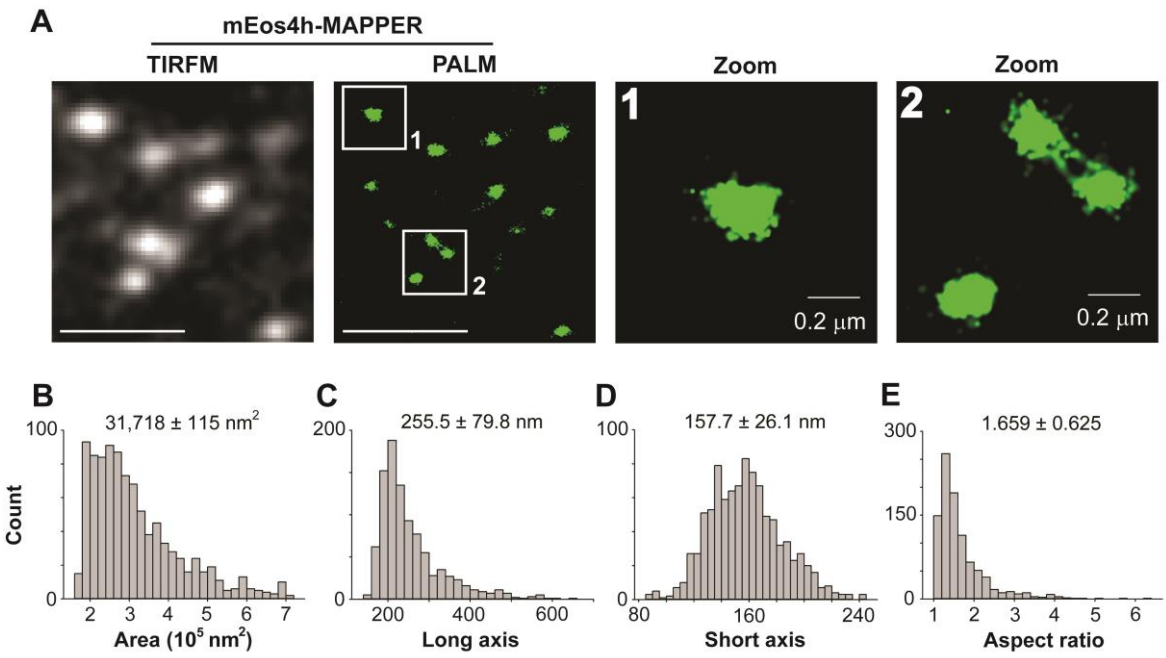

Figure 3-1. Characterization of ER-PM Junctions by Super-Resolution PALM Imaging.

(A) HeLa cells were transfected with mEos4h-tagged MAPPER. TIRFM and PALM images of the same regions were obtained using Nikon N-STORM (left and middle left). Scale bar: 2 μm. Magnified images (middle right and right) reveal the shape of individual junctions in two dimensions.

(B-E) Histograms of area (B), long axis (C), short axis (D) and aspect ratio (E) were derived from PALM images as described in Methods. Total of 956 junctions from seven PALM images were analyzed. Mean ± SD of each category are shown on the top in (B-E).

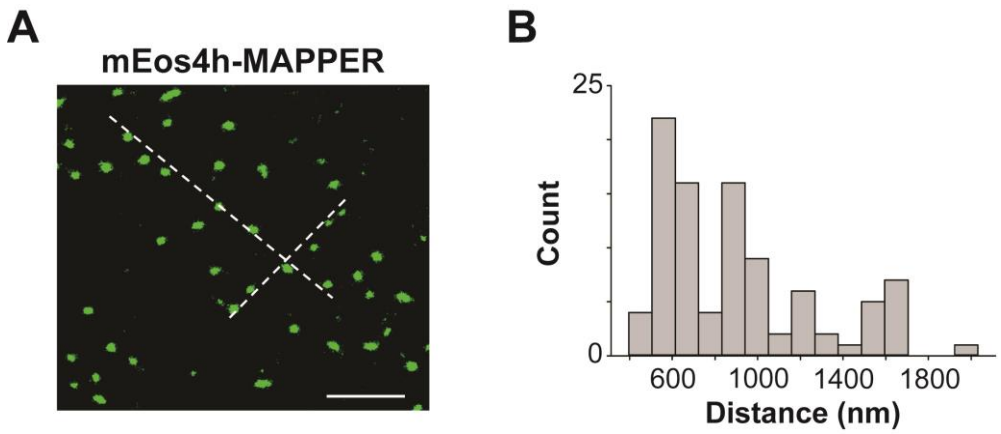

Figure 3-2. Distribution of ER-PM Junctions.

(A) A representative PALM image of mEos4h-MAPPER expressing HeLa cells obtained using Nikon N-STORM. Dashed lines indicate the streaks of ER-PM junctions. Scale bar: 2 μm.

(B) The histogram of distance to nearest neighbor of individual ER-PM junctions labeled by mEos4h-MAPPER. Data derived from 95 ER-PM junctions of one images is shown.

Table 1. Multi-Modal Distribution of Distance to Nearest Neighbor

Mode Center (nm)	Fold to Minimal of 319 nm	Fraction
619	2X	35%
925	3X	35%
1326	4X	23.5%
2218	7X	6.5%

Table 2. R Value Derived from Distance to Nearest Neighbor

Image Name	R Value
C1-1	1.1272
C2-1	1.2477
C2-3	1.2248
C4-1	1.1235
C4-2	1.2249
C6-1	1.1964
C7-1	1.1564
C7-2	1.3919

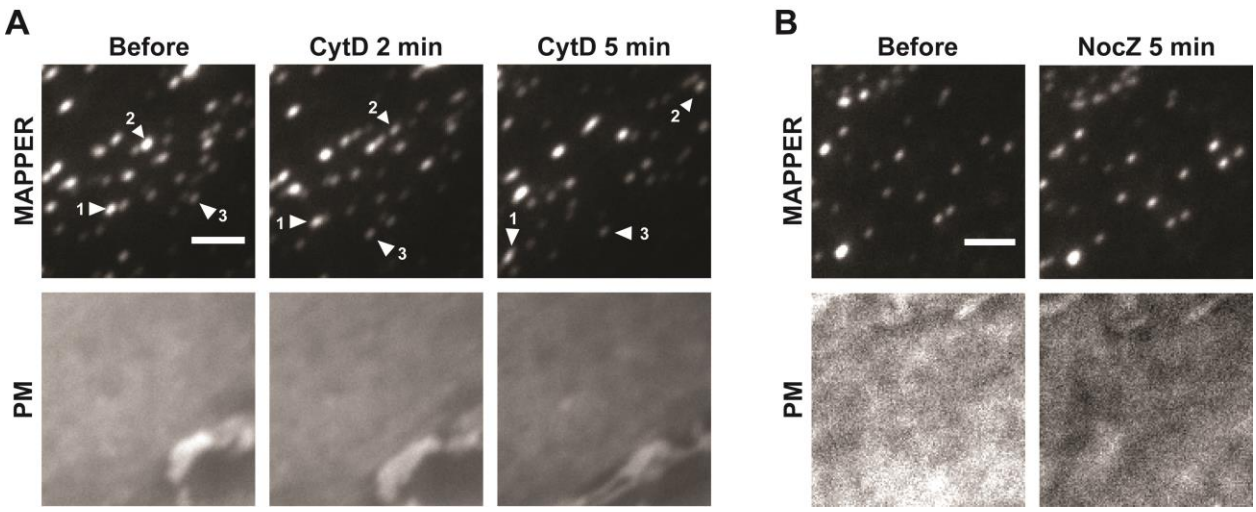

Figure 3-3. Dynamic Movement of ER-PM Junctions.

(A and B) Dynamic movement of ER-PM junctions monitored by TIRF microscopy in MAPPER-expressing HeLa cells transfected with a PM marker treated with 10 μM CytD (A) and 10 μM NocZ (B). Numbers in (A) indicate identical ER-PM junctions in different imaging time points. The scale bar represents 2 μm.

Chapter 4

Enhanced ER-to-PM Connection during Ca^{2+} Signaling

4.1 Dynamic Regulation of ER-PM Junctions Following TG Treatment

Since ER-PM junctions are the spatial platform for Ca^{2+} signaling and lipid metabolism, regulation of ER-PM junctions are likely to exert profound effects on these cellular functions. Previous EM studies showed that TG treatment increased the percentage of the PM in close contact with the ER in HeLa and Jurkat cells, suggesting that ER-to-PM connection can be regulated during Ca^{2+} signaling (Orci et al., 2009; Wu et al., 2006). To first confirm these observations are reproducible in live cells, I applied MAPPER to examine the dynamic regulation of ER-PM junctions and detected a marked increase in MAPPER signal following TG treatment using TIRF microscopy (Figure 4-1A). Similar increases in MAPPER signal were found in cells treated with histamine (Figure 4-1D), which stimulates G-protein-coupled histamine receptors and activates Ca^{2+} signaling. The increased MAPPER signal was not a result of cell movement or a focus drift, because no increase was detected by the PM marker cotransfected into the same cells (Figures 4-1A and 4-1D). Further analysis revealed a significant increase in density of ER-PM junctions detected by MAPPER from 0.21 to 0.27 following TG treatment (Figure 4-1B), indicating that new junctions are formed during Ca^{2+} signaling. Interestingly, a significant 1.9-fold increase in intensity of preexisting ER-PM junctions was also detected following TG treatment (Figure 4-1C). The increase in density and intensity of ER-PM junctions was not solely caused by MAPPER expression or an increased recruitment of MAPPER to ER-PM junctions via its PM targeting motif because similar increase of ER-PM junctions labeled by YFP-ER was also detected by TIRF microscopy after TG treatment (Figure 4-1E).

The other possible cause of the increase in intensity of MAPPER is an increase in area of single ER-PM junctions. To test this idea, I further applied PALM super-resolution microscopy to measure the area

of ER-PM junctions labeled by mEos4h-MAPPER. As shown in Figure 4-2A, area and shape of ER-PM junctions appeared to be similar in both untreated and TG-treated cells. Further analysis of more than 400 single ER-PM junctions in each sample showed no significant change in junctional area (Figure 4-2B). PALM imaging process often takes minutes to acquire sufficient images to reconstruct single ER-PM junctions. Therefore, live-cell imaging using PALM is technically difficult. To track TG-induced changes in single ER-PM junctions in live cells, stimulated emission depletion (STED) super-resolution imaging technique with faster acquisition time was employed (Willig et al., 2006). I found that the area and shape of the same ER-PM junctions labeled by MAPPER remained similar before and after TG treatment (Figures 4-2C and 4-2D). Of notice, an increase in intensity was also observed in most of the ER-PM junctions imaged by live-cell STED microscopy (Figure 4-2C). The lengths of the long and short axes of individual ER-PM junctions were further quantified by performing double Gaussian fitting (Figure 4-2E). Before TG treatment, the long and short axes were 272.7 ± 49.5 nm and 176.1 ± 22.5 nm, respectively (Figure 4-2F), comparable to those obtained from PALM imaging (Figures 3-1C and 3-1D). No significant changes were detected following TG treatment (Figure 4-2F). These results suggest that the area and shape of ER-PM junctions remained constant during Ca^{2+} signaling.

TIRF microscopy technique generates an evanescent field that only penetrates from the PM to the cytosol for approximate 100 nm. The intensity of this evanescent field decays exponentially with the distance from the interface, which makes TIRF extremely sensitive to changes in distance between a fluorescent protein and the PM (Steyer and Almers, 2001). MAPPER contains a GFP in the ER lumen away from the PM, and several flexible linkers in its cytosolic portion which can be extended or bent to fit into ER-PM junctions with different gap distance from 10 to 25 nm (Wu et al., 2006). Therefore, it is plausible to hypothesize that the intensity increase induced by TG results from a decrease in gap distance of ER-PM junctions. To test this hypothesis, I generated MAPPER-s, which contains a shorter cytosolic region than MAPPER. Thus, MAPPER-s is likely to restrict the range of gap distance of labeled ER-PM junctions to approximate 10 nm or less (Figure 4-3A). Following TG stimulation, an increase in density

of MAPPER-s-labeled ER-PM junctions similar to that in MAPPER-transfected cells was observed (Figures 4-3B and 4-3C). However, intensity of MAPPER-s-labeled ER-PM junctions appeared to remain similar during TG treatment (Figure 4-3B). Further analysis showed that TG-induced increase in MAPPER-s-labeled ER-PM junctions was significantly less than in MAPPER-labeled junctions (Figures 4-3D and 4-1C). These results suggested that the TG-induced increase in MAPPER intensity reflects a decrease in gap distance of ER-PM junctions. To directly measure the gap distance, ER-PM junctions labeled by MAPPER and MAPPER-s were examined by conventional EM using post-staining methods. In MAPPER expressing cells, a marked decrease in average gap distance from 12.09 to 9.47 nm was observed following TG/Histamine treatment (Figure 4-3E). Notably, the gap distance measured in MAPPER-s transfected cells was 9.05 nm at basal indicating that MAPPER-s indeed restricted ER-PM junctions as expected (Figure 4-3E). Also, further decrease in the gap distance following stimulus was observed in MAPPER-s transfected cells (Figure 4-3E). Altogether, this data suggest that treatment with either TG or histamine induces an enhanced ER-to-PM connection by triggering new junction formation and by shortening the gap between the ER and the PM.

4.2 Elevation of Cytosolic Ca^{2+} Is Sufficient to Enhance the Connection between the ER and the PM

To dissect the molecular mechanisms underlying the enhanced ER-to-PM connection following TG or histamine treatment, I first tested whether an increase in cytosolic Ca^{2+} was required for the enhanced connection. I found that TG-induced increase in density and intensity of MAPPER-labeled ER-PM junctions was abolished in cells preloaded with BAPTA, a cytosolic Ca^{2+} chelator (phase I and II; Figures 4-4A to 4-4D). When 10 mM Ca^{2+} was added to cells to overcome chelation by BAPTA, an elevation in cytosolic Ca^{2+} was accompanied by a robust increase in intensity and density of ER-PM junctions (phase III and IV; Figures 4-4A to 4-4D). These results demonstrate that the enhanced ER-to-PM connection induced by TG is dependent on an increase in cytosolic Ca^{2+}. Notably, exogenous STIM1 translocation in BAPTA-AM-loaded cells did not enhance ER-to-PM connection, suggesting that neither ER Ca^{2+} depletion nor STIM1 translocation is sufficient for the enhanced ER-to-PM connection induced by TG

(Figure 4-4E). In addition, enhanced ER-to-PM connection following TG treatment was still observed in STIM1 knockdown cells with abolished SOCE (Figures 4-4F and 4-4G), indicating that endogenous STIM1 and SOCE were not necessary for TG-mediated enhanced ER-to-PM connection. In summary, these results suggested that elevation of cytosolic Ca^{2+} levels is the key to trigger the enhanced ER-to-PM connection.

I then tested whether an increase in cytosolic Ca^{2+} alone was sufficient to promote ER-to-PM connection. Cells were cotransfected with MAPPER and R-GECO1, a genetically encoded Ca^{2+} indicator (Zhao et al., 2011), and loaded with NP-EGTA, a photolabile Ca^{2+} chelator. Photolysis of NP-EGTA by UV illumination resulted in a transient but robust increase in cytosolic Ca^{2+} as indicated by changes in intensity of R-GECO1 (Figures 4-5A and 4-5B). A dynamic increase with similar kinetics in intensity of MAPPER-labeled ER-PM junctions was also observed (Figures 4-5A and 4-5C). Increase in MAPPER intensity peaked with maximal cytosolic Ca^{2+} level at 2 min, and the intensity dropped significantly accompanied with a decrease in cytosolic Ca^{2+} level at 5 min. These results indicate that the connection between the ER and the PM is dynamically controlled by cytosolic Ca^{2+} levels, and implied the existence of a cytosolic Ca^{2+} sensor for the enhanced ER-to-PM connection.

The PALM image analysis in this chapter was performed in collaboration with a current graduate student in the Liou lab, Ting-Sung Hsieh.

The live cell STED imaging work presented in this chapter was performed in collaboration with Jung-Chi Lia, Ph.D. at Columbia University.

The EM work presented in this chapter was performed in collaboration with Karen Rothberg, Ph.D. in the Live Cell Imaging Core Facility, UTSW.

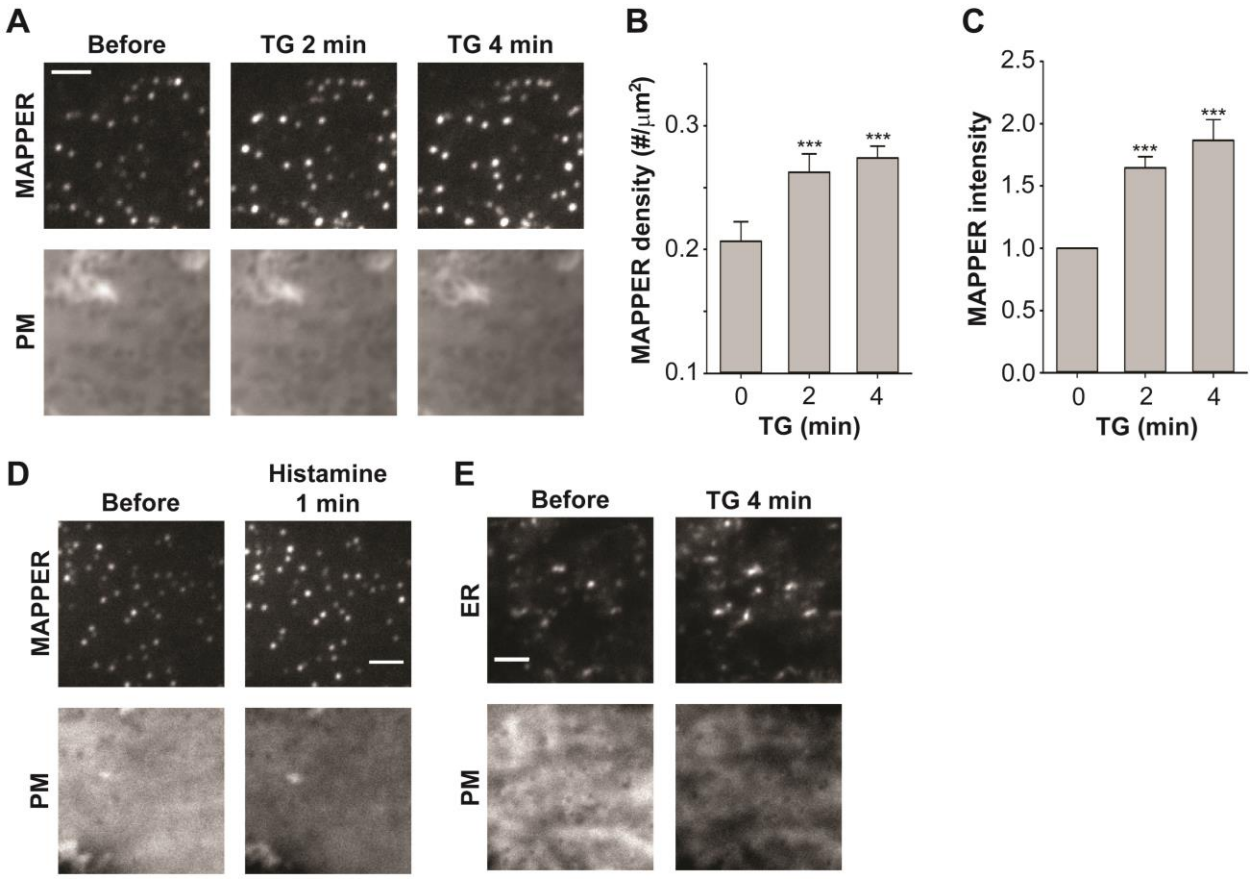

Figure 4-1. Enhanced ER-to-PM Connection Following TG Treatment.

(A) Dynamic changes in ER-PM junctions induced by 1 μM TG monitored by TIRF microscopy in MAPPER-expressing HeLa cells transfected with a PM marker. The scale bar represents 2 μm.

(B and C) Quantification of the dynamic changes in density (B) and intensity (C) of ER-PM junctions monitored as described in (A). Mean ± SD is shown (three to eight cells from at least three independent experiments). The triple asterisks denote $p < 0.001$.

(D) Dynamic changes in ER-PM junctions induced by 100 μM histamine monitored by TIRF microscopy in MAPPER-expressing HeLa cells transfected with a PM marker. Scale bar, 2 μm.

(E) Dynamic changes in ER-PM junctions induced by 1 μM TG monitored by TIRF microscopy in HeLa cells transfected with an ER marker and a PM marker. Scale bar, 2 μm.

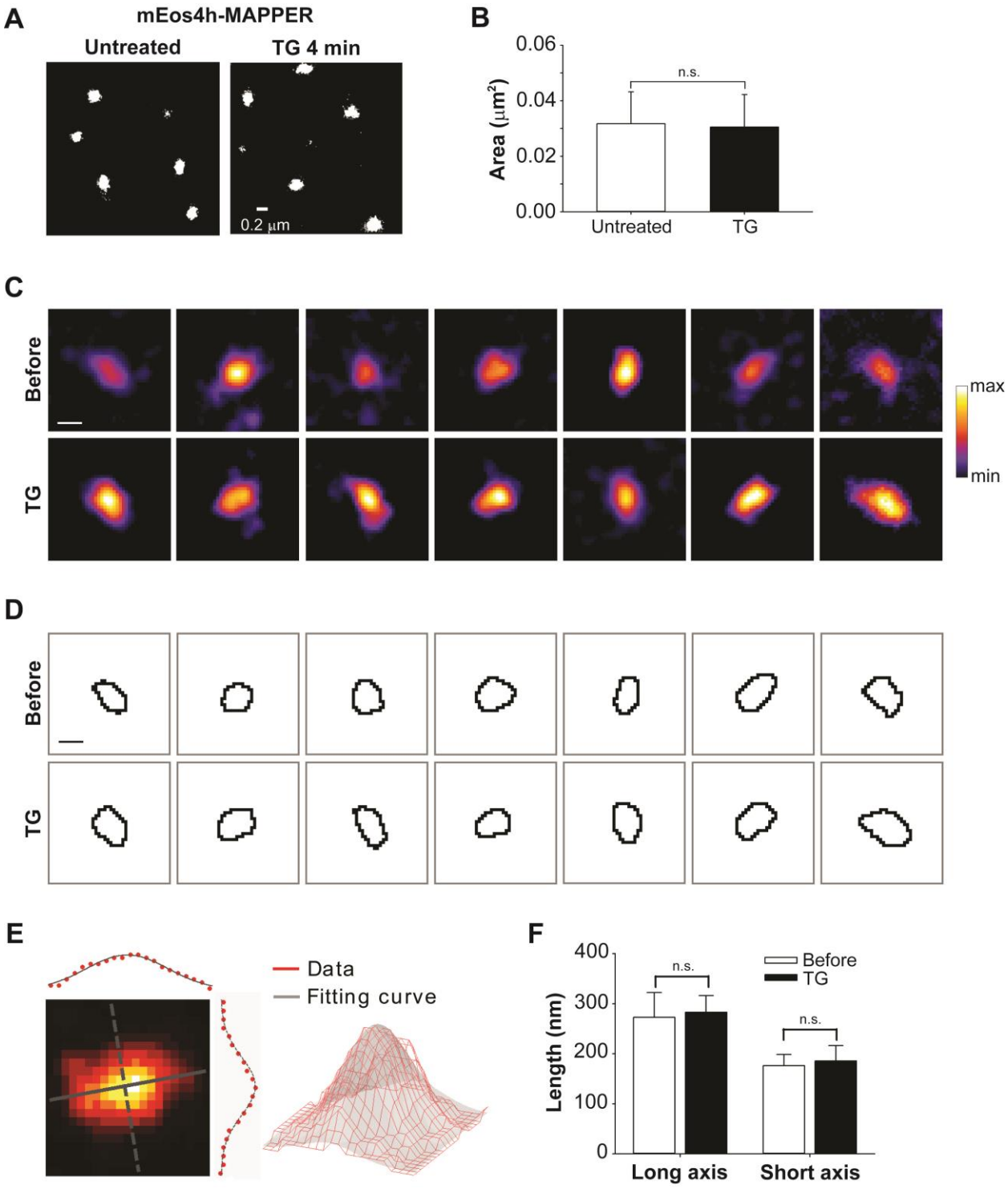
A
mEos4h-MAPPER
Untreated
TG 4 min
0.2 μm
B
Area (μm²)
0.06
0.04
0.02
0.00
n.s.
Untreated
TG
C
Before
TG
max
min
D
Before
TG
E
Data
Fitting curve
F
Length (nm)
400
300
200
100
0
n.s.
n.s.
Before
TG
Long axis
Short axis

Figure 4-2. The Area and Shape of ER-PM Junctions Remains Unchanged Following TG Treatment Monitored by Super-Resolution PALM and STED Imaging.

(A) Representative PALM images of untreated or TG-treated mEos4h-MAPPER transfected HeLa cells.

(B) Area of individual junctions was analyzed from PALM images of seven untreated samples (total 956 junctions) and six TG-treated samples (total 428 junctions), respectively. Mean ± SD are shown.

(C) Live-cell STED images of seven representative ER-PM junctions in MAPPER-expressing HeLa cells taken before and 5 minutes after TG treatment. Scale bar, 200 nm.

(D) The contours of half maxima for the corresponding regions in (C) illustrating the sizes and shapes of these representative ER-PM junctions before and after TG treatment. Scale bar, 200 nm.

(E) A representative illustration of double-Gaussian fitting employed to obtain the principal axes and to quantify the axis lengths of an ER-PM junction.

(F) Average lengths of long and short axes obtained from 16 ER-PM junctions in two independent live-cell STED imaging experiments. Mean ± SD are shown.

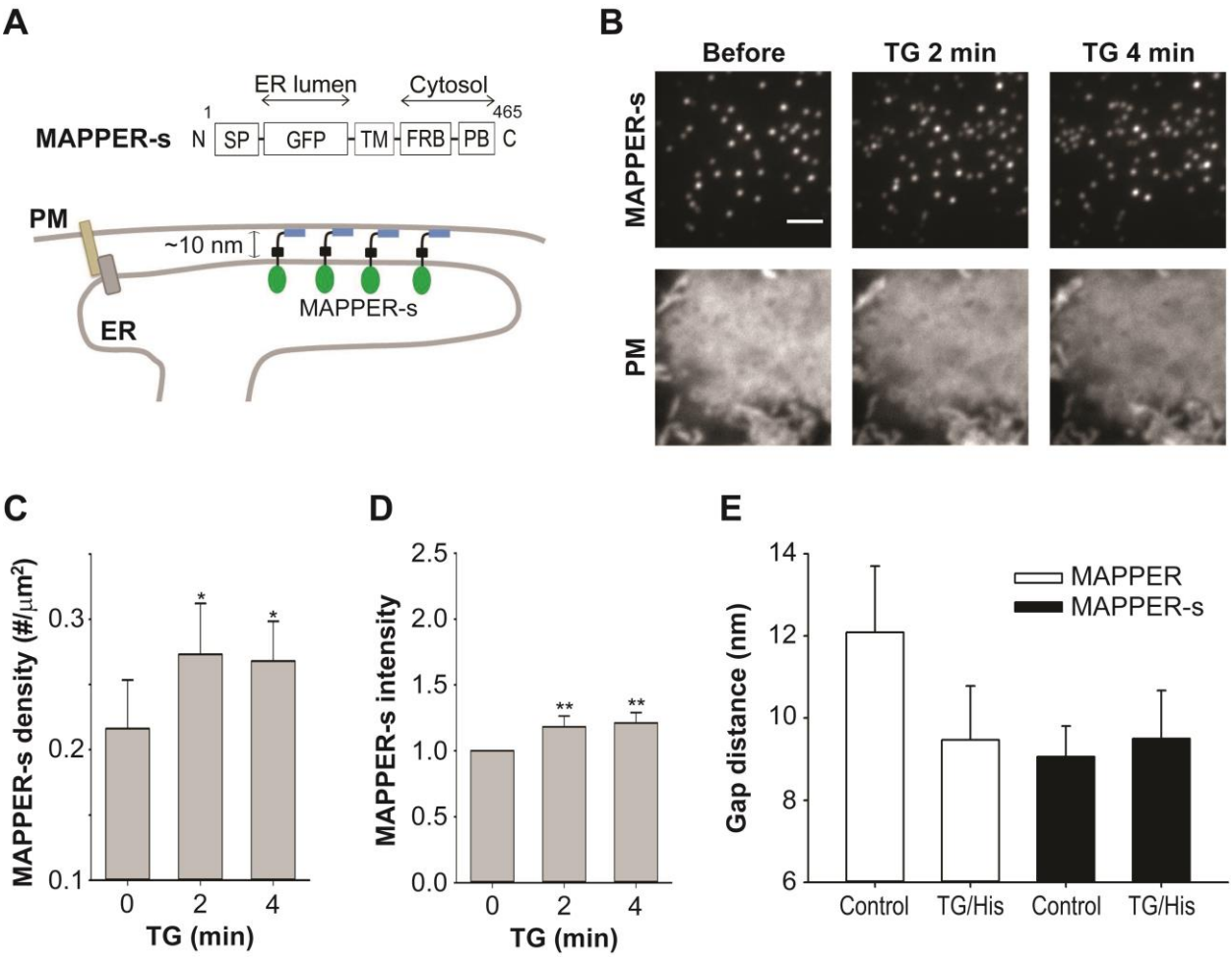

Figure 4-3. Decrease in Gap Distance of ER-PM Junctions during Ca^{2+} Signaling.

(A) Diagram of MAPPER-s (top) and a schematic depicting how MAPPER-s restricts the gap distance of labeled ER-PM junctions (bottom).

(B) Dynamic change of ER-PM junctions induced by 1 μM TG monitored by TIRF microscopy in HeLa cells co-transfected with MAPPER-s and a PM marker. Scale bar, 2 μm.

(C and D) Quantification of the dynamic changes in density (C) and intensity (E) of ER-PM junctions induced by 1 μM TG monitored by TIRF microscopy in HeLa cells transfected with MAPPER-s. Mean ± SD is shown (four to six cells from two independent experiments). The asterisk denotes $p < 0.05$ and double asterisks denote $p < 0.01$.

(E) Gap distance of ER-PM junctions labeled by MAPPER or MAPPER-s induced by 1 μM TG and 100 μM histamine measured by EM. Mean ± SEM is shown (at least 15 ER-PM junctions in total from 2 to 3 cells in each group were measured).

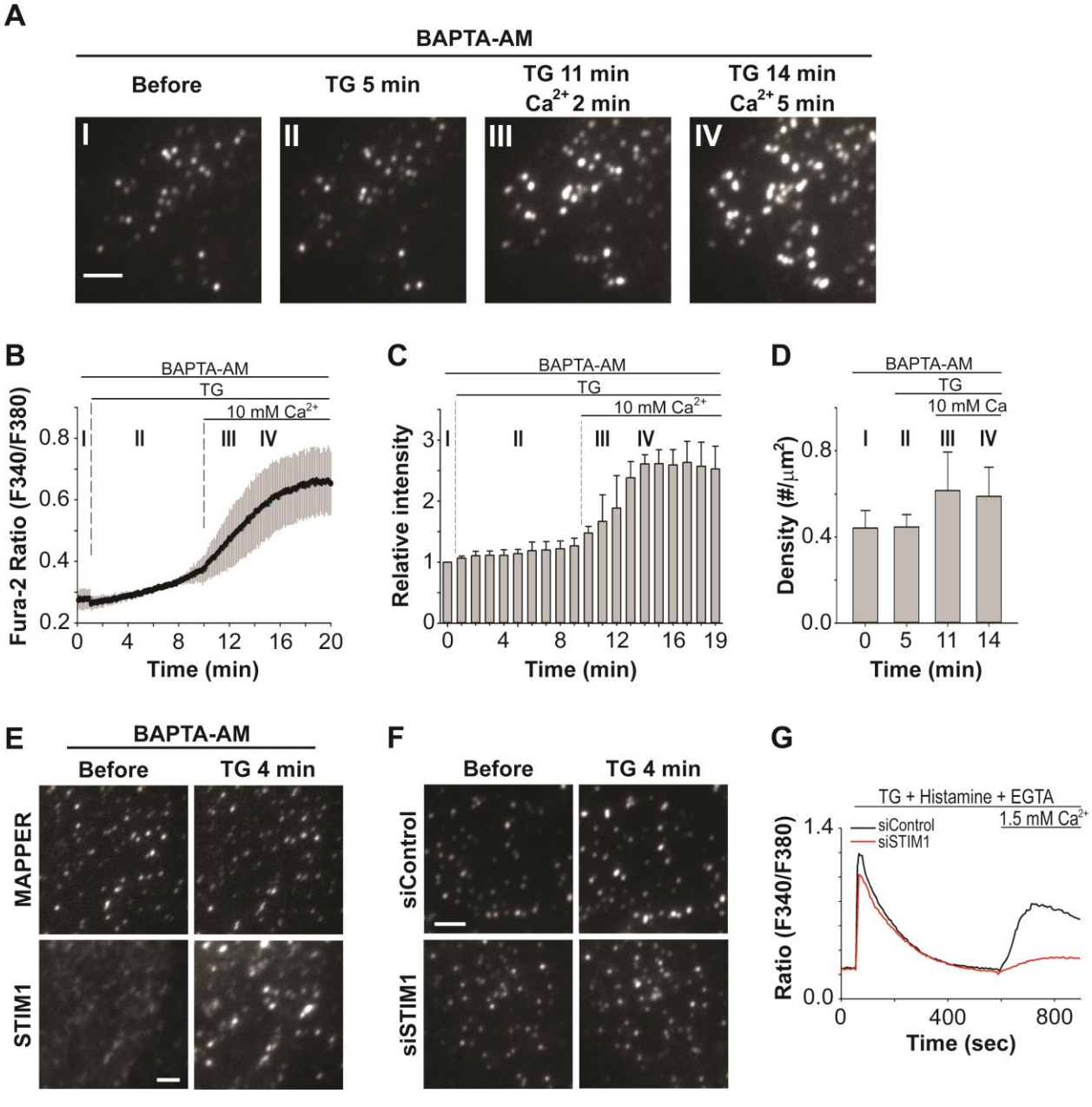
A
BAPTA-AM
Before
TG 5 min
TG 11 min
Ca2+ 2 min
TG 14 min
Ca2+ 5 min
I
II
III
IV
B
BAPTA-AM
TG
10 mM Ca2+
Fura-2 Ratio (F340/F380)
Time (min)
C
BAPTA-AM
TG
10 mM Ca2+
Relative intensity
Time (min)
D
BAPTA-AM
TG
10 mM Ca
Density (#/μm2)
Time (min)
E
BAPTA-AM
Before
TG 4 min
MAPPER
STIM1
F
Before
TG 4 min
siControl
siSTIM1
G
TG + Histamine + EGTA
1.5 mM Ca2+
siControl
siSTIM1
Ratio (F340/F380)
Time (sec)

Figure 4-4. Elevation of Cytosolic Ca^{2+} but Not SOCE Is Required for TG-Induced Enhanced ER-to-PM Connection.

(A) HeLa cells expressing MAPPER were loaded with BAPTA-AM (phase I) to prevent the increase in cytosolic Ca^{2+} induced by TG treatment (phase II). Later, 10 mM extracellular Ca^{2+} was added to cells to overcome BAPTA chelation and trigger a rise in cytosolic Ca^{2+} (phases III and IV). Time-lapse TIRF images of MAPPER in a representative cell are shown. Scale bar, 2 μm. See also Movie S3.

(B) Changes in cytosolic Ca^{2+} levels monitored by the intensity ratio of Fura-2. Mean ± SD from three independent experiments are shown.

(C and D) Quantification of changes in intensities (C) and densities (D) of ER-PM junctions monitored as described in (A). Mean ± SD from at least three independent experiments are shown.

(E) Dynamic changes of MAPPER and STIM1 induced by 1 μM TG monitored by TIRF microscopy in BAPTA-loaded MAPPER-expressing HeLa cells transfected with mCherry-STIM1. The scale bar represents 2 μm.

(F) Dynamic change of ER-PM junctions induced by 1 μM TG monitored by TIRF microscopy in MAPPER-expressing HeLa cells transfected with siControl or siSTIM1. The scale bar represents 2 μm.

(G) SOCE triggered by 1 μM TG and 100 μM histamine in siControl or siSTIM1-transfected HeLa cells. Shown are average traces derived from 357 cells in siControl and 617cells in siSTIM1.

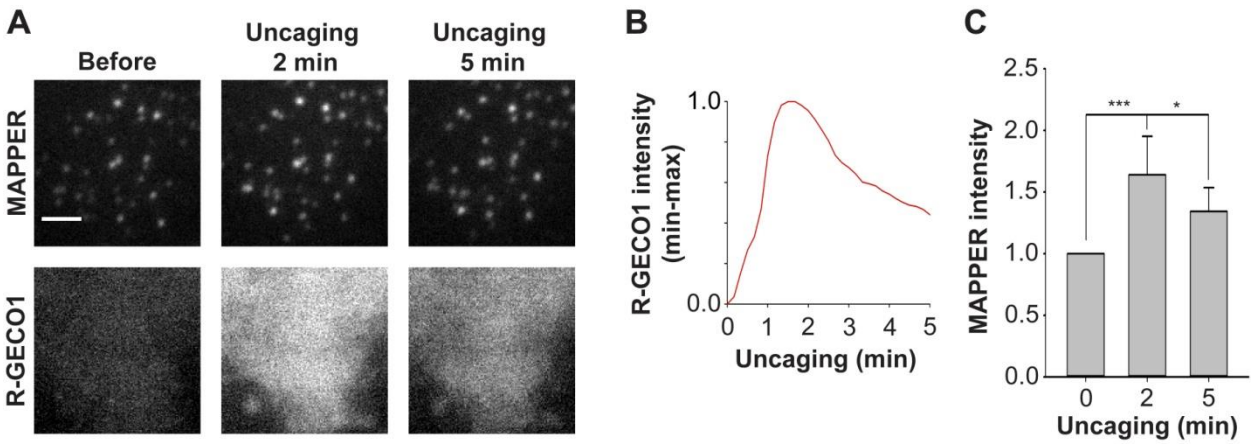

Figure 4-5. Elevation of Cytosolic Ca^{2+} Is Sufficient for TG-Induced Enhanced ER-to-PM Connection.

(A) Dynamic changes in ER-PM junctions and R-GECO1 intensities monitored by TIRF microscopy during UV-induced Ca^{2+} uncaging in MAPPER-expressing HeLa cells transfected with R-GECO1 and loaded with NP-EGTA. The scale bar represents 2 μm.

(B) Relative changes in R-GECO1 intensity monitored as described in (G). Shown is the average R-GECO1 intensity trace (five cells from two independent experiments).

(C) Dynamic changes in intensity of ER-PM junctions monitored as described in (G). Mean ± SD is shown (seven cells from two independent experiments). The asterisk denotes $p < 0.05$ and triple asterisks denote $p < 0.001$.

Chapter 5

E-Syt1 Mediates Enhanced ER-to-PM Connection

5.1 Elevation of Cytosolic Ca^{2+} Induces E-Syt1 Translocation to ER-PM Junctions

Because elevation of cytosolic Ca^{2+} alone is sufficient to enhance ER-to-PM connection, it is plausible to assume the existence of a cytosolic Ca^{2+} sensor that promotes ER-to-PM connection. I hypothesized that the cytosolic Ca^{2+} sensor is present at ER-PM junctions to mediate the enhanced connection. Recent studies showed that E-Syt1/E-Syt2/E-Syt3 and their yeast orthologs, tricalbins, are a family of C2 domain-containing proteins and capable of binding to Ca^{2+} and phospholipids. They localize to ER-PM junctions and contribute to ER-to-PM tethering (Giordano et al., 2013; Manford et al., 2012; Toulmay and Prinz, 2012). E-Syt1 is distinct from E-Syt2 and E-Syt3 as it contains two additional C2 domains (Figures 1-4A and 5-1A). Moreover, E-Syt1 is evenly expressed in most tissues, whereas the expression of E-Syt2 and E-Syt3 is more abundant in cerebellum and at low level in most tissues (Min et al., 2007).

The dynamic regulation of ER-PM junctions is likely to be a universal process in many cell types, and thus I tested whether the widely expressed E-Syt1 is the Ca^{2+} sensor that promotes ER-to-PM connection. Consistent with previous findings, E-Syt1, tagged with mCherry at the N terminus, was localized to the bulk of ER in resting cells (Figures 5-1B) (Giordano et al., 2013; Min et al., 2007). Remarkably, TG treatment triggered E-Syt1 translocation into puncta (Figures 5-1B). These puncta were subsequently identified as ER-PM junctions in cells cotransfected with MAPPER and E-Syt1, in which E-Syt1 translocated into MAPPER-labeled ER-PM junctions (Figures 5-1C). To test whether an increase in cytosolic Ca^{2+} was sufficient to induce E-Syt1 translocation, NP-EGTA was loaded into cells cotransfected with mCherry-E-Syt1 and GEM-GECO1, a genetically encoded Ca^{2+} indicator (Zhao et al., 2011). UV-induced photolysis of NP-EGTA triggered a quick increase in cytosolic Ca^{2+} followed by E-

Syt1 translocation to ER-PM junctions, and this translocation was reversible when elevated cytosolic Ca^{2+} diminished (Figures 5-1D). Further analysis showed that the kinetics of cytosolic Ca^{2+} level and E-Syt1 translocation were tightly coupled (Figures 5-1E).

Out of the five C2 domains of E-Syt1, only the C2A and the C2C domains contain canonical residues for Ca^{2+} binding by comparing the sequence homology to C2 domain in synaptotagmin (Min et al., 2007; Rizo and Sudhof, 1998). To dissect the mechanism by which E-Syt1 senses Ca^{2+} and translocates to ER-PM junctions, I mutated a key aspartic acid residue to alanine in the probable Ca^{2+} binding loops of C2A and C2C domains to generate the corresponding E-Syt1-D406A and E-Syt1-D724A mutants (Figure 5-2A). Following TG treatment, the E-Syt1-D406A mutant translocated to ER-PM junctions (Figure 5-2B), whereas no translocation of the E-Syt1-D724A mutant was observed (Figure 5-2C). Similar results were obtained using C-terminal tagged-E-Syt1 mutants following cytosolic Ca^{2+} increase via the photolysis of NP-EGTA (Figures 5-2D and 5-2E). These observations indicate that E-Syt1 binds to Ca^{2+} via its C2C domain, and Ca^{2+} binding is important for E-Syt1 translocation to ER-PM junctions. In addition, the C2E domain of E-Syt1 contains a polybasic stretch that is similar to the C2C domains of E-Syt2 and E-Syt3, which have been showed to bind to PIP_2 at PM (Giordano et al., 2013; Min et al., 2007). Thus, C2E domain may provide PM targeting for E-Syt1 translocation to ER-PM junctions. To test this hypothesis, I introduced a stop codon before the amino acid number 998 to generate E-Syt1-dC2E mutant (Figure 5-2A). As expected, E-Syt1-dC2E failed to translocate to ER-PM junctions after TG treatment or NP-EGTA photolysis (Figures 5-2D and 5-2G). These results indicate that E-Syt1 senses elevation of cytosolic Ca^{2+} via its C2C domain and translocated to ER-PM junctions likely via its C2E domain binding to PIP_2 at PM. Similar results were also shown in a recent report (Giordano et al., 2013).

5.2 Enhanced ER-to-PM Connection Is Mediated by E-Syt1 Translocation to ER-PM Junctions

Given that E-Syt1 senses cytosolic Ca2+ increase and translocates to ER-PM junctions, it is tempting to hypothesize that E-Syt1 is the Ca2+ sensor for enhanced ER-to-PM connection. To test this idea, siRNAs targeting either the coding sequence (siE-Syt1_cds) or the 3′ UTR (siE-Syt1_3′ UTR) of *E-Syt1* were used. TG-induced increase in ER-to-PM connection, as indicated by the intensity increase of MAPPER-labeled ER-PM junctions, was greatly diminished in cells transfected with siE-Syt1_cds or siE-Syt1_3′ UTR compared to cells transfected with control siRNA (siControl) (Figures 5-3A and 5-3B). In addition, reconstitution of mCherry-E-Syt1 in cells treated with siE-Syt1_3′ UTR restored the enhanced ER-to-PM accompanied by mCherry-S-Syt1 translocation following TG treatment (Figures 5-3C and 5-3E). By contrast, expression of the E-Syt1-D724A mutant, which neither senses Ca^{2+} nor translocates to ER-PM junctions, failed to rescue the defects in enhancing ER-to-PM connection in siE-Syt1_3′ UTR-treated cells (Figures 5-3D and 5-3E). These results indicate that E-Syt1 promotes the enhanced ER-to-PM connection during Ca^{2+} signaling via its translocation to ER-PM junctions following Ca^{2+} binding.

5.3 Enhanced ER-to-PM Connection Is Not Required for SOCE

Since ER-PM junctions are the spatial platform for SOCE, I then tested if enhanced ER-to-PM connection is important for SOCE. E-Syt1 knockdown by siE-Syt1 and MAPPER-s overexpression were applied to abolish and to enhance ER-to-PM connection, respectively. Surprisingly, SOCE measured by Ca^{2+} influx following ER Ca^{2+} depletion by TG and histamine appeared to be similar in siControl and siE-Syt1 transfected cells. Consistently, no change in SOCE was observed in MAPPER-s expressing cells. These results suggest that SOCE is not regulated by enhanced ER-to-PM connection. Similar results were shown in a recent report (Giordano et al., 2013).

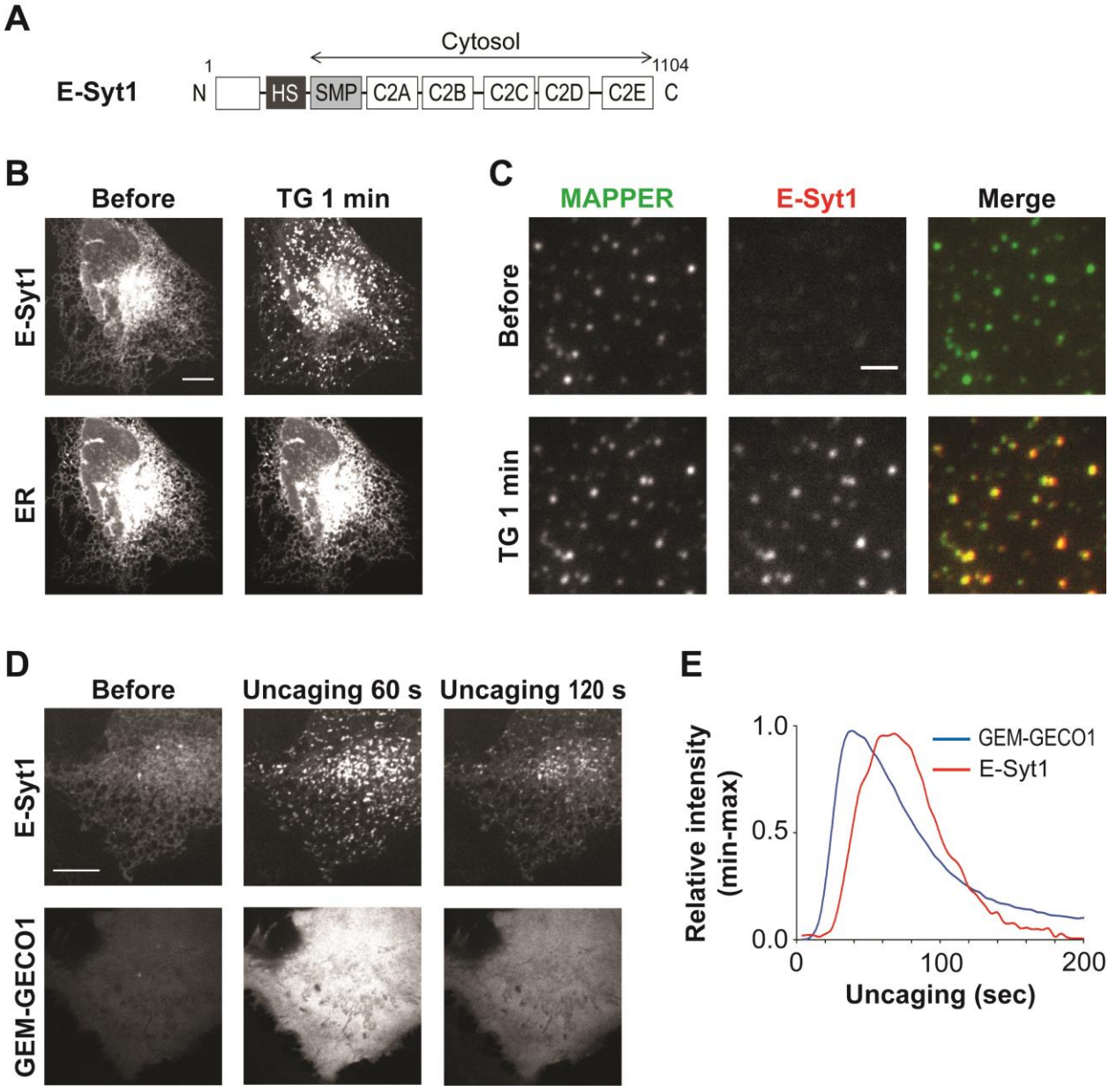
A
Cytosol
1
1104
E-Syt1
N
HS
SMP
C2A
C2B
C2C
C2D
C2E
C
B
Before
TG 1 min
E-Syt1
ER
C
MAPPER
E-Syt1
Merge
Before
TG 1 min
D
Before
Uncaging 60 s
Uncaging 120 s
E-Syt1
GEM-GECO1
E
Relative intensity (min-max)
1.0
0.5
0.0
0
100
200
Uncaging (sec)
GEM-GECO1
E-Syt1

Figure 5-1. E-Syt1 Translocates to ER-PM Junctions Following Cytosolic Ca^{2+} Increase.

(A) Diagram of E-Syt1. Amino acid numbers are indicated. HS, hydrophobic patches; SMP, synaptotagmin-like-mitochondrial-lipid binding protein; C2, C2 doamin.

(B) E-Syt1 translocation induced by 1 μM TG monitored by confocal microscopy in HeLa cells co-transfected with mCherry-E-Syt1 and YFP-ER. Scale bar, 10 μm.

(C) E-Syt1 translocation to ER-PM junctions induced by 1 μM TG monitored by TIRF microscopy in MAPPER-expressing HeLa cells transfected with mCherry-E-Syt1. Scale bar, 2 μm.

(D) Changes in E-Syt1 localization and GEM-GECO1 intensity (CFP emission) monitored by confocal microscopy during UV illumination-induced Ca^{2+} uncaging in NP-EGTA-loaded HeLa cells co-transfected with mCherry-E-Syt1 and GEM-GECO1. Scale bar, 10 μm.

(E) Relative changes in cellular GEM-GECO1 intensities (CFP emission/GFP emission) and E-Syt1 translocation to ER-PM junctions monitored as described in (C). Shown are the average traces of four cells.

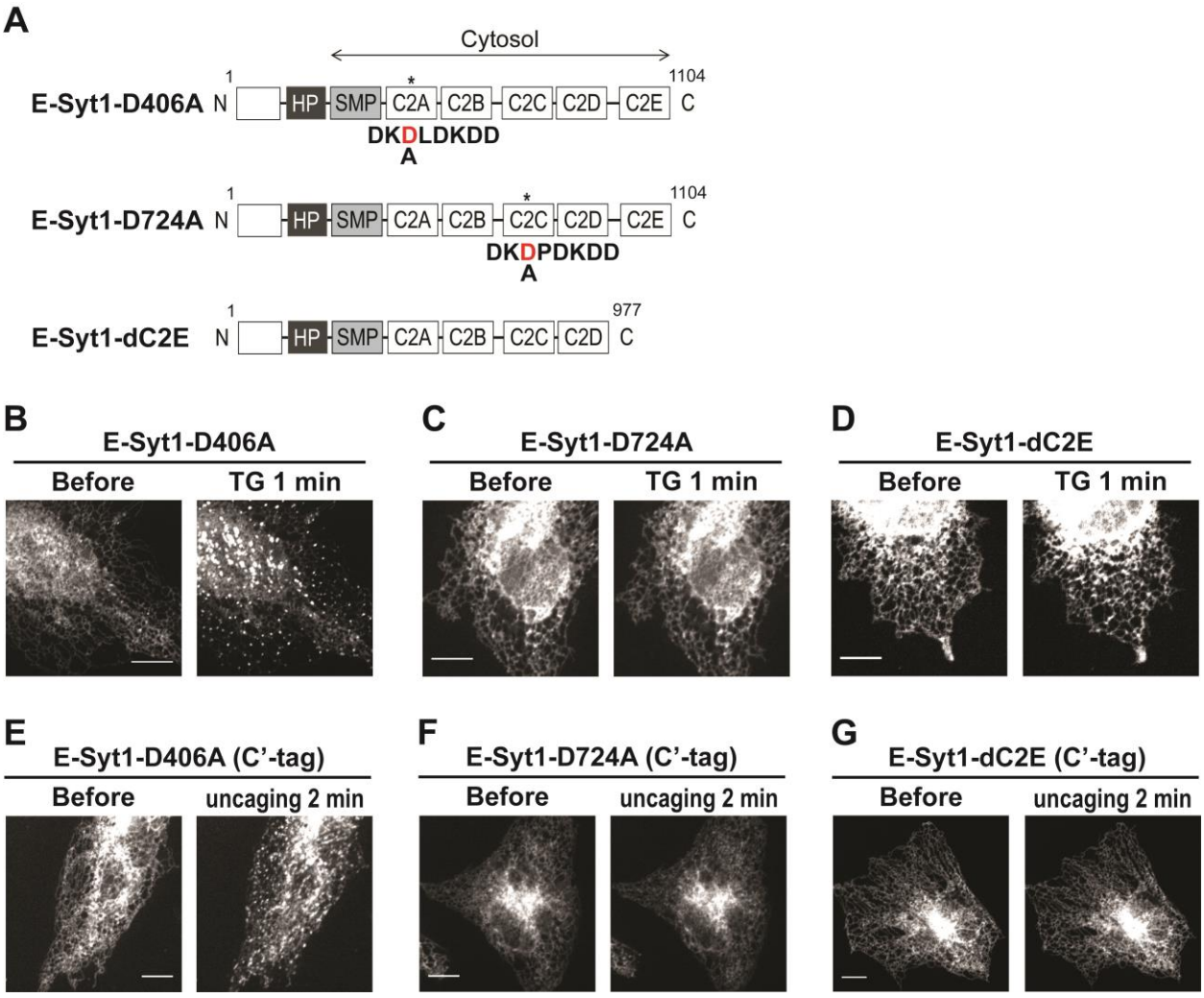

Figure 5-2. E-Syt1 Translocation to ER-PM Junctions is Dependent on C2C and C2E Domains.

(A) Diagrams of E-Syt1-D406A, E-Syt1-D724A, and E-Syt1-dC2E.

(B, C, and D) Confocal images of HeLa cells transfected with E-Syt1-D406A (B), E-Syt1-D724A (C), or E-Syt1-dC2E (D) before and after 1 μM TG treatment. Scale bar, 10 μm.

(E, F, and G) Confocal images of NP-EGTA loaded HeLa cells expressing with C-terminal tagged E-Syt1-D406A (E), E-Syt1-D724A (F), or E-Syt1-dC2E (G) before and 2 min after Ca^{2+} uncaging. Scale bar, 10 μm.

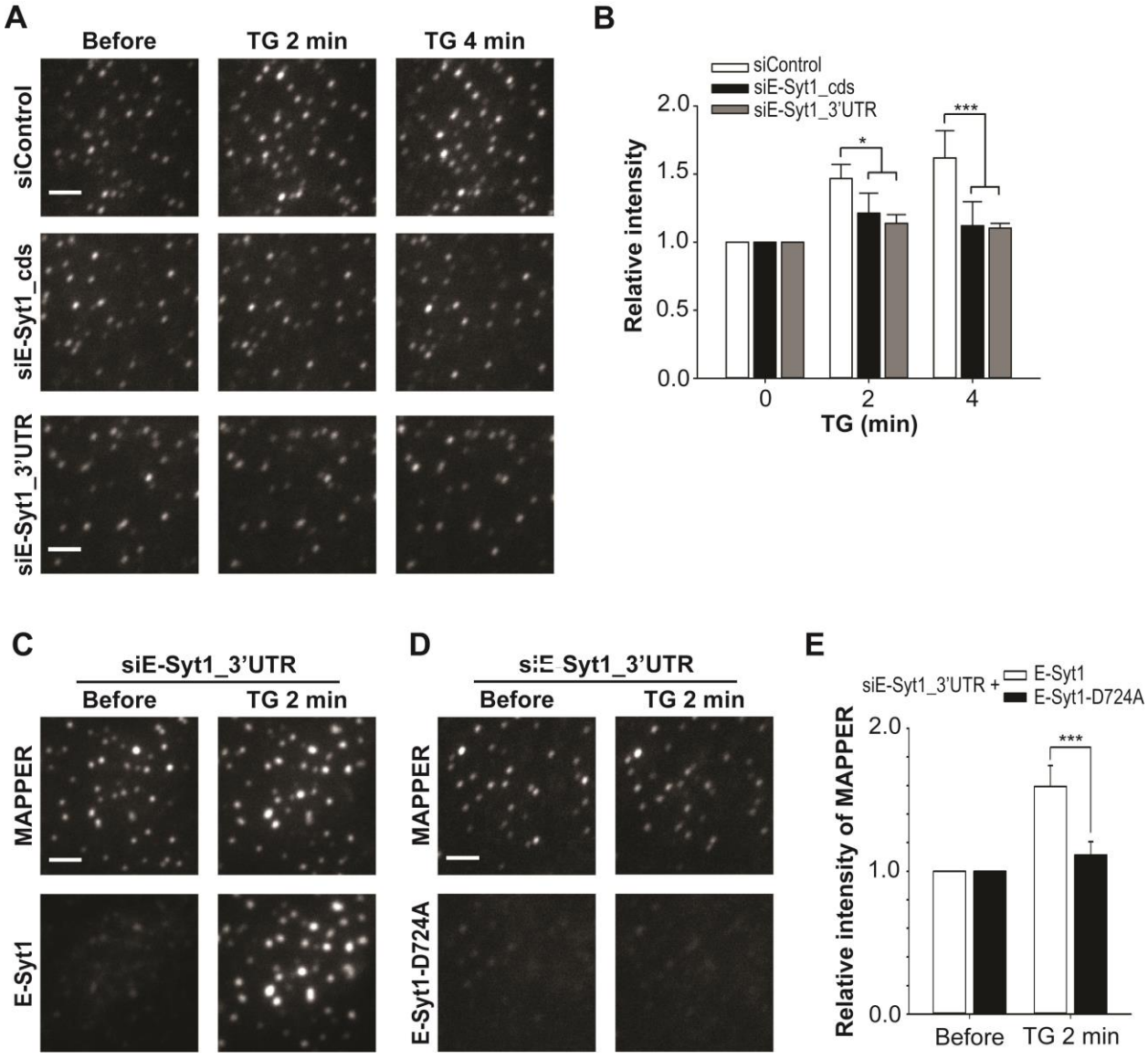
A
Before
TG 2 min
TG 4 min
siControl
siE-Syt1_cds
siE-Syt1_3'UTR
B
siControl
siE-Syt1_cds
siE-Syt1_3'UTR
Relative intensity
2.0
1.5
1.0
0.5
0.0
*
***
0
2
4
TG (min)
C
siE-Syt1_3'UTR
Before
TG 2 min
MAPPER
E-Syt1
D
siE-Syt1_3'UTR
Before
TG 2 min
MAPPER
E-Syt1-D724A
E
siE-Syt1_3'UTR +
E-Syt1
E-Syt1-D724A
Relative intensity of MAPPER
2.0
1.0
0.0
***
Before
TG 2 min

Figure 5-3. Enhanced ER-to-PM Connection during Ca^{2+} Signaling Is Mediated by E-Syt1 Translocation to ER-PM Junctions.

(A) Dynamic changes in ER-PM junctions induced by 1 μM TG monitored by TIRF microscopy in MAPPER-expressing HeLa cells transfected with siControl, siE-Syt1_cds or siE-Syt1_3′ UTR. The scale bar represents 2 μm.

(B) Quantification of the dynamic changes in intensities of ER-PM junctions monitored as described in (A). Mean ± SD are shown (four to six cells from at least three independent experiments). The asterisk denotes $p < 0.05$ and triple asterisks denote $p < 0.001$.

(C and D) Dynamic changes in ER-PM junctions and E-Syt1 translocation induced by 1 μM TG monitored by TIRF microscopy in MAPPER-expressing HeLa cells cotransfected with siE-Syt1_3′ UTR and mCherry-E-Syt1 or mCherry-E-Syt1-D724A. The scale bar represents 2 μm.

(E) Quantification of the dynamic changes in intensity of ER-PM junctions monitored as described in (C) and (D). Mean ± SD is shown (four to six cells from three independent experiments). Triple asterisks denote $p < 0.001$.

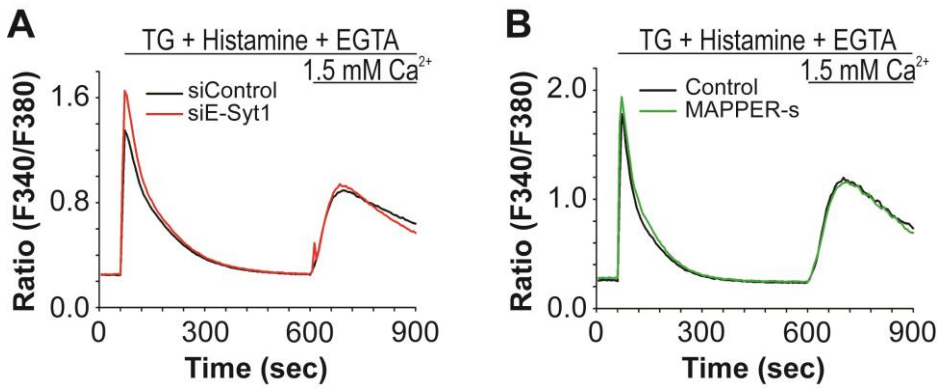

Figure 5-4. Enhanced ER-to-PM Connection Is Not Required for SOCE.

(A) SOCE triggered by 1 μM TG and 100 μM histamine in siControl or siE-Syt1-transfected HeLa cells. Shown are average traces derived from at least 700 cells in each group.

(B) SOCE triggered by 1 μM TG and 100 μM histamine in HeLa cells transfected with Control or MAPPER-s. Shown are average traces derived from at least 250 cells in each group.

Chapter 6

Feedback Regulation of Receptor-Induced Ca^{2+} Signaling at ER-PM Junctions

6.1 Nir2 Translocates to ER-PM Junctions and Promotes PIP_2 Replenishment after Receptor Stimulation

ER-PM junctions have been proposed as loci for non-vesicular PI transport. The only piece of evidence to support this hypothesis was obtained from genetics studies in *Drosophila*. In *Drosophila* photoreceptor cells, deletion of a PITP called RdgBα localized at ER-PM junctions, led to defective photoreceptor activation mediated by rhodopsin-induced Ca^{2+} signaling (Hotta and Benzer, 1970). Ca^{2+} signaling is generally triggered by receptor-induced PLC activation and PM PIP_2 hydrolysis (Berridge et al., 2000), and the decreased PM PIP_2 level need to be restored to maintain cellular homeostasis. Therefore, it is plausible to hypothesize that the enhanced ER-to-PM connection by E-Syt1 facilitates PM PIP_2 replenishment at ER-PM junctions during Ca^{2+} signaling. To test this idea, I first examined whether Nir2, a mammalian ortholog of *Drosophila* RdgB, is localized to ER-PM junctions. Overexpression of a mCherry-tagged Nir2 showed cytosolic distribution (Figure 6-1A, top panel). Strikingly, histamine stimulation triggered Nir2 translocation into puncta in HeLa cells overexpressing histamine H1 receptor (Figure 6-1A, bottom panel). These puncta were subsequently identified as ER-PM junctions in cells cotransfected with MAPPER and Nir2, in which Nir2 translocated into MAPPER-labeled ER-PM junctions (Figure 6-1B).

Since Nir2 is a PITP, I then examined whether Nir2 is involved in replenishing PM PIP_2 after receptor-induced hydrolysis during Ca^{2+} signaling. PIP_2 levels at the PM were monitored using TIRF microscopy and GFP-PLCδ-PH, a PIP_2 biosensor (Stauffer et al., 1998), in HeLa cells overexpressing H1 receptor to augment PIP_2 hydrolysis induced by histamine stimulation. In siControl-transfected cells, a sharp decrease of PLCδ-PH intensity at the PM was observed following histamine stimulation (Figure 6-

1C), indicating PIP_2 hydrolysis. This decrease was followed by a partial recovery, reflecting replenishment of PIP_2 at the PM. Notably, in cells treated with siRNA targeting *Nir2* (siNir2), PIP_2 replenishment was reduced compared to siControl-transfected cells (Figure 6-1C). In contrast, overexpression of Nir2 strongly augmented PIP_2 replenishment after hydrolysis compared with control-transfected cells (Figure 6-1D). Similar results were obtained using Tubby-GFP (Figure 6-1E), another biosensor that binds PIP_2 selectively (Quinn et al., 2008). These results suggest that Nir2 translocates to ER-PM junctions and mediates PM PIP_2 replenishment following receptor-induced hydrolysis.

6.2 PI Transfer Activity and ER-PM Junction Targeting Are Important for Nir2 to Promote PIP_2 Replenishment following Receptor Stimulation

Nir2 contains a N-terminal conserved PITP domain, a FFAT motif that binds to VAPs in the ER (Amarilio et al., 2005), and C-terminal DDHD and LNS2 domain that are likely for PM targeting (Kim et al., 2013) (Figure 6-2A). The PITP domain of Nir2 has been shown to bind PI in vitro and contains the key residues that make hydrogen bond contact with the inositol head group for the PI transfer activity (Aikawa et al., 1999; Cockcroft, 2012). To test whether the PI transfer activity is required for Nir2 to mediate PIP_2 replenishment, I mutated two of the key residues to generate the Nir2-K61A,N90F mutant. Similar to wild-type Nir2, the Nir2-K61A,N90F mutant was recruited to ER-PM junctions following histamine treatment (Figure 6-2B). Nevertheless, it failed to enhance PIP_2 replenishment compared to wild-type Nir2 (Figure 6-2C). Similar results were obtained with the Nir2-T59E,N90F mutant (Figures 6-2D and 6-2E), and the PITP domain deleted Nir2-ΔPITP mutant (Figures 6-2F and 6-2G). These results indicate that a functional PITP domain is essential for Nir2 to promote PM PIP_2 replenishment but is not required for Nir2 translocation to ER-PM junctions following receptor stimulation.

The translocation of Nir2 from the cytosol to ER-PM junctions suggests that it binds to the ER and the PM simultaneously following receptor stimulation. Nir2 has been shown to interact with the ER membrane proteins VAP-A and VAP-B via its FFAT motif (Amarilio et al., 2005). I first confirmed the

interaction between Nir2 and VAPs by demonstrating an accumulation of VAP-A and VAP-B colocalizing with Nir2 at ER-PM junctions following receptor stimulation (Figures 6-3A and 6-3B). These results indicate that VAP-A or VAP-B binding supports Nir2 recruitment to ER-PM junctions. To test if Nir2 translocation to ER-PM junctions are important for PIP_2 replenishment at PM, I generated a FFAT mutant of Nir2 (Nir2-FM) that cannot bind VAP proteins as described previously (Amarilio et al., 2005). Nir2-FM was recruited to the PM but failed to concentrate at ER-PM junctions following receptor stimulation, as observed by TIRF microscopy (top panels, Figures 6-3C and 6-3D). Consistently, the accumulation of VAP-A and VAP-B at ER-PM junctions was not detected following receptor stimulation (bottom panels, Figures 6-3C and 6-3D). These observations suggest that receptor stimulation induces concurrent PM targeting and VAP binding of Nir2, leading to the simultaneous recruitment of Nir2 and VAPs to ER-PM junctions. Nir2-FM containing a functional PITP domain promoted PIP_2 replenishment at PM following receptor stimulation as compared to control (Figure 6-3E). Interestingly, the degree of PIP_2 replenishment mediated by Nir2-FM was reduced comparing with cells overexpressing wild-type Nir2 (Figure 6-3E). These results confirmed that PITP domain is important for the replenishment PIP_2 in cells overexpressing Nir2. In addition, localization to ER-PM junctions further facilitated the efficiency of Nir2 to replenish PIP_2 at the PM.

6.3 Enhanced ER-to-PM Connection by E-Syt1 Facilitates Nir2 Translocation to ER-PM Junctions

Given that Nir2 targeting to ER-PM junctions supports its functions, I further tested a hypothesis that the enhanced ER-to-PM connection by E-Syt1 contributes to Nir2 translocation to ER-PM junctions following receptor stimulation. To manipulate ER-to-PM connection, *E-Syt1* knockdown and MAPPER-s overexpression were applied to abolish and to enhance this connection, respectively. Nir2 translocation to ER-PM junctions occurred quickly after histamine stimulation in siControl-transfected cells (Figure 6-4A). In contrast, aborted cycles of Nir2 translocation were observed in cells treated with siE-Syt1 (Figure 6-4A). As a result, the maximal fold increase of Nir2 intensity at single ER-PM junctions was significantly reduced in siE-Syt1-transfected cells (Figure 6-4B). To further confirm that the enhanced

ER-to-PM connection is important for Nir2 translocation, MAPPER-s was applied to restrict the range of gap distance of ER-PM junctions. Nir2 translocation was monitored in cells without overexpressing H1 receptor to demonstrate the enhancing effect of MAPPER-s. In MAPPER-expressing cells, histamine stimulation induced a weak translocation of Nir2, which was greatly potentiated in cells expressing MAPPER-s (Figure 6-4C). Further analyses showed that histamine stimulation induced a significantly higher increase of Nir2-mCherry intensity at ER-PM junctions in MAPPER-s-transfected cells than in MAPPER-transfected cells (Figure 6-4D).These results suggest that the decrease in gap distance of ER-PM junctions E-Syt1 facilitates Nir2 translocation and then accumulation to ER-PM junctions after receptor stimulation.

6.4 Enhanced ER-to-PM Connection Promotes PIP_2 Replenishment and Supports Receptor-Induced Ca^{2+} Signaling

Because the enhanced ER-to-PM connection mediated by E-Syt1 is important for Nir2 translocation to ER-PM junctions, I then tested the effect of *E-Syt1* knockdown on PM PIP_2 replenishment after receptor-induced hydrolysis. PM PIP_2 replenishment was markedly reduced in cells transfected with siE-Syt1_3′ UTR compared to that in siControl-transfected cells following histamine stimulation (Figure 6-5A). These results are consistent with the defective Nir2 translocation in siE-Syt1-treated cells. Expression of wild-type, but not the D724A mutant of E-Syt1 rescued the defective PM PIP_2 replenishment in *E-Syt1* knockdown cells (Figure 6-5A). This data indicate that E-Syt1 translocation to ER-PM junctions is crucial for replenishing PM PIP_2 after receptor-induced hydrolysis. Consistently, overexpression of MAPPER-s, which facilitates Nir2 translocation to ER-PM junctions, promoted PM PIP_2 replenishment after hydrolysis (Figure 6-5B). Together, these results suggest that the enhanced ER-to-PM connection induced by E-Syt1 translocation to ER-PM junctions is essential for recruiting Nir2 and subsequent replenishing PM PIP_2 after receptor stimulation.

It is likely that defective PM PIP_2 replenishment after the initial receptor-induced hydrolysis affects the ability of cells to respond to subsequent stimulation. To test this hypothesis, Ca^{2+} signaling responses induced by periodic treatment of histamine was monitored in cells treated with siRNA targeting *E-Syt1* and *Nir2*. I observed that the first pulse of histamine stimulation triggered comparable amplitude increases in Ca^{2+} responses in siControl-, siE-Syt1- and siNir2-transfected cells (Figures 6-5C and 6-5D). Strikingly, a profound decrease in amplitude of Ca^{2+} responses to subsequent histamine pulses was observed in siE-Syt1- and siNir2-transfected cells. These results suggest that the enhanced ER-to-PM connection and PM PIP_2 replenishment are important for the recovery of the Ca^{2+} signaling system following receptor stimulation.

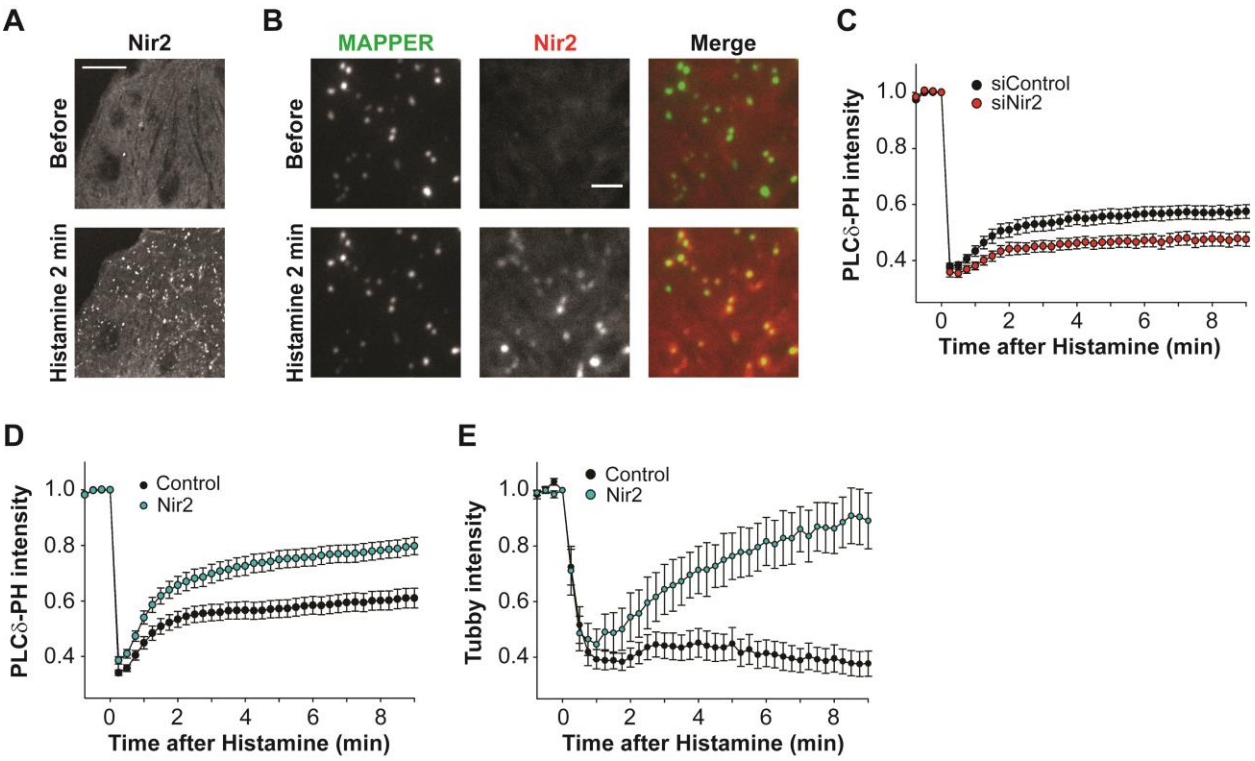

Figure 6-1. Nir2 Translocates to ER-PM Junctions and Promotes PIP_2 Replenishment following Receptor Stimulation.

(A) Nir2 translocation induced by 100 μM histamine monitored by confocal microscopy in HeLa cells cotransfected with H1 receptor and Nir2-mCherry. The scale bar represents 10 μm.

(B) Nir2 translocation to ER-PM junctions induced by 100 μM histamine monitored by TIRF microscopy in MAPPER-expressing HeLa cells transfected with H1 receptor and Nir2-mCherry. The scale bar represents 2 μm.

(C) Dynamic changes of PLCδ-PH intensity induced by 100 μM histamine monitored by TIRF microscopy in HeLa cells cotransfected with H1 receptor, GFP-PLCδ-PH, and siControl or siNir2. Mean ± SEM is shown (6 to 17 cells from three independent experiments).

(D and E) Dynamic changes of PLCδ-PH (D) or Tubby (E) intensity induced by 100 μM histamine monitored by TIRF microscopy in HeLa cells cotransfected with H1 receptor, GFP-PLCδ-PH or GFP-Tubby, and control (mCherry-N1 vector) or Nir2-mCherry. Mean ± SEM is shown (25 cells from six independent experiments in GFP-PLCδ-PH; 5 to 8 cells from two independent experiments in GFP-Tubby).

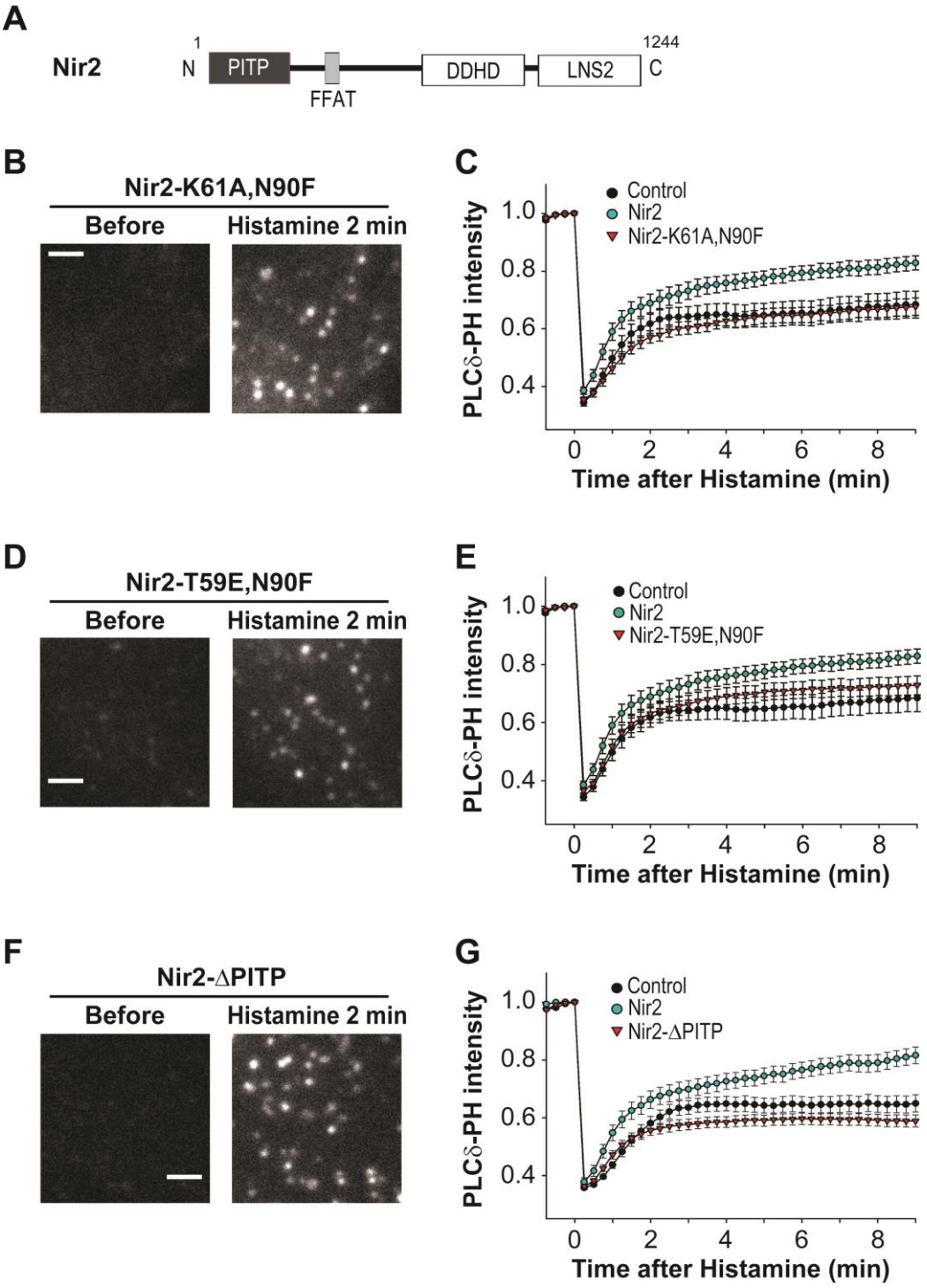
A
Nir2
1
N
PITP
FFAT
DDHD
LNS2
1244
C
B
Nir2-K61A,N90F
Before
Histamine 2 min
C
Control
Nir2
Nir2-K61A,N90F
PLCδ-PH intensity
1.0
0.8
0.6
0.4
0
2
4
6
8
Time after Histamine (min)
D
Nir2-T59E,N90F
Before
Histamine 2 min
E
Control
Nir2
Nir2-T59E,N90F
PLCδ-PH intensity
Time after Histamine (min)
F
Nir2-ΔPITP
Before
Histamine 2 min
G
Control
Nir2
Nir2-ΔPITP
PLCδ-PH intensity
Time after Histamine (min)

Figure 6-2. PI Transfer Activity Is Important for Nir2 to Promote PIP_2 Replenishment following Receptor Stimulation.

(A) Diagram of Nir2. Amino acid numbers are indicated.

(B) Nir2-K61A,N90F mutant translocation induced by 100 μM histamine monitored by TIRF microscopy in HeLa cells cotransfected with H1 receptor and Nir2-K61A,N90F-mCherry. The scale bar represents 2 μm.

(C) Dynamic changes of PLCδ-PH intensity induced by 100 μM histamine monitored by TIRF microscopy in HeLa cells cotransfected with H1 receptor, GFP-PLCδ-PH, and control, Nir2-mCherry or Nir2-K61A,N90F-mCherry. Mean ± SEM is shown (18–27 cells from three independent experiments).

(D) Translocation of the Nir2-T59E,N90F mutant induced by 100 μM histamine monitored by TIRF microscopy in HeLa cells co-transfected with H1 receptor and Nir2- T59E,N90F-mCherry. Scale bar, 2 μm.

(E) Changes in PLCδ-PH intensity induced by 100 μM histamine monitored by TIRF microscopy in HeLa cells co-transfected with H1 receptor, GFP-PLCδ-PH, and control, Nir2-mCherry or Nir2-T59E,N90F-mCherry. Mean ± SEM are shown (18 to 27 cells from 3 independent experiments).

(F) Nir2-ΔPITP mutant translocation induced by 100 μM histamine monitored by TIRF microscopy in HeLa cells cotransfected with H1 receptor and Nir2-ΔPITP-mCherry. The scale bar represents 2 μm.

(G) Dynamic changes of PLCδ-PH intensity induced by 100 μM histamine monitored by TIRF microscopy in HeLa cells cotransfected with H1 receptor, GFP-PLCδ-PH, and control, Nir2-mCherry or Nir2-ΔPITP-mCherry. Mean ± SEM is shown (14–32 cells from three independent experiments).

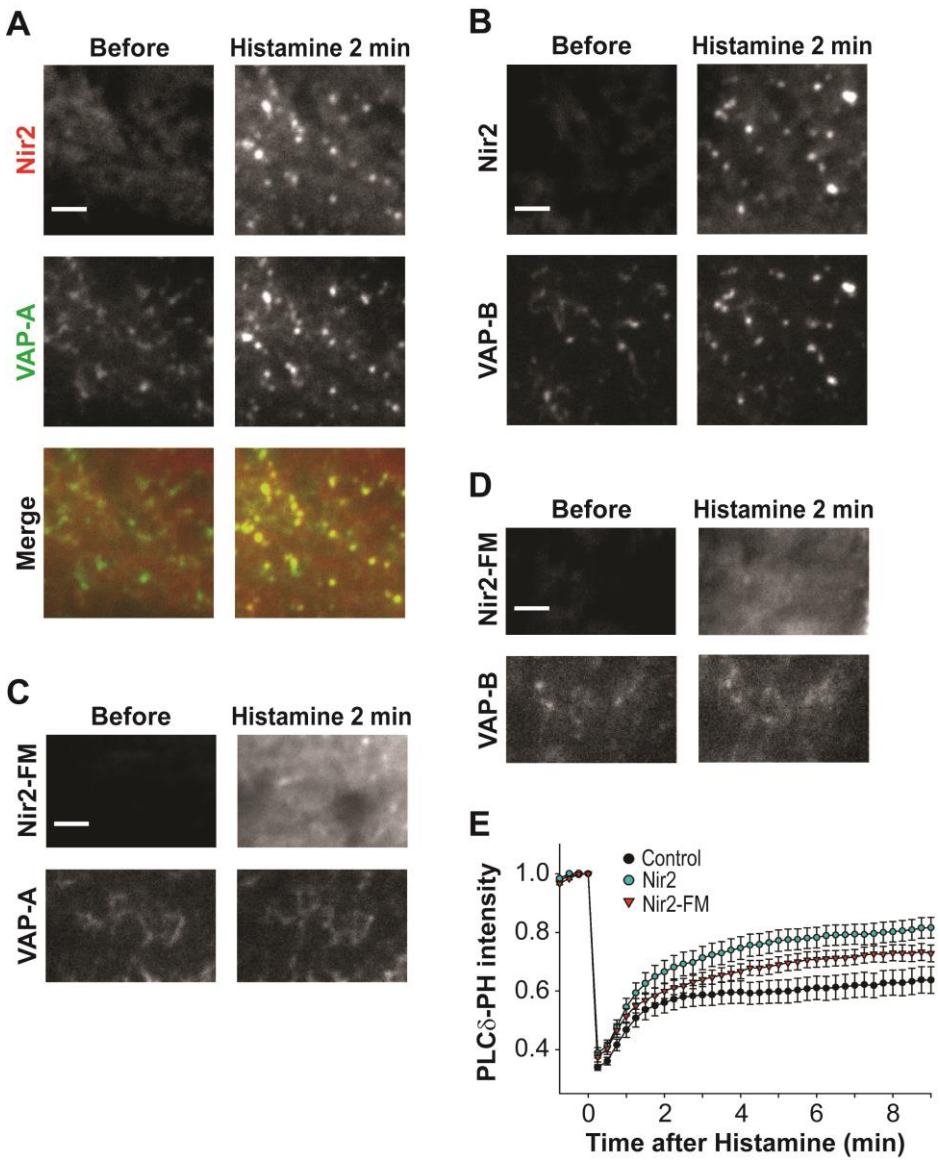
A
Before
Histamine 2 min
Nir2
VAP-A
Merge
B
Before
Histamine 2 min
Nir2
VAP-B
C
Before
Histamine 2 min
Nir2-FM
VAP-A
D
Before
Histamine 2 min
Nir2-FM
VAP-B
E
Control
Nir2
Nir2-FM
PLCδ-PH intensity
1.0
0.8
0.6
0.4
0
2
4
6
8
Time after Histamine (min)

Figure 6-3. ER-PM Junction Targeting Is Important for Nir2 to Promote PIP2 Replenishment following Receptor Stimulation.

(A and B) VAP-A (A) or VAP-B (B) and Nir2 translocation induced by 100 μM histamine monitored by TIRF microscopy in HeLa cells cotransfected with H1 receptor, VAP-A-YFP (A) or VAP-B-YFP (B), and Nir2-mCherry. The scale bar represents 2 μm.

(C and D) VAP-A (C) or VAP-B (D) and Nir2-FM (FFAT mutant) localizations during 100 μM histamine treatment monitored by TIRF microscopy in HeLa cells cotransfected with H1 receptor, VAP-A-YFP (C) or VAP-B-YFP (D), and Nir2-FM-mCherry. The scale bar represents 2 μm.

(E) Dynamic changes of PLCδ-PH intensity induced by 100 μM histamine monitored by TIRF microscopy in HeLa cells cotransfected with H1 receptor, GFP-PLCδ-PH, and control, Nir2-mCherry or Nir2-FM-mCherry. Mean ± SEM are shown (13–18 cells from three independent experiments).

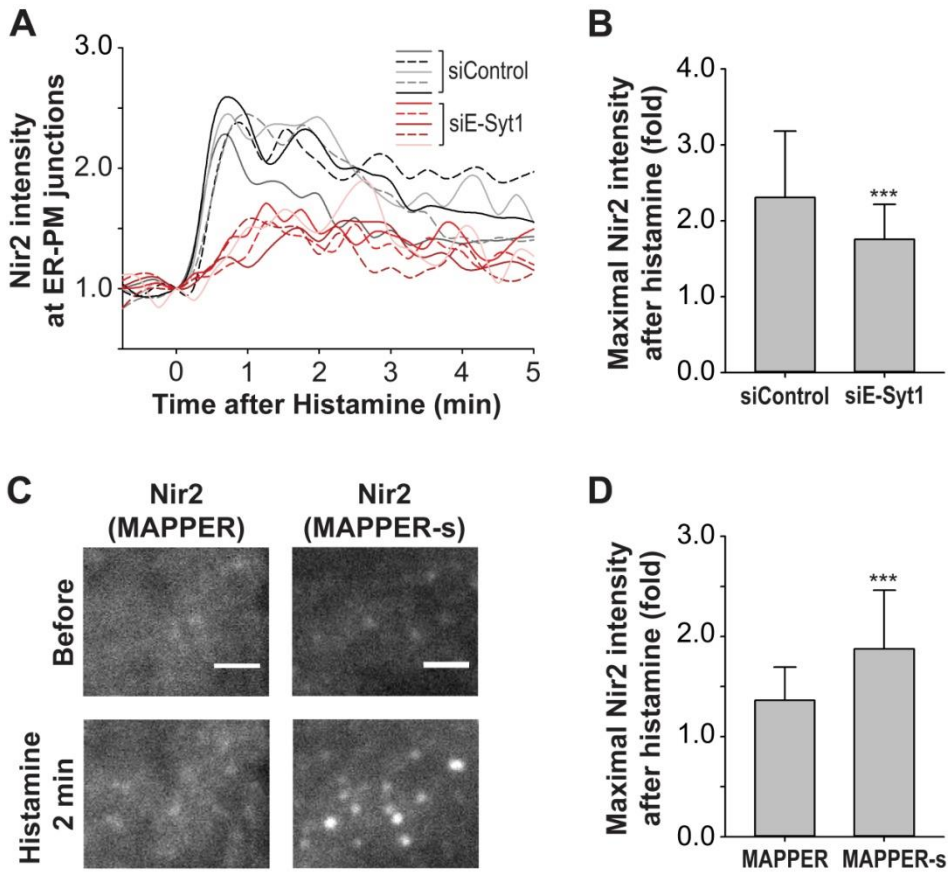

Figure 6-4. Enhancement of ER-to-PM Connection by E-Syt1 Facilitates Nir2 Translocation following Receptor Stimulation.

(A) Nir2 accumulation at single ER-PM junctions induced by 100 μM histamine monitored by TIRF microscopy in HeLa cells cotransfected with H1 receptor, Nir2-mCherry, and siControl or siE-Syt1. Representative traces of Nir2 intensities at single ER-PM junctions are shown.

(B) Quantification of maximal fold increase of Nir2 intensities at single ER-PM junctions monitored as described in (A). Mean ± SD is shown (more than 250 puncta from two independent experiments). Triple asterisks denote $p < 0.001$.

(C) Nir2 translocation to ER-PM junctions induced by 100 μM histamine monitored by TIRF microscopy in HeLa cells cotransfected with Nir2-mCherry and MAPPER or MAPPER-s. The scale bar represents 2 μm.

(D) Quantification of maximal fold increase of Nir2 intensity at single ER-PM junctions monitored as described in (C). Mean ± SD is shown (more than 60 puncta). Triple asterisks denote $p < 0.001$.

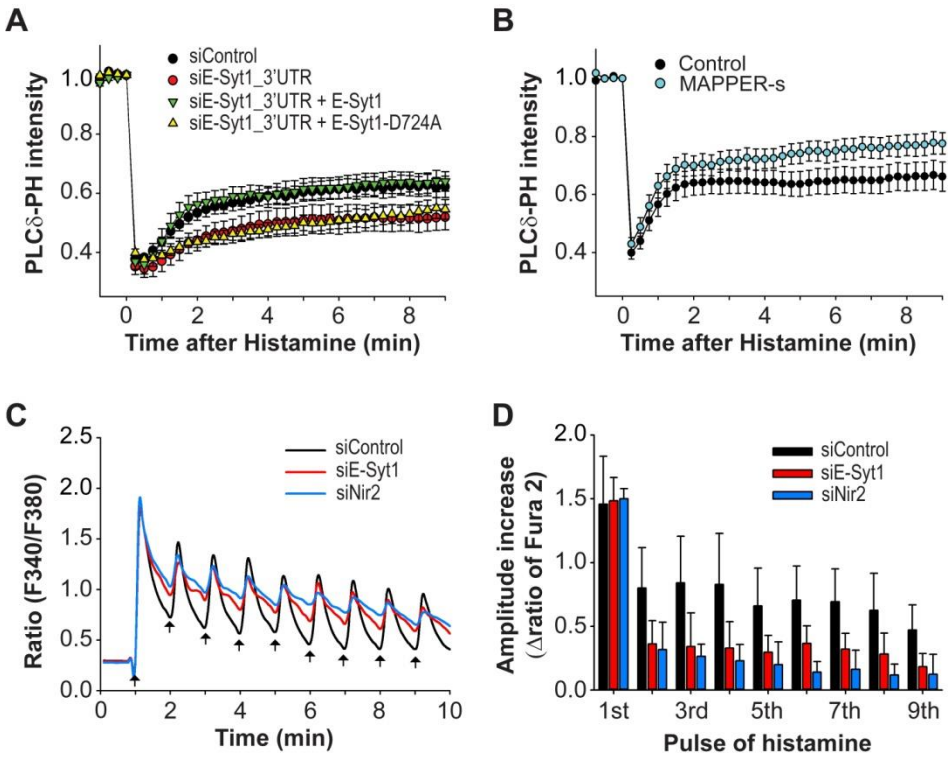

Figure 6-5. Enhanced ER-to-PM Connection by E-Syt1 Facilitates PIP_2 Replenishment following Receptor Stimulation and Supports Repetitive Receptor Activation.

(A) Dynamic changes of PLCδ-PH intensities induced by 100 μM histamine monitored by TIRF microscopy in HeLa cells cotransfected with H1 receptor, GFP-PLCδ-PH, siControl or siE-Syt1, plus mCherry-E-Syt1 or mCherry-E-Syt1-D724A. Mean ± SEM is shown (5 to 9 cells from three independent experiments).

(B) Dynamic changes of PLCδ-PH intensities induced by 100 μM histamine monitored by TIRF microscopy in HeLa cells cotransfected with H1 receptor, mCherry-PLCδ-PH, and control (SP-GFP-TM) or MAPPER-s. Mean ± SEM are shown (13 to 14 cells from two independent experiments).

(C) Relative changes in cytosolic Ca^{2+} concentration monitored by Fura2 ratio in HeLa cells cotransfected with H1 receptor and siControl, siE-Syt1 or siNir2. Cells were subjected to multiple pulses of 100 μM histamine treatment (arrows) in a perfusion system providing a constant flow of ECB. Average traces are shown (at least 6 wells from two independent experiments; each well contained at least 300 cells).

(D) Quantification of amplitude increases of each pulse from data shown in (C). Mean ± SD is shown (at least 6 wells from two independent experiments).

Chapter 7

Discussion

7.1 Feedback Regulation of Receptor-Induced Ca^{2+} Signaling

Based on these findings, I propose a model of a feedback mechanism for receptor-induced Ca^{2+} signaling (Figure 7-1). Stimulation of many cell surface receptors leads to the activation of PLC. Activated PLC hydrolyzes PIP_2 at the PM to generate IP_3 that mediates a release of ER Ca^{2+} to the cytosol through IP_3 receptors. E-Syt1 detects the elevation of cytosolic Ca^{2+} and translocates to ER-PM junctions, triggering an enhanced connection between the ER and the PM. This enhanced ER-to-PM connection facilitates Nir2 recruitment to ER-PM junctions. At these junctions, Nir2 may efficiently transfer PI synthesized in the ER to the PM for a subsequent conversion to PIP_2 to support receptor-induced Ca^{2+} signaling. In this model, elevation of cytosolic Ca^{2+} resulting from receptor-induced PIP_2 hydrolysis, enhancement of ER-to-PM connection mediated by the Ca^{2+} effector E-Syt1, and recruitment of Nir2 at ER-PM junctions to facilitate PI transfer together constitute a feedback mechanism to maintain PM PIP_2 level and to prepare the signaling system for additional stimulation.

7.2 Generation of MAPPER

Previous studies assumed that ER-PM junctions were transient structures that only inducibly form when they are needed (Lavieu et al., 2010; Orci et al., 2009; Varnai et al., 2007). In my study, I first demonstrate the existence of ER-PM junctions in live cells at the resting state using YFP-ER and TIRF microscopy. YFP-ER is an ER luminal marker that does not provide exogenous ER-to-PM tethers to create additional ER-PM junctions when expressed in cells. In comparison to ER tubules that undergo constantly remodeling in live cells, ER-PM junctions are extremely stable, indicating that they are not randomly formed and are likely maintained by molecular tethers. In addition, the existence of stable ER-PM junctions also suggests that they may participate in certain housekeeping functions in resting cells.

Understanding the abundance of endogenous ER-PM junctions is important because it serves as a baseline for further investigation of the mechanisms underlying the formation and regulation of ER-PM junctions.

Several methods have been developed previously to visualize ER-PM junctions in live mammalian cells (Dingsdale et al., 2013; Ercan et al., 2009; Lavieu et al., 2010; Varnai et al., 2007). These approaches often require multiple manipulations of the cells including transfections and treatment of pharmacological agents, which may lead to technical difficulties or experimental artifacts in studying the dynamic properties of ER-PM junctions. By generating MAPPER, a marker that contains minimal ER- and PM-targeting motifs, a fluorescent protein, and several rigid and flexible linkers in the cytosolic region setting the proper gap distance, I successfully labeled ER-PM junctions in live HeLa cells. This method only requires transfection of MAPPER and no further manipulation of cells. Thus, MAPPER can be easily applied to many imaging techniques including confocal microscopy, TIRF microscopy, EM, and super-resolution imaging. In addition, studying other cellular functions in the context of ER-PM junctions labeled by MAPPER is more feasible because of the minimal perturbation. Overexpression of proteins that localize to ER-PM junctions including STIM1, E-Syt2/E-Syt3, and JHPs often creates additional and bigger ER-PM junctions (Giordano et al., 2013; Min et al., 2007; Orci et al., 2009; Takeshima et al., 2000). These proteins have endogenous interacting partners and thus may cause changes in ER-PM junctions when overexpressed. By contrast, overexpression MAPPER, a synthetic protein without protein-interacting motifs, does not significantly affect area, density, or functions of ER-PM junctions. These results indicate that MAPPER is suitable for quantitative studies of the dynamic properties of ER-PM junctions. Moreover, in comparison to other methods MAPPER is more likely to label endogenous ER-PM junctions, because both its ER and PM targeting motifs were designed based on STIM1, a protein that localizes to ER-PM junctions. In addition, the design of flexible cytosolic linkers is of importance, because they provide elasticity and enable MAPPER to report the changes in gap distance of ER-PM junctions. This change in the gap distance is dynamic, which could explain why the change has never been observed in previous EM studies with prolonged (10 to 20 min) TG treatment (Luik et al., 2006; Lur

et al., 2009; Orci et al., 2009). Other ER-PM tethers with a design similar to MAPPER have been recently reported in fission yeast. These tethers constitutively localized to the cortical ER and suppressed the phenotype of the reduction of cortical ER caused by Scs2/Scs22 deletion (Zhang et al., 2012). It is likely that MAPPER may similarly facilitate the formation of ER-PM junctions by providing constitutive tethering, and may not be suitable for studying the formation of ER-PM junctions in siRNA or pharmacological inhibitor treated cells. In summary, the generation of MAPPER significantly advances our understanding of ER-PM junctions. MAPPER labels ER-PM junctions with minimal perturbation in live cells and reflects the dynamic properties of ER-PM junctions in details. In the future, MAPPER will be applied to investigate other cellular functions in the context of ER-PM junctions.

7.3 Area, Shape, and Distribution of ER-PM Junctions

The area and shape of MAPPER-labeled ER-PM junctions, as determined by super-resolution imaging, indicate that ER-PM junctions are a specialized ER subdomain distinct from tubules or cisternae. The average length of the short axis of ER-PM junctions was 157.7 nm and 176.1 nm as measured by PALM and STED imaging techniques, respectively. The short axis is longer than the diameter of ER tubules, at approximate 30 to 40 nm in yeast cells and at 50 to 120 nm in mammalian cells reported by EM and super-resolution imaging (Bernales et al., 2006; Shibata et al., 2010; Shim et al., 2012; West et al., 2011). Previous study in yeast demonstrated that the thickness of the ER lumen at ER-PM junctions, as measured by the distance from the PM face through the lumen to the cytosolic face, is similar to that of other ER subdomains (West et al., 2011). Thus, it is plausible to assume that ER-PM junctions are enlarged ER tubules. This idea is supported by the observation that the volume-to-surface area ratio of ER-PM junctions is slightly greater than that of tubules, indicating a larger lumen of these junctions (West et al., 2011). This unique shape is likely to be maintained by specific membrane shaping proteins. In yeast lacking tubule-generating proteins including Rtn1/Rtn2 and DP1/Yop1, extensive cisternae-like ER-PM junctions with a narrower thickness were observed, indicating the involvement of these proteins in shaping ER-PM junctions. It remains to be determined if ER-shaping proteins participate in generating

ER-PM junctions in mammalian cells. A recent report showed that E-Syt2 and E-Syt3 localize at ER-PM junctions and target to ER membrane via their hydrophobic segments similar to those in tubule-shaping proteins. These findings prompt the hypothesis that E-Syt2 and E-Syt3 may participate in shaping ER-PM junctions via their hydrophobic segments wedging ER membrane. In addition, E-Syt2 and E-Syt3 contribute to ER-to-PM tethering. The binding of E-Syt2/E-Syt3 to the PM may further stabilize the ER membrane, leading to the expansion of ER tubules into ER-PM junctions with larger lumen. Intriguingly, triple knockdown of all E-Syts displayed a 50% decrease in number of ER-PM junctions and a 75% decrease of PM coverage by ER-PM junctions. Although these results were determined by different methods, the greater decrease in PM coverage than in number of ER-PM junctions may reflect the smaller area of remaining ER-PM junctions. It is unclear whether E-Syts are involved in shaping ER membranes. Therefore, it will be of significance to test this membrane-shaping hypothesis to further understand the mechanisms of shaping ER-PM junctions.

In addition to the membrane-shaping molecules, other components, such as cortical cytoskeletons, may also play a role in determining the area and shape of ER-PM junctions. In most cells, actin is thought to be the main cytoskeletal component to form cortical meshwork (Jaqaman and Grinstein, 2012; Kusumi et al., 2011). This cortical actin network is in close apposition to the cytosolic leaflet of the PM within 10.2 nm to generate compartments underneath the PM with a diameter ranging from 100 to 300 nm as revealed by EM tomography (Morone et al., 2006). This partition serves as fences of the PM to confine the short-term diffusion of many transmembrane proteins and phospholipids to an area of 40 to 300 nm in diameter (Kusumi et al., 2011). Similar actin networks in sheet-like cell protrusions were also observed by dual-objective super-resolution imaging (Xu et al., 2012). The size of this cortical actin meshwork is remarkably similar to the size of ER-PM junctions labeled by MAPPER, implicating that this meshwork may contribute to define maximal size of ER-PM junctions. It would be interesting to test if cortical actin network plays a role in determining the area and shape of ER-PM junctions.

The meshwork of cortical actin with a set size likely explains the distance to nearest neighbor and the uniform distribution of ER-PM junctions. The minimal distance between two ER-PM junctions of 319 nm is consistent with the size of the cortical actin meshwork. Intriguingly, up to 70% of ER-PM junctions are either 619 nm or 925 nm away from each other indicating that they are often distributed periodically in every two or every three partitions generated by cortical actin meshwork. In addition, CytD treatment resulted in a drastic lateral movement of some ER-PM junctions indicating the change in distribution. It is not clear what determines the uniform distribution of ER-PM junctions. A recent study in yeast demonstrated that the distribution of cortical ER contributes to positioning the endocytosis events at the PM (Stradalova et al., 2012). Considering the PM is the interface to the extracellular environment, this uniform distribution of ER-PM junctions may reflect an optimal arrangement in which to coordinate other cellular functions within the limited PM space. In addition to cortical actin, septins have been shown to act as diffusion barriers at the PM in sperm annulus, at the base of cilia, and at the bases of dendritic spines in neurons (Mostowy and Cossart, 2012). Moreover, association of septins to cortical actin has been demonstrated and this interaction further regulates the turnover rate of septins (Hagiwara et al., 2011). A recent study showed that septin4 knockdown abolished STIM1-Orail interaction, implicating that ER-PM junctions may be likewise affected (Sharma et al., 2013). Furthermore, spectrins that are composed of 200-nm spectrin tetramers have been reported to assemble into cortical cytoskeletal network with actin and ankyrin (Bennett and Baines, 2001; Byers and Branton, 1985). Therefore, it is likely that multiple cortical cytoskeletal networks together define the meshwork that contributes to the distribution of ER-PM junctions.

7.4 Enhanced ER-to-PM Connection by E-Syt1

Using MAPPER and high-resolution TIRF microscopy, I demonstrate that changes in cytosolic Ca^{2+} levels dynamically regulate ER-PM junctions. In addition to new junction formation, my data suggests that a decrease in gap distance of ER-PM junctions occurs following elevation of cytosolic Ca^{2+}. The dynamic regulation of gap distance of ER-PM junctions has been suggested but never before

demonstrated. In yeast, the gap distance between cortical ER and the PM is in the range from 15.7 to 58.9 nm (West et al., 2011). Interestingly, Osh4p, with a diameter of 6 nm based on structural data, has been shown to localize at cortical ER. Osh4p only contains an OSBP-related domain (ORD) that has been implicated to bind two membranes simultaneously (Schulz et al., 2009). Thus, gap distance between the ER and PM in yeast is likely to be regulated for the retention of Osh4p in cortical ER. One other possibility is that Osh4p may interact with other components at ER-PM junctions to facilitate its accumulation. Consistent with the former idea, I demonstrate that a decrease in gap distance between the ER and PM facilitates the accumulation of Nir2 at ER-PM junctions to promote PIP_2 replenishment at PM. This data suggests that regulation of the gap distance of ER-PM junctions may lead to important functional consequences. On the other hand, the components localized at ER-PM junctions may also contribute to set the gap distance. Triad junctions lacking RyRs displayed a significant decrease in the gap distance from 12.1 ± 1.6 nm to 6.8 ± 1.9 nm (Takekura et al., 1995a). Consistently, ER-PM junctions artificially generated by overexpression of JPH-1 in amphibian embryos that do not express RyRs showed a gap distance of 7.6 ± 0.6 nm (Takeshima et al., 2000). These observations indicated RyRs may act as a spacer to set the gap distance of 12 nm by pushing the membranes away from each other. In addition, a relaxed type of dyad junctions with a gap distance of 30 nm have been reported in cardiac myocytes from embryos (Fawcett and McNutt, 1969; Takeshima et al., 2000). JPH-2 deficiency myotubes with remarkable reduction in 12-nm dyad junctions appeared to have the 30-nm dyad junctions unaffected. These results indicated that an unidentified tether, in addition to JPH-2, must exist to form the 30-nm junctions during heart development. Therefore, it is reasonable to postulate that multiple tethers with different lengths also exist in non-excitable cells to modulate the gap distance of ER-PM junctions during cellular processes.

SOCE is the best understood cellular function occurring at ER-PM junctions. Surprisingly, SOCE was not regulated by the enhanced ER-to-PM connection, as demonstrated in cells with E-Syt1 knockdown and MAPPER-s overexpression. This is consistent with the observation that STIM1

translocation was not affected in BAPTA-AM loaded cells in which the enhanced ER-to-PM connection was inhibited. These findings suggested that the cytosolic portion of STIM1 is long enough to reach to the PM and activate Orai1 at ER-PM junctions without the enhanced connection. Moreover, SOCE also appeared to be unaffected in E-Syt1/E-Syt2/E-Syt3 triple knockdown cells with a significant reduction of ER-PM junctions, implying that the number of ER-PM junctions is not a limiting factor for SOCE. Intriguingly, a sustained SOCE was observed in these triple knockdown cells, suggesting that Ca^{2+} dependent inactivation (CDI) of SOCE may be abolished. CDI is mediated by STIM1, Orai1, Ca^{2+}-bound calmodulin (CaM), and high Ca^{2+} levels at ER-PM junctions (Hoth and Penner, 1993; Litjens et al., 2004; Mullins et al., 2009; Zweifach and Lewis, 1995). The functions of STIM1 and Orai1 in these triple knockdown cells appeared to be unaffected as there was no defect in the initial phase of SOCE. Therefore, the decrease in CDI may result from the low Ca^{2+} levels at ER-PM junctions. It is reasonable to postulate that high Ca^{2+} levels will be generated at the mouth of activated Orai1, and the close apposition between the ER and PM may further create a restricted space to maintain the high Ca^{2+} levels during SOCE to facilitate CDI. This Ca^{2+} microdomains idea has been proposed for a long time. Several studies have demonstrated that Ca^{2+} levels underneath the PM are significantly higher than those in the cytosol (Rizzuto and Pozzan, 2006). However, the Ca^{2+} levels at ER-PM junctions during the resting state or during SOCE have never been directly measured because of the lack of a suitable tool. MAPPER contains a FRB domain in the cytosol capable of recruiting FKBP-linked Ca^{2+} indicators to selectively monitor Ca^{2+} concentration at single ER-PM junction resolution. This measurement may further reveal the distribution of Ca^{2+} microdomains during cellular processes. In addition, MAPPER-s and siE-Syt1 can be applied to test if the enhanced ER-to-PM connection contributes to the generation of Ca^{2+} microdomains.

The function of E-Syt1 has remained elusive since its identification (Min et al., 2007). My work reveals that E-Syt1 is a cytosolic Ca^{2+} effector that enhances the ER-to-PM connection and PIP_2 replenishment during receptor-induced Ca^{2+} signaling. I also demonstrate that the function of E-Syt1 is dependent on Ca^{2+} binding to the C2C domain and the subsequent translocation to ER-PM junctions

following increases in cytosolic Ca^{2+}. The C2E domain is also required for E-Syt1 translocation. This domain contains several basic residues similar to the C2C domain at the very C-termini of E-Syt2 and E-Syt3 to mediate PM targeting via PIP_2 binding (Giordano et al., 2013; Min et al., 2007). Therefore, it is likely that following C2C Ca^{2+} binding the C2E PM targeting motif is exposed leading to E-Syt1 translocation to enhance ER-to-PM connection.

Similar to E-Syt2 and E-Syt3, E-Syt1 also contains a hydrophobic segment for its ER membrane targeting. Thus, E-Syt1 translocation, following the elevation of cytosolic Ca^{2+}, may further increase membrane curvature at ER-PM junctions. Considering that high membrane curvature facilitates desorption of lipid molecules from membranes (McLean and Phillips, 1984), E-Syt1 may generate higher ER membrane curvature at ER-PM junctions to facilitate lipid extraction by Nir2. In addition to C2 domains, E-Syt1 contains a SMP domain. A bioinformatics study showed that SMP domain belongs to the TULIP (tubular lipid-binding proteins) domain superfamily. The structural data of these domains indicated the potential role in lipid trafficking by revealing a center tubular cavity that binds to lipid or other hydrophobic ligands (Kopec et al., 2010). Nevertheless, it is unclear whether the SMP domain-containing proteins directly transfer lipid though this cavity. In yeast, all SMP domain-containing proteins are localized to ER-organelle junctions (Toulmay and Prinz, 2012), implying that these junctions may be dynamically regulated by SMP domain-containing proteins. Further investigation of the molecular mechanisms underlying the E-Syt1-regulated ER-to-PM connection and identification of E-Syt1 interacting proteins may reveal the structural basis of ER-PM junctions and shed light on the regulation of other ER-organelle junctions.

7.5 Non-Vesicular PI Transfer at ER-PM Junctions

Non-vesicular lipid trafficking at ER-organelle junctions has been proposed to distribute lipids between the ER and specific organelles (Lev, 2012). In my study, I demonstrate that Nir2 is localized to ER-PM junctions and promotes PM PIP_2 replenishment during receptor-induced Ca^{2+} signaling. These

findings provide direct evidence supporting a long-standing hypothesis that PITPs mediate a cycle of phospholipid metabolism between the ER and the PM induced by receptor stimulation (Michell, 1975). It has been proposed that PITPs not only mediate PI transfer but may also present PI to its kinases (Cockcroft and Garner, 2011; Ile et al., 2006). It is difficult to test these hypotheses in cells since PI once at the PM is rapidly phosphorylated to generate PIP_2 and no suitable tool for selective PI labeling is currently available. Nonetheless, the observation that Nir2 localized at ER-PM junctions replenished PIP_2 more efficiently than that localized at PM following receptor activation suggests the likelihood of PI transfer at ER-PM junctions. A recent study proposed that PI is delivered to the PM by a highly mobile ER-derived PI-synthesizing compartment that makes repetitive contacts with the PM (Kim et al., 2011). The formation of these compartments requires Sar1 small GTPase, an essential component for COPII complex (Kim et al., 2011; Szul and Sztul, 2011). In addition, these PI-synthesizing compartments have been shown to colocalize with Sec31, an ER exit site marker, and Rab10 (English and Voeltz, 2013; Kim et al., 2011). These results suggested that vesicular trafficking mechanisms may participate in the delivery of PI from these compartments to the PM. However, the mechanisms remain elusive since no membrane fusion was observed when these compartments were making contacts with the PM (Kim et al., 2011). Given that the contacts between the PI-synthesizing compartments and the PM are not regulated during Ca^{2+} signaling, this could be a housekeeping mechanism that constantly provides PI to the PM in the resting state. PIP_2 at the PM involved in many cellular processes is of particular importance (Di Paolo and De Camilli, 2006). Therefore, multiple mechanisms may contribute to PI transfer to the PM to maintain PM PIP_2 levels.

Nir2 is ubiquitously expressed and is implicated in many cell functions including morphogenesis, cytokinesis, and the maintenance of diacylglycerol levels in Golgi (Lev et al., 1999; Litvak et al., 2005; Litvak et al., 2002; Tian et al., 2002). Nir2 deficient mice showed embryonic lethality indicating the requirement of Nir2 during development (Lu et al., 2001). Previously, Nir2 has been described as a peripheral Golgi protein (Litvak et al., 2002). In my study, Nir2-mCherry was localized to the cytosol in

resting cells and translocated to ER-PM junctions following receptor stimulation. The observation of Nir2 localization to ER-PM junctions is consistent with the localization of its *Drosophila* ortholog RdgBα revealed by EM studies (Vihtelic et al., 1993). Furthermore, I found that expression of Nir2-mCherry enhanced PIP_2 replenishment whereas siNir2 caused the opposite effect. These results suggest that the overexpressed Nir2 exerts functions similar to the endogenous Nir2 protein.

The translocation of Nir2 from the cytosol to ER-PM junctions suggests that it binds to the ER and the PM simultaneously following receptor stimulation. I and others demonstrated that Nir2 interacts with the ER membrane protein VAP-A and VAP-B via its FFAT motif (Amarilio et al., 2005). Enrichment of VAPs to ER-PM junctions by Nir2 may further recruit other FFAT-motif-containing proteins to mediate additional cellular functions (Lev et al., 2008). Nir2 only showed apparent translocation to ER-PM junctions with H1 receptor overexpression leading to substantial PIP_2 hydrolysis following receptor activation. This indicates that Nir2 targets to PM via a metabolic product following PIP_2 hydrolysis. A recent report showed that Nir2, either endogenous or overexpressed, translocates to PM via its LNS2 domain binding to PA (Kim et al., 2013), an intermediate product in PI cycle downstream of PIP_2 hydrolysis. This data imply that Nir2 senses the hydrolysis of PM PIP_2 and then translocates to ER-PM junctions to facilitate PIP_2 replenishment. Moreover, Nir2 recruitment to ER-PM junctions is dependent on an enhanced ER-to-PM connection as demonstrated by E-Syt1 knockdown and MAPPER-s overexpression. Based on these findings, I propose that the recruitment of Nir2 to ER-PM junctions during receptor-induced Ca^{2+} signaling requires that three events occur concurrently: (1) Nir2 interaction with VAPs in the ER membrane; (2) Nir2 PM targeting via PA binding; and (3) a decrease in gap distance of ER-PM junctions induced by increases in cytosolic Ca^{2+}. These events may serve as gates to prevent Nir2 translocation by cytosolic Ca^{2+} fluctuation without receptor-induced PIP_2 hydrolysis. In addition, these gates may ensure that PIP_2 replenishment occurs at ER-PM junctions near the subcellular loci of its hydrolysis.

I demonstrate that abortive Nir2 recruitment to ER-PM junctions by siE-Syt1 or knockdown of Nir2 by siNir2 led to abolished PIP_2 replenishment at PM accompanied by defective receptor-induced Ca^{2+} signaling in HeLa cells. These results are consistent to the defects in PIP_2 resynthesis and photo-transduction in flies lacking RdgBα (Hardie et al., 2001; Harris and Stark, 1977; Hotta and Benzer, 1970). The decrease in the amplitude of Ca^{2+} levels following histamine stimuli in both siE-Syt1 and siNir2 treated cells suggests the defects in the generation of IP_3 resulted from insufficient PM PIP_2 levels. In addition, I also observed sustained Ca^{2+} levels during the washout phase in siE-Syt1 and siNir2 treated cells, indicating that the Ca^{2+} clearance machinery was also affected. Given that PMCA activity is sensitive to PM PIP_2 levels (Hilgemann et al., 2001), the sustained Ca^{2+} levels may reflect a reduced PMCA activity. It has been shown that reconstitution of full length RdgBα or its PITP domain, or Nir2 in flies lacking RdgBα, was sufficient to rescue the electrophysiological defects and retinal degeneration (Chang et al., 1997; Milligan et al., 1997). This data further supports the idea that PI transfer and subsequent PIP_2 replenishment is essential to support receptor-induced Ca^{2+} signaling in *Drosophila* photoreceptor and in mammalian cells. Interestingly, Nir1 lacking the conserved PITP domain could partially rescue the degeneration phenotype but failed to restore photo-transduction. This observation implied that the ultrastructure of rhadbomeres may be maintained by a PI transfer-independent mechanism. Nonetheless, the mechanisms underlying the retinal degeneration phenotype remain unclear. All Nirs contain a FFAT motif and a LNS2 domain that have been shown to provide ER and PM targeting, respectively (Amarilio et al., 2005; Kim et al., 2013). Therefore, Nir1 might function as an ER-to-PM tether to rescue the retinal degeneration phenotype in mutant flies. One other possibility is that Nir1 may be involved in other steps of the PI cycle to elicit the rescue. The functional significance of Nir1 has been demonstrated in a human disease called autosomal dominant cone dystrophy. Patients with a mutation in Nir1 showed defective color vision, low visual acuity, and abnormal cone response (Kohn et al., 2008). However, the cellular functions of Nir1 remain to be determined. Nirs are multiple-domain containing proteins. Except for the PITP domain, the functions of rest of the domains have not been fully understood. Intriguingly, both DDHD and LNS2 domains have been implicated to be involved in PA metabolism

(Cockcroft, 2012). Thus, it is possible that Nirs may participate in multiple steps in the PI cycle. Further understanding of the cellular functions of Nirs may shed light on the mechanisms of PI cycle and its significance in the formation and regulation of ER-PM junctions.

7.6 Future Directions

The observations of my dissertation work raised several interesting questions. Firstly, the existence of stable ER-PM junctions implied the underlying structural components to tether the ER to the PM. MAPPER is highly concentrated at ER-PM junctions, and thus MAPPER can be applied as a bait to identify molecular components at ER-PM junctions using biochemical approaches. Secondly, to investigate the governing mechanisms behind the uniform distribution of ER-PM junctions is of importance. It is likely that cortical cytoskeletons may participate in determining this distribution. Understanding the distribution of ER-PM junctions may shed light on how different functional microdomains are arranged at PM. In addition, it is unclear how E-Syt1 translocation leads to the decrease in gap distance of ER-PM junctions. E-Syt1 may function by itself or together with other components at ER-PM junctions to shorten the gap distance. Investigating the mechanisms behind E-Syt1-mediated gap distance change may provide insights to the regulation of other ER-organelle junctions. Furthermore, MAPPER will be applied to understand to regulation of ER-PM junctions in other cellular processes, such as cell migration and mitosis.

7.7 Concluding Remarks

Feedback loops connect output signals to their original inputs and are important for maintaining cellular homeostasis (Brandman and Meyer, 2008). By generating MAPPER, I demonstrate a dynamic regulation of ER-PM junctions and the underlying mechanisms during Ca^{2+} signaling. These observations further reveal a feedback mechanism that connects cytosolic Ca^{2+} signals originating from receptor-induced PM PIP_2 hydrolysis back to the PM by PIP_2 replenishment via E-Syt1 and Nir2 at ER-PM

junctions. Overall, these findings provide mechanistic insights into the crosstalk between Ca^{2+} signaling and PIP_2 metabolism at ER-PM junctions.

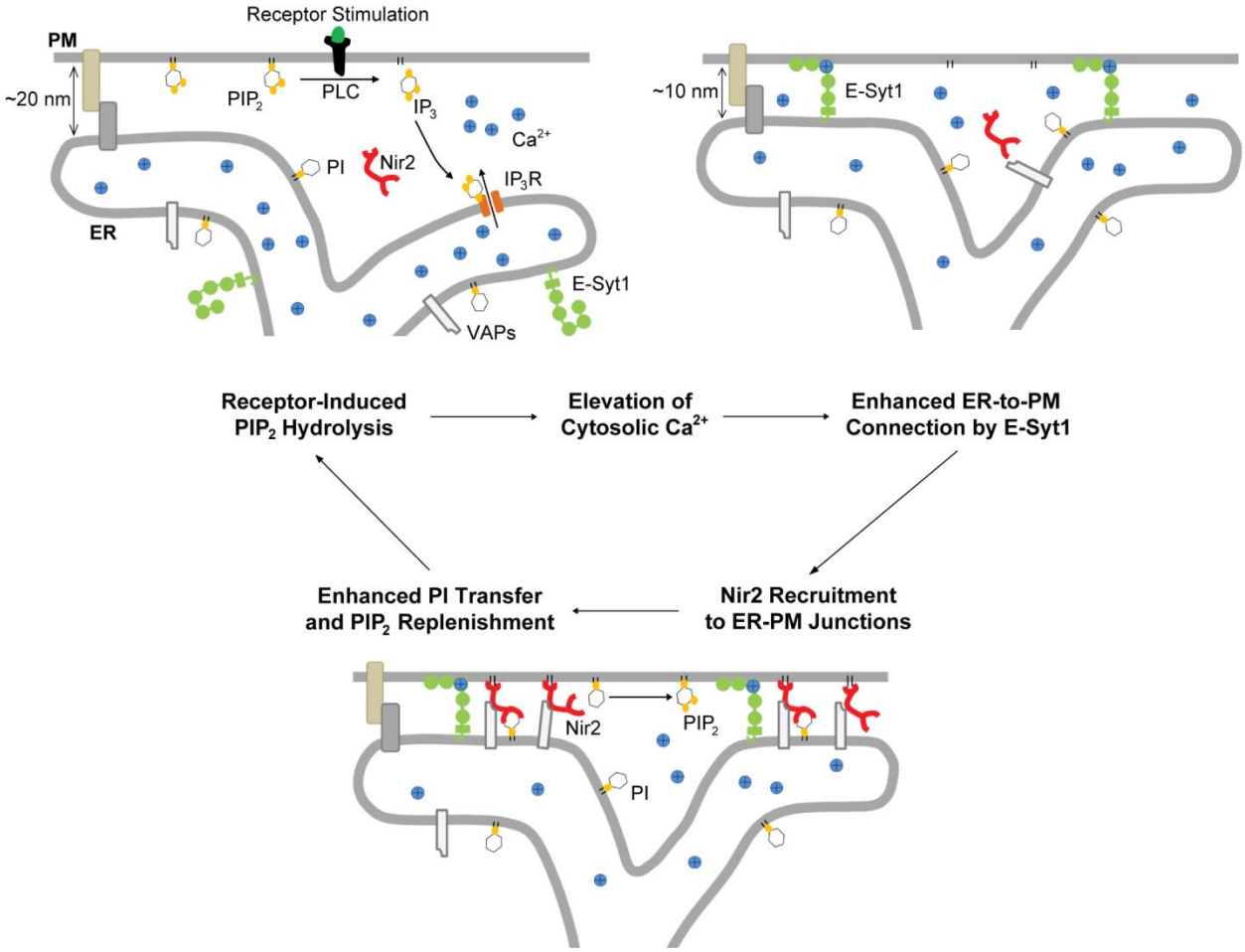

Figure 7-1. Model of a Feedback Mechanism for Receptor-Induced Ca^{2+} Signaling

Stimulation of numerous receptors activates PLC, which hydrolyzes PIP_2 at the PM to produce IP_3. IP_3 triggers a release of ER Ca^{2+} and an increase in cytosolic Ca^{2+}. Subsequently, E-Syt1 binds Ca^{2+} and translocates to ER-PM junctions to induce new junction formation and a decrease in gap distance between the ER and the PM. Enhancement

of ER-to-PM connection induced by E-Syt1 facilitates Nir2 recruitment to ER-PM junctions and PI transfer from the ER to the PM. PI is then converted to PIP_2 at the PM to support receptor-induced Ca^{2+} signaling.

Chapter 8

Materials and Methods

Reagents

Thapsigargin (TG), Pluronic F-127, BAPTA-AM, NP-EGTA, and Fura-2 AM were purchased from Invitrogen (Carlsbad, CA). All chemicals for extracellular buffer (ECB, 125 mM NaCl, 5 mM KCl, 1.5 mM $MgCl_2$, 20 mM HEPES, 10 mM glucose, and 1.5 mM $CaCl_2$, pH 7.4), 100X penicillin and streptomycin solutions, histamine, nocadazole (NocZ), cytochalasin D (CytD), and EGTA were obtained from Sigma (St. Louis, MO). siRNAs used in this study were generated as described previously (Liou et al., 2005). Primers used for siRNA generation are listed in Table 2.

Cell Culture and Transfection

HeLa cells purchased from ATCC (Manassas, VA) were cultured in MEM supplemented with 10% FBS (HyClone, Logan, UT) and 1X penicillin and streptomycin solution. DNA plasmids (15-50 ng) and siRNAs (10-25 nM) were transfected into HeLa cells with TransIT-LT1 reagent and TransIT-TKO reagent, respectively (Muris, Madison, WI).

DNA Constructs

mCherry-tagged human STIM1 (SP-mCherry-STIM1) was constructed by replacing the CFP portion of SP-CFP-STIM1 (Liou et al., 2005) with mCherry. Orai1-mCherry was constructed by replacing the YFP portion of Orai1-YFP (Varnai et al., 2007) with mCherry. mCherry-ER was constructed by replacing the sequence of STIM1 from SP-mCherry-STIM1 with oligonucleotides containing the coding sequence of KDEL and a stop codon. YFP-ER was described previously (Liou et al., 2005). mCherry-E-Syt1 was cloned by replacing the KDEL portion mCherry-ER with a E-Syt1 PCR fragment containing amino acids from residue 53 to residue 1104. E-Syt1-mCherry and Nir2-mCherry were cloned by replacing the Orai1

part of Orai1-mCherry with PCR fragments of full-length E-Syt1 or full-length Nir2, respectively. Both mCherry-E-Syt1 and E-Syt1-mCherry were cloned using In-Fusion-HD cloning kit (Clontech, Mountain View, CA), and E-Syt1 transcript 2 (NM_015292) was retrieved using PCR from a human cDNA library. Mutants of E-Syt1 and Nir2 were generated using QuickChange site-direct mutagenesis kit (Agilent Technologies, Santa Clara, CA) with oligonucleotides containing mutated coding sequences. mCherry-PLCδ-PH was constructed by replacing the GFP part of GFP-PLCδ-PH with mCherry. VAP-A-YFP and VAP-B-YFP were cloned by inserting PCR fragments containing full-length VAP-A and VAP-B into YFP-N1. All constructs listed here were verified by sequencing. All oligonucleotides used in this study are listed in Table 2.

MAPPER-s and MAPPER construction

MAPPER-s was constructed by replacing the mCherry-STIM1 portion of SP-mCherry-STIM with four fragments: 1) GFP or YFP; 2) STIM1 transmembrane (TM) domain (aa 195-240) with a downstream $(GA)_6$ linker PCR amplified from SP-mCherry-STIM1; 3) FKBP12-rapamycin-binding (FRB) with a downstream $(SAGG)_3$ linker PCR amplified from a FRB-STIM1 plasmid (Luik et al., 2008); 4) the polybasic tail (PB) digested from YFP-Rit tail (Heo et al., 2006) using EcoRI and BamHI. To generate MAPPER, two helical linkers, $(EAAAR)_4$ and $(EAAAR)_6$, were cloned into upstream and downstream flanking regions of the FRB, respectively. miniSOG-MAPPER was generated by insertion of PCR amplified miniSOG in between the SP and YFP of MAPPER using In-Fusion-HD cloning kit (Clontech, Mountain View, CA).

Electron Microscopy (EM)

1. miniSOG method

miniSOG-MAPPER were imaged following the method of Shu et al. with some modifications (Shu et al., 2011). In brief, cells grown on MatTek dishes (Ashland, MA) were rinsed to remove serum and fixed in 4% paraformaldehyde in 0.1M phosphate buffer pH7.4 containing 7.5% sucrose for 30

min at room temperature. Cells were washed with 0.1M phosphate buffer and placed on ice. All subsequent steps were done at 4°C. Aldehydes were blocked with 50mM ammonium chloride for 15 min. Cells washed first with phosphate buffer and transferred to 0.1M cacodylate buffer pH7.4. Nonspecific staining wwas blocked by incubating the cells with 50mM glycine, 10mM KCN and 20mM aminotriazole in 0.1 M cacodylate for 30 minutes. Fresh DAB (diaminobenzidine tetrahydrochloride) was prepared at concentration of 1mg/ml, filtered through 0.22 um filter and placed on ice until use. 20mM aminotriazole was added to the DAB solution prior to DAB addition to the cells to help lower nonspecific background.

DAB solution was added to the cells and oxygen was bubbled over the dishes. Cells of interest were identified by YFP or mCherry fluorescence. Cells were photobleached with FITC filter set with an Osram short arc lamp HXP for 3 to 5 minutes. Multiple regions on the same dish were exposed with a change in DAB solution after each exposure. DAB was removed from the cells. Dishes were rinsed with 0.1M cacodylate buffer, fixed with 2% glutaraldehye in 0.1M cacodylate buffer for 20 minutes, rinsed and post-fixed with 1% OsO_4 containing 0.08% potassium ferricyanide in 0.1 M cacodylate buffer for 60 min in the dark. After rinsing with buffer and water, dishes were stained en bloc with 4% uranyl acetate in 50% ethanol for 60 minutes, dehydrated through graded series of ethanol, infiltrated with Epon resin (2:1 and 1:2; ethanol and resin ratios) and embedded in 100% Epon. Beem capsules containing 100% resin were placed over the MaTTek coverslip and samples were polymerized in an oven overnight. MatTek coverslips were removed from the resin by immersing the capsule and MatTek dishes in liquid nitrogen.

The regions of interest were identified on the resin face by the corresponding letter and number pattern that had been photobleached . Ultrathin sections were cut on a microtome, placed on 100 mesh formvar coated grids and imaged on the FEI Tecnai Spirit G2 electron microscope at 120 keV equipped with a Gatan CCD camera.

2. Immunogold labeling method

Immunogold labeling of MAPPER was following the method of (Yamamoto and Masaki, 2010). Cells were rinsed to remove serum and fixed in 4% paraformaldehyde in 0.1M phosphate buffer pH7.4 containing 7.5% sucrose for 30 min at room temperature. Cells were washed with 0.1M phosphate buffer. Aldehydes were blocked with 50mM glycine for 15 min. Cells were permeabilized with 0.25% saponin in 0.1M phosphate for 30 minutes at room temperature, rinsed with 0.02% saponin and then blocked with 0.1M phosphate buffer containing 0.02% saponin, 1% BSA, 0.2% fish gelatin and 10% goat serum (blocking buffer) for 30 minutes. Cells were incubated with no antibody (control) or with monoclonal antibody rabbit anti-GFP (Life Technologies) overnight at 4°C. Cells were rinsed with 0.1 M phosphate buffer containing 0.02% saponin and 1% BSA. Secondary antibody (goat-anti rabbit Fab'-covalently conjugated to 1.4 nm nanogold particles (Nanoprobes, Inc) in blocking buffer was added to the cells and incubated for 2 hours at room temperature. Cells were rinsed with buffer containing 0.02% saponin and 1% BSA, then .02% saponin and finally just 0.1M phosphate buffer. Cells were fixed with 1% glutaraldehyde for 10 min. Aldehydes were blocked with 50 mM glycine. Cells were rinsed with phosphate buffer and then distilled water.

The 1.4 nm gold was intensified with the GoldEnhance EM (Nanoprobes) for 2 minute and immediately treated with freshly prepared 1 % (w/v) aqueous sodium thiosulfate solution. Cells were rinsed with water and placed in 0.1M cacodylate buffer pH 7.4. Cells were postfixed in OsO_4 and processed for electron microscopy as described above. Ultrathin sections were cut on a microtome and imaged on the Tenai G2 Spirit electron microscope without any further post-staining.

Live-Cell Confocal and TIRF Microscopy

HeLa cells were cultured and transfected on Lab-Tek chambered #1 coverglass (NUNC, Rochester, NY). Before imaging, cells were washed with ECB to remove the residual serum and phenol red. Live-cell confocal and TIRF imaging experiments were performed at room temperature (25°C) with 60X or 100X

objectives and a confocal-TIRF microscope custom-built using a Nikon Eclipse Ti microscope (Melville, NY). The microscope was controlled by Micro-Manager software (Edelstein et al., 2010). In order to manipulate intracellular Ca^{2+} levels, cells were loaded with 10 μM BAPTA-AM or 20 μM NP-EGTA in ECB containing 0.05% Pluronic F-127 and 0.1% of BSA at room temperature for 30 minutes. Loaded cells were then washed twice with ECB containing 0.1% BSA and incubated in ECB for another 15 to 30 minutes before the experiments. To release Ca^{2+} from NP-EGTA, cells were exposed to a 405-nm laser pulse for 400-800 ms at imaging rates of 6 sec or 10 sec per frame. The PM PIP_2 level was determined by the intensity of GFP-PLCδ-PH, mCherry-PLCδ-PH, or Tubby-GFP using TIRF microscopy, and an ND8 filter was introduced to the light path to prevent photobleaching.

Ca^{2+} Measurements

HeLa cells were loaded with 0.5 μM fura-2 AM in ECB containing 0.05% pluronic F-127 and 0.1% of BSA for 30 minutes at room temperature. Loaded cells were then washed twice with ECB containing 0.1% BSA, and incubated in ECB for another 15 to 30 minutes before the experiments. Single-cell Ca^{2+} images were taken with a 4X objective and an automated microscope custom-built on Nikon Eclipse Ti microscope. Changes of intracellular Ca^{2+} levels were indicated by the change of ratio of 510 nm excited at 340 nm to those at 380 nm (F340/F380). For periodic histamine stimulation experiments, Fura-2 loaded cells were placed in a perfusion system built in the lab providing a constant ECB flow of 1.5 to 2 ml per minute. Histamine (100 μM) was added every minute.

Photo-activated Localization Microscopy (PALM) Imaging and Analysis

PALM imaging was performed on Nikon N-STORM microscopy (Nikon Instruments Inc.) following the method of Jones et al (Jones et al., 2011). In brief, regions of interests were identified by minimal illumination of GFP fluorescence. Since ER-PM junctions are very close to the PM, we used a highly-oblique-incidence imaging geometry to reduce the background. mEos4h-MAPPER was activated by weak 405 nm laser and the activated mEos4h was imaged with a 561 nm laser in a continuous imaging mode.

The intensity of 405 nm laser was ramped up to compensate the photobleaching during imaging process. Camera rate was set to 62.5 frames per second. PALM images were generated using the build-in algorithm of Nikon Element software.

To further characterize ER-PM junctions, PALM images were first converted to binary images with an appropriate threshold that preserve individual structures. The converted binary images were then subjected to a morphological closing to smooth the outer edge and fill the inner holes of each identified structure. To remove the noise, incompletely-labeled structures and artificially enlarged ER-PM junctions caused by mEos4h-MAPPER overexpression, those with areas smaller than $75^2\pi$ nm^2 (150 nm in diameter) or larger than $150^2\pi$ nm^2 (300 nm in diameter) were excluded from the analysis. To measure the dimensional properties for the identified structures, the MATLAB (MathWorks) function regionprops was employed.

To characterize spatial distribution of ER-PM junctions, the distance from one centroid of an ER-PM junction to its nearest neighbor was first measured. The distribution of the distance to nearest neighbor was further analyzed using the MATLAB function gmdistribution.fit, which is based on an expectation-maximization algorithm and the Akaike information criterion, to construct a Gaussian mixture model. The Clark-Evans nearest neighbor measure together with a test of significance was the applied to quantify the degree to which the spatial distribution of ER-PM junctions deviates from random distribution (Clark and Evans, 1954).

Live-Cell Stimulated Emission Depletion (STED) Imaging and Analysis

Images were acquired with a custom-built CW STED microscope in which the excitation beam and depletion beam were delivered by a CW laser (491 nm, Calypso 25, Cobolt AB) and a 1W CW laser (VFL-P-1000-592, MPB Communications Inc). A vortex phase plate (VPP-1, RPC Photonics Inc) was used to create a central-zero doughnut-shaped depletion light in overlapping with the excitation beam to switch off the fluorophores in the region covered by the depletion beam. Two laser lights were focused

onto the sample plane by a 100X oil immersion objective (Olympus UPLSAPO100x-1.4 NA). The fluorescence was cleaned via a 535/22 band-pass filter and then photos were registered by an avalanche photodiode (APD) single photon counting module (SPCM-AQR-15, PerkinElmer Optoelectronics). Images were reconstructed pixel-by-pixel using a three-axis piezostage scanner (Nano-PDQ375HS, Mad City Labs Inc) (Yang et al., 2013).

HeLa cells were grown on glass-bottom dishes in DMEM supplemented with 10% FBS and Pen-Strep at 37°C and 5% CO_2 for 48 hours. The media were changed with phenol red-free DMEM prior to imaging. TG was pre-diluted to 5μM in the culture media and maintained at 37°C. STED imaging of the cells were first acquired before the treatment of TG and then the 5μM TG solution was added into the dishes to make the final working concentration of 1μM. The same cells with treatment were imaged again by STED microscopy around 3 to 5 minutes after adding TG.

STED Images were acquired over an area up to 20 μm by 20 μm with a pixel size of 25 nm and a dwell time of 20 μs per pixels. The STED image shown was processed by a mean filter of 2 pixels, background subtraction of 50 pixels, and contrast stretching using ImageJ. The STED images for dimensional analysis were first denoised by a mean filter of 0.5 pixels and then each junction was analyzed using a fitting routine written in Matlab with a two-dimension Gaussian function to statically estimate their width along the direction of major or minor axis of the fitted Gaussian function.

Image Analyses

To determine the intensity change of individual ER-PM junctions, at least 30 stable puncta were selected in each cell from MAPPER-s or MAPPER TIRF images. The intensity traces of selected regions from the same cell were background subtracted, normalized to time zero, and averaged. To obtain the total number of ER-PM junctions in each cell, TIRF images of cells expressing MAPPER-s or MAPPER were background subtracted and subjected to Fourier transform with a high-pass filter to create “binary-like” images that helped identify dim puncta and define the edges. The transformed images were subjected to

threshold analysis to obtain the total number of ER-PM junctions. PM areas detected by a fluorescent PM marker were measured to obtain the density of ER-PM junctions. For the analyses of E-Syt1 or Nir2 translocation, puncta of E-Syt1 or Nir2 from TIRF or confocal images were selected. The intensity traces of selected regions from the same cell were background subtracted, normalized to time zero, and averaged. To determine the maximal fold increase of Nir2 at ER-PM junctions, moving averages of 5 consecutive data points were applied to smooth out the fluctuations of Nir2 translocation traces.

Statistical Analyses

Data were statistically analyzed by t-test or one-way analysis of variance (ANOVA) using SigmaPlot software (Systat Software Inc., San Jose, CA).

Table 3. Oligonucleotides used in this study.

Name	Sequence (5'- 3')
STIM1-TM-F	ggactagtctggatacagtgctctttgg
STIM1-TM-R	ggctcgagagcacctgctccagctccggcaccagcgcccgctccgtgctccttggagtaacggt
FRB-F	ggctcgagatcctctggcatgagatgtg
FRB-R	gggaattctacctccggcagagccacctgcactgcctccagctgactttgagattcgtcggaacac
PB-F	atcggaattctaatggagaaaaaatctaagcc
PB-R	atcgggatcctcaagttactgaatctttcttc
Linker EcoRI-F	attctagaagctgctgctagagaagctgctgctagagaagctgctgctagagaagctgctgctagagaagctgctgctagagaagctgctgctagagc
Linker EcoRI-R	aattgctctagcagcagcttctctagcagcagcttctctagcagcagcttctctagcagcagcttctctagcagcagcttctctagcagcagcttctag
Linker XhoI-F	tcgaggaagcagcagcacgagaagctgctgctagagaagctgctgctagagaagcagcagcacgag
Linker XhoI-R	tcgactcgtgctgctgcttctctagcagcagcttctctagcagcagcttctcgtgctgctgcttcc
miniSOG-F	ggccagagcctcgcaccggtcgagaaaagtttcgtgataactgat
miniSOG-R	ctcaccatggtggcgaccggtgctccatccagctgcactcc
KDEL-F	ctagtaaggacgagctgtaaa
KDEL-R	gatctttacagctcgtcctta
mCherry-E-Syt1-F	tccggatcaactagtgcggtgctgacttcattcg
mCherry-E-Syt1-R	agatccggtggatccctaggagctgcccttgtcctt
E-Syt1-mCherry-F	gtcagatccgctagcgacaatggagcgatctccag
E-Syt1-mCherry-R	accagcacctgaattcgcggagctgcccttgtcctt
E-Syt1-D406A-F	gaggtgttcgacaaggctccagataaagatgactttctg
E-Syt1-D406A-R	gtcatctttatctggagccttgtcgaacacctccacttc
E-Syt1-D724A-F	gaagtctttgacaaggccttggacaaggatgattttctgg

E-Syt1-D724A-R	atcatccttgtccaaggccttgtcaaagacttcaacctc
Nir2-mCherry-F	atcggctagccaggatgctcatcaaggaat
Nir2-mCherry-R	atcggaattcgcctcctcgctgtccagctt
Nir2-T59E-F	Agcgggcaatacgaacacaaggtgtaccacgtggg
Nir2-T59E-R	gtggtacaccttgtgttcgtattgcccgctgcccc
Nir2-K61A-F	caatacacacacgcggtgtaccacgtgggctccc
Nir2-K61A-R	cacgtggtacaccgcgtgtgtgtattgcccgctgc
Nir2-N90F-F	gaggaatcctggtttgcctacccctacacccg
Nir2-N90F-R	gtaggggtaggcaaaccaggattcctcttctacctg
Nir2-FM-F	gctccgaggaagcgttgttggctggccacgaaggcttctcggacagt
Nir2-FM-F	gaagccttcgtggccagccaacaacgcttcctcggagctgttctca
VAP-A-YFP-F	atcggctagcggaacatggcgtccgcctcaggg
VAP-A-YFP-R	atcggaattctcaagatgaatttccctagaaagaatcc
VAP-B-YFP-F	atcggctagcggaacatggcgaaggtgg
VAP-B-YFP-R	atcggaattctcaaggcaatcttcccaataattac
siE-Syt1cdsF	gcgtaatacgactcactataggctggtgtcccagcactc
siE-Syt1cdsR	gcgtaatacgactcactatagggttgtccatcaggtcatacc
siE-Syt13’UTRF	gcgtaatacgactcactatagggcctgactgctctgtcttcc
siE-Syt13’UTRR	gcgtaatacgactcactatagggaagtcctccaaagccctctc
siNir2cdsF	gcgtaatacgactcactataggtcgtgtatgtcacaggcc
siNir2cdsR	gcgtaatacgactcactataggcaggctgatgctccg

BIBLIOGRAPHY

Aikawa, Y., Kuraoka, A., Kondo, H., Kawabuchi, M., and Watanabe, T. (1999). Involvement of PITPnm, a mammalian homologue of Drosophila rdgB, in phosphoinositide synthesis on Golgi membranes. J Biol Chem *274*, 20569-20577.

Airey, J.A., Beck, C.F., Murakami, K., Tanksley, S.J., Deerinck, T.J., Ellisman, M.H., and Sutko, J.L. (1990). Identification and localization of two triad junctional foot protein isoforms in mature avian fast twitch skeletal muscle. J Biol Chem *265*, 14187-14194.

Amarilio, R., Ramachandran, S., Sabanay, H., and Lev, S. (2005). Differential regulation of endoplasmic reticulum structure through VAP-Nir protein interaction. J Biol Chem *280*, 5934-5944.

Arregui, C.O., Balsamo, J., and Lilien, J. (1998). Impaired integrin-mediated adhesion and signaling in fibroblasts expressing a dominant-negative mutant PTP1B. J Cell Biol *143*, 861-873.

Baba, Y., Nishida, K., Fujii, Y., Hirano, T., Hikida, M., and Kurosaki, T. (2008). Essential function for the calcium sensor STIM1 in mast cell activation and anaphylactic responses. Nat Immunol *9*, 81-88.

Bai, J., and Pagano, R.E. (1997). Measurement of spontaneous transfer and transbilayer movement of BODIPY-labeled lipids in lipid vesicles. Biochemistry *36*, 8840-8848.

Baumann, O., and Walz, B. (2001). Endoplasmic reticulum of animal cells and its organization into structural and functional domains. International review of cytology *205*, 149-214.

Bennett, V., and Baines, A.J. (2001). Spectrin and ankyrin-based pathways: metazoan inventions for integrating cells into tissues. Physiol Rev *81*, 1353-1392.

Bernales, S., McDonald, K.L., and Walter, P. (2006). Autophagy counterbalances endoplasmic reticulum expansion during the unfolded protein response. PLoS biology *4*, e423.

Berridge, M.J., Lipp, P., and Bootman, M.D. (2000). The versatility and universality of calcium signalling. Nat Rev Mol Cell Biol *1*, 11-21.

Betzig, E., Patterson, G.H., Sougrat, R., Lindwasser, O.W., Olenych, S., Bonifacino, J.S., Davidson, M.W., Lippincott-Schwartz, J., and Hess, H.F. (2006). Imaging intracellular fluorescent proteins at nanometer resolution. Science *313*, 1642-1645.

Boute, N., Boubekeur, S., Lacasa, D., and Issad, T. (2003). Dynamics of the interaction between the insulin receptor and protein tyrosine-phosphatase 1B in living cells. EMBO Rep *4*, 313-319.

Brandman, O., and Meyer, T. (2008). Feedback loops shape cellular signals in space and time. Science *322*, 390-395.

Byers, T.J., and Branton, D. (1985). Visualization of the protein associations in the erythrocyte membrane skeleton. Proc Natl Acad Sci U S A *82*, 6153-6157.

Cai, H., Reinisch, K., and Ferro-Novick, S. (2007). Coats, tethers, Rabs, and SNAREs work together to mediate the intracellular destination of a transport vesicle. Dev Cell *12*, 671-682.

Carrasco, S., and Meyer, T. (2011). STIM proteins and the endoplasmic reticulum-plasma membrane junctions. Annual review of biochemistry *80*, 973-1000.

Chang, J.T., Milligan, S., Li, Y., Chew, C.E., Wiggs, J., Copeland, N.G., Jenkins, N.A., Campochiaro, P.A., Hyde, D.R., and Zack, D.J. (1997). Mammalian homolog of Drosophila retinal degeneration B rescues the mutant fly phenotype. The Journal of neuroscience : the official journal of the Society for Neuroscience *17*, 5881-5890.

Cheng, A., Bal, G.S., Kennedy, B.P., and Tremblay, M.L. (2001). Attenuation of adhesion-dependent signaling and cell spreading in transformed fibroblasts lacking protein tyrosine phosphatase-1B. J Biol Chem *276*, 25848-25855.

Clark, P.J., and Evans, F.C. (1954). Distance to nearest neighbor as a measure of spatial relationships in populations. Ecology, 445-453.

Cockcroft, S. (2012). The diverse functions of phosphatidylinositol transfer proteins. Current topics in microbiology and immunology *362*, 185-208.

Cockcroft, S., and Garner, K. (2011). Function of the phosphatidylinositol transfer protein gene family: is phosphatidylinositol transfer the mechanism of action? Critical reviews in biochemistry and molecular biology *46*, 89-117.

Cockcroft, S., and Garner, K. (2013). Potential role for phosphatidylinositol transfer protein (PITP) family in lipid transfer during phospholipase C signalling. Advances in biological regulation *53*, 280-291.

Csordas, G., Renken, C., Varnai, P., Walter, L., Weaver, D., Buttle, K.F., Balla, T., Mannella, C.A., and Hajnoczky, G. (2006). Structural and functional features and significance of the physical linkage between ER and mitochondria. J Cell Biol *174*, 915-921.

D'Angelo, G., Vicinanza, M., and De Matteis, M.A. (2008). Lipid-transfer proteins in biosynthetic pathways. Curr Opin Cell Biol *20*, 360-370.

Darbellay, B., Arnaudeau, S., Bader, C.R., Konig, S., and Bernheim, L. (2011). STIM1L is a new actin-binding splice variant involved in fast repetitive Ca2+ release. J Cell Biol *194*, 335-346.

de Brito, O.M., and Scorrano, L. (2008). Mitofusin 2 tethers endoplasmic reticulum to mitochondria. Nature *456*, 605-610.

de Brouwer, A.P., Versluis, C., Westerman, J., Roelofsen, B., Heck, A.J., and Wirtz, K.W. (2002). Determination of the stability of the noncovalent phospholipid transfer protein-lipid complex by electrospray time-of-flight mass spectrometry. Biochemistry *41*, 8013-8018.

De Matteis, M.A., and D'Angelo, G. (2007). The role of the phosphoinositides at the Golgi complex. Biochemical Society symposium, 107-116.

Di Paolo, G., and De Camilli, P. (2006). Phosphoinositides in cell regulation and membrane dynamics. Nature *443*, 651-657.

Dingsdale, H., Okeke, E., Awais, M., Haynes, L., Criddle, D.N., Sutton, R., and Tepikin, A.V. (2013). Saltatory formation, sliding and dissolution of ER-PM junctions in migrating cancer cells. Biochem J *451*, 25-32.

Dupont, G., Combettes, L., Bird, G.S., and Putney, J.W. (2011). Calcium oscillations. Cold Spring Harbor perspectives in biology *3*.

Edelstein, A., Amodaj, N., Hoover, K., Vale, R., and Stuurman, N. (2010). Computer control of microscopes using microManager. Curr Protoc Mol Biol *Chapter 14*, Unit14 20.

Eden, E.R., White, I.J., Tsapara, A., and Futter, C.E. (2010). Membrane contacts between endosomes and ER provide sites for PTP1B-epidermal growth factor receptor interaction. Nat Cell Biol *12*, 267-272.

Endo, M. (2009). Calcium-induced calcium release in skeletal muscle. Physiol Rev *89*, 1153-1176.

English, A.R., and Voeltz, G.K. (2013). Rab10 GTPase regulates ER dynamics and morphology. Nat Cell Biol *15*, 169-178.

Ercan, E., Momburg, F., Engel, U., Temmerman, K., Nickel, W., and Seedorf, M. (2009). A conserved, lipid-mediated sorting mechanism of yeast Ist2 and mammalian STIM proteins to the peripheral ER. Traffic *10*, 1802-1818.

Fawcett, D.W., and McNutt, N.S. (1969). The ultrastructure of the cat myocardium. I. Ventricular papillary muscle. J Cell Biol *42*, 1-45.

Fenteany, G., and Zhu, S. (2003). Small-molecule inhibitors of actin dynamics and cell motility. Curr Top Med Chem *3*, 593-616.

Feske, S., Gwack, Y., Prakriya, M., Srikanth, S., Puppel, S.H., Tanasa, B., Hogan, P.G., Lewis, R.S., Daly, M., and Rao, A. (2006). A mutation in Orai1 causes immune deficiency by abrogating CRAC channel function. Nature *441*, 179-185.

Feske, S., Picard, C., and Fischer, A. (2010). Immunodeficiency due to mutations in ORAI1 and STIM1. Clin Immunol *135*, 169-182.

Flucher, B.E. (1992). Structural analysis of muscle development: transverse tubules, sarcoplasmic reticulum, and the triad. Dev Biol *154*, 245-260.

Flucher, B.E., Phillips, J.L., and Powell, J.A. (1991). Dihydropyridine receptor alpha subunits in normal and dysgenic muscle in vitro: expression of alpha 1 is required for proper targeting and distribution of alpha 2. J Cell Biol *115*, 1345-1356.

Fosset, M., Jaimovich, E., Delpont, E., and Lazdunski, M. (1983). [3H]nitrendipine receptors in skeletal muscle. J Biol Chem *258*, 6086-6092.

Foti, M., Audhya, A., and Emr, S.D. (2001). Sac1 lipid phosphatase and Stt4 phosphatidylinositol 4-kinase regulate a pool of phosphatidylinositol 4-phosphate that functions in the control of the actin cytoskeleton and vacuole morphology. Mol Biol Cell *12*, 2396-2411.

Fox, P.D., Haberkorn, C.J., Weigel, A.V., Higgins, J.L., Akin, E.J., Kennedy, M.J., Krapf, D., and Tamkun, M.M. (2013). Plasma membrane domains enriched in cortical endoplasmic reticulum function as membrane protein trafficking hubs. Mol Biol Cell *24*, 2703-2713.

Frangioni, J.V., Beahm, P.H., Shifrin, V., Jost, C.A., and Neel, B.G. (1992). The nontransmembrane tyrosine phosphatase PTP-1B localizes to the endoplasmic reticulum via its 35 amino acid C-terminal sequence. Cell *68*, 545-560.

Franzini-Armstrong, C. (1972). Studies of the triad. 3. Structure of the junction in fast twitch fibers. Tissue & cell *4*, 469-478.

Franzini-Armstrong, C., and Jorgensen, A.O. (1994). Structure and development of E-C coupling units in skeletal muscle. Annual review of physiology *56*, 509-534.

Franzini-Armstrong, C., Pincon-Raymond, M., and Rieger, F. (1991). Muscle fibers from dysgenic mouse in vivo lack a surface component of peripheral couplings. Dev Biol *146*, 364-376.

Fujii, Y., Shiota, M., Ohkawa, Y., Baba, A., Wanibuchi, H., Kinashi, T., Kurosaki, T., and Baba, Y. (2012). Surf4 modulates STIM1-dependent calcium entry. Biochem Biophys Res Commun *422*, 615-620.

Garbino, A., van Oort, R.J., Dixit, S.S., Landstrom, A.P., Ackerman, M.J., and Wehrens, X.H. (2009). Molecular evolution of the junctophilin gene family. Physiol Genomics *37*, 175-186.

Gardiner, D.M., and Grey, R.D. (1983). Membrane junctions in Xenopus eggs: their distribution suggests a role in calcium regulation. J Cell Biol *96*, 1159-1163.

Garner, K., Hunt, A.N., Koster, G., Somerharju, P., Groves, E., Li, M., Raghu, P., Holic, R., and Cockcroft, S. (2012). Phosphatidylinositol transfer protein, cytoplasmic 1 (PITPNC1) binds and transfers phosphatidic acid. J Biol Chem *287*, 32263-32276.

Giordano, F., Saheki, Y., Idevall-Hagren, O., Colombo, S.F., Pirruccello, M., Milosevic, I., Gracheva, E.O., Bagriantsev, S.N., Borgese, N., and De Camilli, P. (2013). PI(4,5)P(2)-dependent and Ca(2+)-regulated ER-PM interactions mediated by the extended synaptotagmins. Cell *153*, 1494-1509.

Guo, S., Stolz, L.E., Lemrow, S.M., and York, J.D. (1999). SAC1-like domains of yeast SAC1, INP52, and INP53 and of human synaptojanin encode polyphosphoinositide phosphatases. J Biol Chem *274*, 12990-12995.

Gwack, Y., Srikanth, S., Oh-Hora, M., Hogan, P.G., Lamperti, E.D., Yamashita, M., Gelinas, C., Neems, D.S., Sasaki, Y., Feske, S., *et al.* (2008). Hair loss and defective T- and B-cell function in mice lacking ORAI1. Mol Cell Biol *28*, 5209-5222.

Hagiwara, A., Tanaka, Y., Hikawa, R., Morone, N., Kusumi, A., Kimura, H., and Kinoshita, M. (2011). Submembranous septins as relatively stable components of actin-based membrane skeleton. Cytoskeleton *68*, 512-525.

Haj, F.G., Verveer, P.J., Squire, A., Neel, B.G., and Bastiaens, P.I. (2002). Imaging sites of receptor dephosphorylation by PTP1B on the surface of the endoplasmic reticulum. Science *295*, 1708-1711.

Hanada, K., Kumagai, K., Yasuda, S., Miura, Y., Kawano, M., Fukasawa, M., and Nishijima, M. (2003). Molecular machinery for non-vesicular trafficking of ceramide. Nature *426*, 803-809.

Hardie, R.C., Raghu, P., Moore, S., Juusola, M., Baines, R.A., and Sweeney, S.T. (2001). Calcium influx via TRP channels is required to maintain PIP2 levels in Drosophila photoreceptors. Neuron *30*, 149-159.

Harris, W.A., and Stark, W.S. (1977). Hereditary retinal degeneration in Drosophila melanogaster. A mutant defect associated with the phototransduction process. J Gen Physiol *69*, 261-291.

Henkart, M., Landis, D.M., and Reese, T.S. (1976). Similarity of junctions between plasma membranes and endoplasmic reticulum in muscle and neurons. J Cell Biol *70*, 338-347.

Henkart, M.P., and Nelson, P.G. (1979). Evidence for an intracellular calcium store releasable by surface stimuli ifibroblasts (L cells). J Gen Physiol *73*, 655-673.

Heo, W.D., Inoue, T., Park, W.S., Kim, M.L., Park, B.O., Wandless, T.J., and Meyer, T. (2006). PI(3,4,5)P3 and PI(4,5)P2 lipids target proteins with polybasic clusters to the plasma membrane. Science *314*, 1458-1461.

Hernandez, M.V., Sala, M.G., Balsamo, J., Lilien, J., and Arregui, C.O. (2006). ER-bound PTP1B is targeted to newly forming cell-matrix adhesions. J Cell Sci *119*, 1233-1243.

Hilgemann, D.W., Feng, S., and Nasuhoglu, C. (2001). The complex and intriguing lives of PIP2 with ion channels and transporters. Science's STKE : signal transduction knowledge environment *2001*, re19.

Hirata, Y., Brotto, M., Weisleder, N., Chu, Y., Lin, P., Zhao, X., Thornton, A., Komazaki, S., Takeshima, H., Ma, J., *et al.* (2006). Uncoupling store-operated Ca2+ entry and altered Ca2+ release from sarcoplasmic reticulum through silencing of junctophilin genes. Biophys J *90*, 4418-4427.

Hogan, P.G., Lewis, R.S., and Rao, A. (2010). Molecular basis of calcium signaling in lymphocytes: STIM and ORAI. Annu Rev Immunol *28*, 491-533.

Holthuis, J.C., and Levine, T.P. (2005). Lipid traffic: floppy drives and a superhighway. Nat Rev Mol Cell Biol *6*, 209-220.

Hoth, M., and Penner, R. (1992). Depletion of intracellular calcium stores activates a calcium current in mast cells. Nature *355*, 353-356.

Hoth, M., and Penner, R. (1993). Calcium release-activated calcium current in rat mast cells. J Physiol *465*, 359-386.

Hotta, Y., and Benzer, S. (1970). Genetic dissection of the Drosophila nervous system by means of mosaics. Proc Natl Acad Sci U S A *67*, 1156-1163.

Hu, J., Shibata, Y., Voss, C., Shemesh, T., Li, Z., Coughlin, M., Kozlov, M.M., Rapoport, T.A., and Prinz, W.A. (2008). Membrane proteins of the endoplasmic reticulum induce high-curvature tubules. Science *319*, 1247-1250.

Hu, J., Shibata, Y., Zhu, P.P., Voss, C., Rismanchi, N., Prinz, W.A., Rapoport, T.A., and Blackstone, C. (2009). A class of dynamin-like GTPases involved in the generation of the tubular ER network. Cell *138*, 549-561.

Ikemoto, T., Komazaki, S., Takeshima, H., Nishi, M., Noda, T., Iino, M., and Endo, M. (1997). Functional and morphological features of skeletal muscle from mutant mice lacking both type 1 and type 3 ryanodine receptors. J Physiol *501 (Pt 2)*, 305-312.

Ile, K.E., Schaaf, G., and Bankaitis, V.A. (2006). Phosphatidylinositol transfer proteins and cellular nanoreactors for lipid signaling. Nature chemical biology *2*, 576-583.

Jaqaman, K., and Grinstein, S. (2012). Regulation from within: the cytoskeleton in transmembrane signaling. Trends Cell Biol *22*, 515-526.

Jones, S.A., Shim, S.H., He, J., and Zhuang, X. (2011). Fast, three-dimensional super-resolution imaging of live cells. Nat Methods *8*, 499-508.

Kaplan, M.R., and Simoni, R.D. (1985). Intracellular transport of phosphatidylcholine to the plasma membrane. J Cell Biol *101*, 441-445.

Kawasaki, T., Lange, I., and Feske, S. (2009). A minimal regulatory domain in the C terminus of STIM1 binds to and activates ORAI1 CRAC channels. Biochem Biophys Res Commun *385*, 49-54.

Kim, S., Kedan, A., Marom, M., Gavert, N., Keinan, O., Selitrennik, M., Laufman, O., and Lev, S. (2013). The phosphatidylinositol-transfer protein Nir2 binds phosphatidic acid and positively regulates phosphoinositide signalling. EMBO Rep *14*, 891-899.

Kim, Y.J., Guzman-Hernandez, M.L., and Balla, T. (2011). A highly dynamic ER-derived phosphatidylinositol-synthesizing organelle supplies phosphoinositides to cellular membranes. Dev Cell *21*, 813-824.

Kohn, L., Kadzhaev, K., Burstedt, M.S., Haraldsson, S., Sandgren, O., and Golovleva, I. (2008). Mutation in the PYK2-binding domain of PITPNM3 causes autosomal dominant cone dystrophy (CORD5) in two Swedish families. Adv Exp Med Biol *613*, 229-234.

Kopec, K.O., Alva, V., and Lupas, A.N. (2010). Homology of SMP domains to the TULIP superfamily of lipid-binding proteins provides a structural basis for lipid exchange between ER and mitochondria. Bioinformatics *26*, 1927-1931.

Korzeniowski, M.K., Popovic, M.A., Szentpetery, Z., Varnai, P., Stojilkovic, S.S., and Balla, T. (2009). Dependence of STIM1/Orai1-mediated calcium entry on plasma membrane phosphoinositides. J Biol Chem *284*, 21027-21035.

Krapivinsky, G., Krapivinsky, L., Stotz, S.C., Manasian, Y., and Clapham, D.E. (2011). POST, partner of stromal interaction molecule 1 (STIM1), targets STIM1 to multiple transporters. Proc Natl Acad Sci U S A *108*, 19234-19239.

Kusumi, A., Suzuki, K.G., Kasai, R.S., Ritchie, K., and Fujiwara, T.K. (2011). Hierarchical mesoscale domain organization of the plasma membrane. Trends in biochemical sciences *36*, 604-615.

Lalanne, F., and Ponsin, G. (2000). Mechanism of the phospholipid transfer protein-mediated transfer of phospholipids from model lipid vesicles to high density lipoproteins. Biochim Biophys Acta *1487*, 82-91.

Launikonis, B.S., and Rios, E. (2007). Store-operated Ca2+ entry during intracellular Ca2+ release in mammalian skeletal muscle. J Physiol *583*, 81-97.

Lavieu, G., Orci, L., Shi, L., Geiling, M., Ravazzola, M., Wieland, F., Cosson, P., and Rothman, J.E. (2010). Induction of cortical endoplasmic reticulum by dimerization of a coatomer-binding peptide anchored to endoplasmic reticulum membranes. Proc Natl Acad Sci U S A *107*, 6876-6881.

Lee, I., and Hong, W. (2006). Diverse membrane-associated proteins contain a novel SMP domain. FASEB J *20*, 202-206.

Lev, S. (2010). Non-vesicular lipid transport by lipid-transfer proteins and beyond. Nat Rev Mol Cell Biol *11*, 739-750.

Lev, S. (2012). Nonvesicular lipid transfer from the endoplasmic reticulum. Cold Spring Harbor perspectives in biology *4*.

Lev, S., Ben Halevy, D., Peretti, D., and Dahan, N. (2008). The VAP protein family: from cellular functions to motor neuron disease. Trends Cell Biol *18*, 282-290.

Lev, S., Hernandez, J., Martinez, R., Chen, A., Plowman, G., and Schlessinger, J. (1999). Identification of a novel family of targets of PYK2 related to Drosophila retinal degeneration B (rdgB) protein. Mol Cell Biol *19*, 2278-2288.

Levine, T. (2004). Short-range intracellular trafficking of small molecules across endoplasmic reticulum junctions. Trends Cell Biol *14*, 483-490.

Levine, T., and Loewen, C. (2006). Inter-organelle membrane contact sites: through a glass, darkly. Curr Opin Cell Biol *18*, 371-378.

Lewis, R.S. (2011). Store-operated calcium channels: new perspectives on mechanism and function. Cold Spring Harbor perspectives in biology *3*.

Lewis, R.S., and Cahalan, M.D. (1989). Mitogen-induced oscillations of cytosolic Ca2+ and transmembrane Ca2+ current in human leukemic T cells. Cell regulation *1*, 99-112.

Li, H., Ding, X., Lopez, J.R., Takeshima, H., Ma, J., Allen, P.D., and Eltit, J.M. (2010). Impaired Orai1-mediated resting Ca2+ entry reduces the cytosolic [Ca2+] and sarcoplasmic reticulum Ca2+ loading in quiescent junctophilin 1 knock-out myotubes. J Biol Chem *285*, 39171-39179.

Liou, J., Fivaz, M., Inoue, T., and Meyer, T. (2007). Live-cell imaging reveals sequential oligomerization and local plasma membrane targeting of stromal interaction molecule 1 after Ca2+ store depletion. Proc Natl Acad Sci U S A *104*, 9301-9306.

Liou, J., Kim, M.L., Heo, W.D., Jones, J.T., Myers, J.W., Ferrell, J.E., Jr., and Meyer, T. (2005). STIM is a Ca2+ sensor essential for Ca2+-store-depletion-triggered Ca2+ influx. Curr Biol *15*, 1235-1241.

Litjens, T., Harland, M.L., Roberts, M.L., Barritt, G.J., and Rychkov, G.Y. (2004). Fast Ca(2+)-dependent inactivation of the store-operated Ca2+ current (ISOC) in liver cells: a role for calmodulin. J Physiol *558*, 85-97.

Litvak, V., Dahan, N., Ramachandran, S., Sabanay, H., and Lev, S. (2005). Maintenance of the diacylglycerol level in the Golgi apparatus by the Nir2 protein is critical for Golgi secretory function. Nat Cell Biol *7*, 225-234.

Litvak, V., Shaul, Y.D., Shulewitz, M., Amarilio, R., Carmon, S., and Lev, S. (2002). Targeting of Nir2 to lipid droplets is regulated by a specific threonine residue within its PI-transfer domain. Curr Biol *12*, 1513-1518.

Liu, Y., Boukhelifa, M., Tribble, E., Morin-Kensicki, E., Uetrecht, A., Bear, J.E., and Bankaitis, V.A. (2008). The Sac1 phosphoinositide phosphatase regulates Golgi membrane morphology and mitotic spindle organization in mammals. Mol Biol Cell *19*, 3080-3096.

Loesser, K.E., Castellani, L., and Franzini-Armstrong, C. (1992). Dispositions of junctional feet in muscles of invertebrates. Journal of muscle research and cell motility *13*, 161-173.

Loewen, C.J., Roy, A., and Levine, T.P. (2003). A conserved ER targeting motif in three families of lipid binding proteins and in Opi1p binds VAP. EMBO J *22*, 2025-2035.

Loewen, C.J., Young, B.P., Tavassoli, S., and Levine, T.P. (2007). Inheritance of cortical ER in yeast is required for normal septin organization. J Cell Biol *179*, 467-483.

Lu, C., Peng, Y.W., Shang, J., Pawlyk, B.S., Yu, F., and Li, T. (2001). The mammalian retinal degeneration B2 gene is not required for photoreceptor function and survival. Neuroscience *107*, 35-41.

Lu, L., Ladinsky, M.S., and Kirchhausen, T. (2009). Cisternal organization of the endoplasmic reticulum during mitosis. Mol Biol Cell *20*, 3471-3480.

Luik, R.M., Wang, B., Prakriya, M., Wu, M.M., and Lewis, R.S. (2008). Oligomerization of STIM1 couples ER calcium depletion to CRAC channel activation. Nature *454*, 538-542.

Luik, R.M., Wu, M.M., Buchanan, J., and Lewis, R.S. (2006). The elementary unit of store-operated Ca2+ entry: local activation of CRAC channels by STIM1 at ER-plasma membrane junctions. J Cell Biol *174*, 815-825.

Lur, G., Haynes, L.P., Prior, I.A., Gerasimenko, O.V., Feske, S., Petersen, O.H., Burgoyne, R.D., and Tepikin, A.V. (2009). Ribosome-free terminals of rough ER allow formation of STIM1 puncta and segregation of STIM1 from IP(3) receptors. Curr Biol *19*, 1648-1653.

Ma, H., Lou, Y., Lin, W.H., and Xue, H.W. (2006). MORN motifs in plant PIPKs are involved in the regulation of subcellular localization and phospholipid binding. Cell Res *16*, 466-478.

Madl, J., Weghuber, J., Fritsch, R., Derler, I., Fahrner, M., Frischauf, I., Lackner, B., Romanin, C., and Schutz, G.J. (2010). Resting state Orai1 diffuses as homotetramer in the plasma membrane of live mammalian cells. J Biol Chem *285*, 41135-41142.

Manford, A.G., Stefan, C.J., Yuan, H.L., Macgurn, J.A., and Emr, S.D. (2012). ER-to-plasma membrane tethering proteins regulate cell signaling and ER morphology. Dev Cell *23*, 1129-1140.

McKinney, S.A., Murphy, C.S., Hazelwood, K.L., Davidson, M.W., and Looger, L.L. (2009). A bright and photostable photoconvertible fluorescent protein. Nat Methods *6*, 131-133.

McLean, L.R., and Phillips, M.C. (1984). Cholesterol transfer from small and large unilamellar vesicles. Biochim Biophys Acta *776*, 21-26.

Mesmin, B., Bigay, J., Moser von Filseck, J., Lacas-Gervais, S., Drin, G., and Antonny, B. (2013). A four-step cycle driven by PI(4)P hydrolysis directs sterol/PI(4)P exchange by the ER-Golgi tether OSBP. Cell *155*, 830-843.

Miao, Y., Miner, C., Zhang, L., Hanson, P.I., Dani, A., and Vig, M. (2013). An essential and NSF independent role for alpha-SNAP in store-operated calcium entry. eLife *2*, e00802.

Michell, R.H. (1975). Inositol phospholipids and cell surface receptor function. Biochim Biophys Acta *415*, 81-47.

Milligan, S.C., Alb, J.G., Jr., Elagina, R.B., Bankaitis, V.A., and Hyde, D.R. (1997). The phosphatidylinositol transfer protein domain of Drosophila retinal degeneration B protein is essential for photoreceptor cell survival and recovery from light stimulation. J Cell Biol *139*, 351-363.

Min, S.W., Chang, W.P., and Sudhof, T.C. (2007). E-Syts, a family of membranous Ca2+-sensor proteins with multiple C2 domains. Proc Natl Acad Sci U S A *104*, 3823-3828.

Monteleone, M.C., Gonzalez Wusener, A.E., Burdisso, J.E., Conde, C., Caceres, A., and Arregui, C.O. (2012). ER-bound protein tyrosine phosphatase PTP1B interacts with Src at the plasma membrane/substrate interface. PLoS One *7*, e38948.

Morone, N., Fujiwara, T., Murase, K., Kasai, R.S., Ike, H., Yuasa, S., Usukura, J., and Kusumi, A. (2006). Three-dimensional reconstruction of the membrane skeleton at the plasma membrane interface by electron tomography. J Cell Biol *174*, 851-862.

Mostowy, S., and Cossart, P. (2012). Septins: the fourth component of the cytoskeleton. Nat Rev Mol Cell Biol *13*, 183-194.

Mullins, F.M., Park, C.Y., Dolmetsch, R.E., and Lewis, R.S. (2009). STIM1 and calmodulin interact with Orai1 to induce Ca2+-dependent inactivation of CRAC channels. Proc Natl Acad Sci U S A *106*, 15495-15500.

Nishi, M., Sakagami, H., Komazaki, S., Kondo, H., and Takeshima, H. (2003). Coexpression of junctophilin type 3 and type 4 in brain. Brain Res Mol Brain Res *118*, 102-110.

Oh-Hora, M., Yamashita, M., Hogan, P.G., Sharma, S., Lamperti, E., Chung, W., Prakriya, M., Feske, S., and Rao, A. (2008). Dual functions for the endoplasmic reticulum calcium sensors STIM1 and STIM2 in T cell activation and tolerance. Nat Immunol *9*, 432-443.

Orci, L., Ravazzola, M., Le Coadic, M., Shen, W.W., Demaurex, N., and Cosson, P. (2009). From the Cover: STIM1-induced precortical and cortical subdomains of the endoplasmic reticulum. Proc Natl Acad Sci U S A *106*, 19358-19362.

Orso, G., Pendin, D., Liu, S., Tosetto, J., Moss, T.J., Faust, J.E., Micaroni, M., Egorova, A., Martinuzzi, A., McNew, J.A., *et al.* (2009). Homotypic fusion of ER membranes requires the dynamin-like GTPase atlastin. Nature *460*, 978-983.

Palty, R., Raveh, A., Kaminsky, I., Meller, R., and Reuveny, E. (2012). SARAF inactivates the store operated calcium entry machinery to prevent excess calcium refilling. Cell *149*, 425-438.

Parekh, A.B., and Penner, R. (1997). Store depletion and calcium influx. Physiol Rev *77*, 901-930.

Park, C.Y., Hoover, P.J., Mullins, F.M., Bachhawat, P., Covington, E.D., Raunser, S., Walz, T., Garcia, K.C., Dolmetsch, R.E., and Lewis, R.S. (2009). STIM1 clusters and activates CRAC channels via direct binding of a cytosolic domain to Orai1. Cell *136*, 876-890.

Park, S.H., and Blackstone, C. (2010). Further assembly required: construction and dynamics of the endoplasmic reticulum network. EMBO Rep *11*, 515-521.

Park, S.H., Zhu, P.P., Parker, R.L., and Blackstone, C. (2010). Hereditary spastic paraplegia proteins REEP1, spastin, and atlastin-1 coordinate microtubule interactions with the tubular ER network. J Clin Invest *120*, 1097-1110.

Penner, R., Matthews, G., and Neher, E. (1988). Regulation of calcium influx by second messengers in rat mast cells. Nature *334*, 499-504.

Pichler, H., Gaigg, B., Hrastnik, C., Achleitner, G., Kohlwein, S.D., Zellnig, G., Perktold, A., and Daum, G. (2001). A subfraction of the yeast endoplasmic reticulum associates with the plasma membrane and has a high capacity to synthesize lipids. European journal of biochemistry / FEBS *268*, 2351-2361.

Porter, K.R., and Palade, G.E. (1957). Studies on the endoplasmic reticulum. III. Its form and distribution in striated muscle cells. The Journal of biophysical and biochemical cytology *3*, 269-300.

Putney, J.W., Jr. (1986). A model for receptor-regulated calcium entry. Cell Calcium *7*, 1-12.

Putney, J.W., Jr., and Bird, G.S. (1993). The inositol phosphate-calcium signaling system in nonexcitable cells. Endocrine reviews *14*, 610-631.

Putyrski, M., and Schultz, C. (2012). Protein translocation as a tool: The current rapamycin story. FEBS Lett *586*, 2097-2105.

Quinn, K.V., Behe, P., and Tinker, A. (2008). Monitoring changes in membrane phosphatidylinositol 4,5-bisphosphate in living cells using a domain from the transcription factor tubby. J Physiol *586*, 2855-2871.

Rivas, M.P., Kearns, B.G., Xie, Z., Guo, S., Sekar, M.C., Hosaka, K., Kagiwada, S., York, J.D., and Bankaitis, V.A. (1999). Pleiotropic alterations in lipid metabolism in yeast sac1 mutants: relationship to "bypass Sec14p" and inositol auxotrophy. Mol Biol Cell *10*, 2235-2250.

Rizo, J., and Sudhof, T.C. (1998). C2-domains, structure and function of a universal Ca2+-binding domain. J Biol Chem *273*, 15879-15882.

Rizzuto, R., and Pozzan, T. (2006). Microdomains of intracellular Ca2+: molecular determinants and functional consequences. Physiol Rev *86*, 369-408.

Roos, J., DiGregorio, P.J., Yeromin, A.V., Ohlsen, K., Lioudyno, M., Zhang, S., Safrina, O., Kozak, J.A., Wagner, S.L., Cahalan, M.D., *et al.* (2005). STIM1, an essential and conserved component of store-operated Ca2+ channel function. J Cell Biol *169*, 435-445.

Rosenbluth, J. (1962). Subsurface cisterns and their relationship to the neuronal plasma membrane. J Cell Biol *13*, 405-421.

Rossi, A.E., and Dirksen, R.T. (2006). Sarcoplasmic reticulum: the dynamic calcium governor of muscle. Muscle & nerve *33*, 715-731.

Rust, M.J., Bates, M., and Zhuang, X. (2006). Sub-diffraction-limit imaging by stochastic optical reconstruction microscopy (STORM). Nat Methods *3*, 793-795.

Schulz, T.A., Choi, M.G., Raychaudhuri, S., Mears, J.A., Ghirlando, R., Hinshaw, J.E., and Prinz, W.A. (2009). Lipid-regulated sterol transfer between closely apposed membranes by oxysterol-binding protein homologues. J Cell Biol *187*, 889-903.

Sharma, S., Quintana, A., Findlay, G.M., Mettlen, M., Baust, B., Jain, M., Nilsson, R., Rao, A., and Hogan, P.G. (2013). An siRNA screen for NFAT activation identifies septins as coordinators of store-operated Ca2+ entry. Nature *499*, 238-242.

Shibata, Y., Shemesh, T., Prinz, W.A., Palazzo, A.F., Kozlov, M.M., and Rapoport, T.A. (2010). Mechanisms determining the morphology of the peripheral ER. Cell *143*, 774-788.

Shibata, Y., Voeltz, G.K., and Rapoport, T.A. (2006). Rough sheets and smooth tubules. Cell *126*, 435-439.

Shim, S.H., Xia, C., Zhong, G., Babcock, H.P., Vaughan, J.C., Huang, B., Wang, X., Xu, C., Bi, G.Q., and Zhuang, X. (2012). Super-resolution fluorescence imaging of organelles in live cells with photoswitchable membrane probes. Proc Natl Acad Sci U S A *109*, 13978-13983.

Shu, X., Lev-Ram, V., Deerinck, T.J., Qi, Y., Ramko, E.B., Davidson, M.W., Jin, Y., Ellisman, M.H., and Tsien, R.Y. (2011). A genetically encoded tag for correlated light and electron microscopy of intact cells, tissues, and organisms. PLoS biology *9*, e1001041.

Sleight, R.G. (1987). Intracellular lipid transport in eukaryotes. Annual review of physiology *49*, 193-208.

Srikanth, S., Jew, M., Kim, K.D., Yee, M.K., Abramson, J., and Gwack, Y. (2012). Junctate is a Ca2+-sensing structural component of Orai1 and stromal interaction molecule 1 (STIM1). Proc Natl Acad Sci U S A *109*, 8682-8687.

Stathopulos, P.B., Zheng, L., Li, G.Y., Plevin, M.J., and Ikura, M. (2008). Structural and mechanistic insights into STIM1-mediated initiation of store-operated calcium entry. Cell *135*, 110-122.

Stauffer, T.P., Ahn, S., and Meyer, T. (1998). Receptor-induced transient reduction in plasma membrane PtdIns(4,5)P2 concentration monitored in living cells. Curr Biol *8*, 343-346.

Stefan, C.J., Manford, A.G., Baird, D., Yamada-Hanff, J., Mao, Y., and Emr, S.D. (2011). Osh proteins regulate phosphoinositide metabolism at ER-plasma membrane contact sites. Cell *144*, 389-401.

Steyer, J.A., and Almers, W. (2001). A real-time view of life within 100 nm of the plasma membrane. Nat Rev Mol Cell Biol *2*, 268-275.

Stiber, J., Hawkins, A., Zhang, Z.S., Wang, S., Burch, J., Graham, V., Ward, C.C., Seth, M., Finch, E., Malouf, N., *et al.* (2008). STIM1 signalling controls store-operated calcium entry required for development and contractile function in skeletal muscle. Nat Cell Biol *10*, 688-697.

Stradalova, V., Blazikova, M., Grossmann, G., Opekarova, M., Tanner, W., and Malinsky, J. (2012). Distribution of cortical endoplasmic reticulum determines positioning of endocytic events in yeast plasma membrane. PLoS One *7*, e35132.

Szul, T., and Sztul, E. (2011). COPII and COPI traffic at the ER-Golgi interface. Physiology *26*, 348-364.

Takekura, H., Nishi, M., Noda, T., Takeshima, H., and Franzini-Armstrong, C. (1995a). Abnormal junctions between surface membrane and sarcoplasmic reticulum in skeletal muscle with a mutation targeted to the ryanodine receptor. Proc Natl Acad Sci U S A *92*, 3381-3385.

Takekura, H., Takeshima, H., Nishimura, S., Takahashi, M., Tanabe, T., Flockerzi, V., Hofmann, F., and Franzini-Armstrong, C. (1995b). Co-expression in CHO cells of two muscle proteins involved in excitation-contraction coupling. Journal of muscle research and cell motility *16*, 465-480.

Takeshima, H., Komazaki, S., Nishi, M., Iino, M., and Kangawa, K. (2000). Junctophilins: a novel family of junctional membrane complex proteins. Mol Cell *6*, 11-22.

Tavassoli, S., Chao, J.T., Young, B.P., Cox, R.C., Prinz, W.A., de Kroon, A.I., and Loewen, C.J. (2013). Plasma membrane--endoplasmic reticulum contact sites regulate phosphatidylcholine synthesis. EMBO Rep *14*, 434-440.

Ter Keurs, H.E., and Boyden, P.A. (2007). Calcium and arrhythmogenesis. Physiol Rev *87*, 457-506.

Terasaki, M., Shemesh, T., Kasthuri, N., Klemm, R.W., Schalek, R., Hayworth, K.J., Hand, A.R., Yankova, M., Huber, G., Lichtman, J.W., *et al.* (2013). Stacked endoplasmic reticulum sheets are connected by helicoidal membrane motifs. Cell *154*, 285-296.

Thastrup, O., Dawson, A.P., Scharff, O., Foder, B., Cullen, P.J., Drobak, B.K., Bjerrum, P.J., Christensen, S.B., and Hanley, M.R. (1989). Thapsigargin, a novel molecular probe for studying intracellular calcium release and storage. Agents and actions *27*, 17-23.

Tian, D., Litvak, V., Toledo-Rodriguez, M., Carmon, S., and Lev, S. (2002). Nir2, a novel regulator of cell morphogenesis. Mol Cell Biol *22*, 2650-2662.

Tilley, S.J., Skippen, A., Murray-Rust, J., Swigart, P.M., Stewart, A., Morgan, C.P., Cockcroft, S., and McDonald, N.Q. (2004). Structure-function analysis of human [corrected] phosphatidylinositol transfer protein alpha bound to phosphatidylinositol. Structure *12*, 317-326.

Toulmay, A., and Prinz, W.A. (2012). A conserved membrane-binding domain targets proteins to organelle contact sites. J Cell Sci *125*, 49-58.

Treves, S., Anderson, A.A., Ducreux, S., Divet, A., Bleunven, C., Grasso, C., Paesante, S., and Zorzato, F. (2005). Ryanodine receptor 1 mutations, dysregulation of calcium homeostasis and neuromuscular disorders. Neuromuscular disorders : NMD *15*, 577-587.

Treves, S., Feriotto, G., Moccagatta, L., Gambari, R., and Zorzato, F. (2000). Molecular cloning, expression, functional characterization, chromosomal localization, and gene structure of junctate, a novel integral calcium binding protein of sarco(endo)plasmic reticulum membrane. J Biol Chem *275*, 39555-39568.

Treves, S., Franzini-Armstrong, C., Moccagatta, L., Arnoult, C., Grasso, C., Schrum, A., Ducreux, S., Zhu, M.X., Mikoshiba, K., Girard, T., *et al.* (2004). Junctate is a key element in calcium entry induced by activation of InsP3 receptors and/or calcium store depletion. J Cell Biol *166*, 537-548.

Treves, S., Vukcevic, M., Griesser, J., Armstrong, C.F., Zhu, M.X., and Zorzato, F. (2010). Agonist-activated Ca2+ influx occurs at stable plasma membrane and endoplasmic reticulum junctions. J Cell Sci *123*, 4170-4181.

Trivedi, D., and Padinjat, R. (2007). RdgB proteins: functions in lipid homeostasis and signal transduction. Biochim Biophys Acta *1771*, 692-699.

Vance, J.E., Aasman, E.J., and Szarka, R. (1991). Brefeldin A does not inhibit the movement of phosphatidylethanolamine from its sites for synthesis to the cell surface. J Biol Chem *266*, 8241-8247.

Varga-Szabo, D., Braun, A., Kleinschnitz, C., Bender, M., Pleines, I., Pham, M., Renne, T., Stoll, G., and Nieswandt, B. (2008). The calcium sensor STIM1 is an essential mediator of arterial thrombosis and ischemic brain infarction. J Exp Med *205*, 1583-1591.

Varnai, P., Toth, B., Toth, D.J., Hunyady, L., and Balla, T. (2007). Visualization and manipulation of plasma membrane-endoplasmic reticulum contact sites indicates the presence of additional molecular components within the STIM1-Orai1 Complex. J Biol Chem *282*, 29678-29690.

Vig, M., DeHaven, W.I., Bird, G.S., Billingsley, J.M., Wang, H., Rao, P.E., Hutchings, A.B., Jouvin, M.H., Putney, J.W., and Kinet, J.P. (2008). Defective mast cell effector functions in mice lacking the CRACM1 pore subunit of store-operated calcium release-activated calcium channels. Nat Immunol *9*, 89-96.

Vig, M., Peinelt, C., Beck, A., Koomoa, D.L., Rabah, D., Koblan-Huberson, M., Kraft, S., Turner, H., Fleig, A., Penner, R., *et al.* (2006). CRACM1 is a plasma membrane protein essential for store-operated Ca2+ entry. Science *312*, 1220-1223.

Vihtelic, T.S., Goebl, M., Milligan, S., O'Tousa, J.E., and Hyde, D.R. (1993). Localization of Drosophila retinal degeneration B, a membrane-associated phosphatidylinositol transfer protein. J Cell Biol *122*, 1013-1022.

Voelker, D.R. (1989). Reconstitution of phosphatidylserine import into rat liver mitochondria. J Biol Chem *264*, 8019-8025.

Voeltz, G.K., Prinz, W.A., Shibata, Y., Rist, J.M., and Rapoport, T.A. (2006). A class of membrane proteins shaping the tubular endoplasmic reticulum. Cell *124*, 573-586.

Vordtriede, P.B., Doan, C.N., Tremblay, J.M., Helmkamp, G.M., Jr., and Yoder, M.D. (2005). Structure of PITPbeta in complex with phosphatidylcholine: comparison of structure and lipid transfer to other PITP isoforms. Biochemistry *44*, 14760-14771.

Walsh, C.M., Chvanov, M., Haynes, L.P., Petersen, O.H., Tepikin, A.V., and Burgoyne, R.D. (2010). Role of phosphoinositides in STIM1 dynamics and store-operated calcium entry. Biochem J *425*, 159-168.

Wang, S., Romano, F.B., Field, C.M., Mitchison, T.J., and Rapoport, T.A. (2013). Multiple mechanisms determine ER network morphology during the cell cycle in Xenopus egg extracts. J Cell Biol *203*, 801-814.

Wei, H.C., Sanny, J., Shu, H., Baillie, D.L., Brill, J.A., Price, J.V., and Harden, N. (2003). The Sac1 lipid phosphatase regulates cell shape change and the JNK cascade during dorsal closure in Drosophila. Curr Biol *13*, 1882-1887.

West, M., Zurek, N., Hoenger, A., and Voeltz, G.K. (2011). A 3D analysis of yeast ER structure reveals how ER domains are organized by membrane curvature. J Cell Biol *193*, 333-346.

Williams, R.T., Manji, S.S., Parker, N.J., Hancock, M.S., Van Stekelenburg, L., Eid, J.P., Senior, P.V., Kazenwadel, J.S., Shandala, T., Saint, R., *et al.* (2001). Identification and characterization of the STIM (stromal interaction molecule) gene family: coding for a novel class of transmembrane proteins. Biochem J *357*, 673-685.

Willig, K.I., Rizzoli, S.O., Westphal, V., Jahn, R., and Hell, S.W. (2006). STED microscopy reveals that synaptotagmin remains clustered after synaptic vesicle exocytosis. Nature *440*, 935-939.

Wirtz, K.W., and Zilversmit, D.B. (1968). Exchange of phospholipids between liver mitochondria and microsomes in vitro. J Biol Chem *243*, 3596-3602.

Wu, M.M., Buchanan, J., Luik, R.M., and Lewis, R.S. (2006). Ca2+ store depletion causes STIM1 to accumulate in ER regions closely associated with the plasma membrane. J Cell Biol *174*, 803-813.

Xu, K., Babcock, H.P., and Zhuang, X. (2012). Dual-objective STORM reveals three-dimensional filament organization in the actin cytoskeleton. Nat Methods *9*, 185-188.

Yamamoto, A., and Masaki, R. (2010). Pre-embedding nanogold silver and gold intensification. Methods in molecular biology *657*, 225-235.

Yang, T.T., Hampilos, P.J., Nathwani, B., Miller, C.H., Sutaria, N.D., and Liao, J.C. (2013). Superresolution STED microscopy reveals differential localization in primary cilia. Cytoskeleton *70*, 54-65.

Yuan, J.P., Zeng, W., Dorwart, M.R., Choi, Y.J., Worley, P.F., and Muallem, S. (2009). SOAR and the polybasic STIM1 domains gate and regulate Orai channels. Nat Cell Biol *11*, 337-343.

Yuan, S.H., Arnold, W., and Jorgensen, A.O. (1991). Biogenesis of transverse tubules and triads: immunolocalization of the 1,4-dihydropyridine receptor, TS28, and the ryanodine receptor in rabbit skeletal muscle developing in situ. J Cell Biol *112*, 289-301.

Zhang, D., Vjestica, A., and Oliferenko, S. (2012). Plasma membrane tethering of the cortical ER necessitates its finely reticulated architecture. Curr Biol *22*, 2048-2052.

Zhang, S.L., Yeromin, A.V., Zhang, X.H., Yu, Y., Safrina, O., Penna, A., Roos, J., Stauderman, K.A., and Cahalan, M.D. (2006). Genome-wide RNAi screen of Ca(2+) influx identifies genes that regulate Ca(2+) release-activated Ca(2+) channel activity. Proc Natl Acad Sci U S A *103*, 9357-9362.

Zhao, Y., Araki, S., Wu, J., Teramoto, T., Chang, Y.F., Nakano, M., Abdelfattah, A.S., Fujiwara, M., Ishihara, T., Nagai, T., *et al.* (2011). An expanded palette of genetically encoded Ca(2)(+) indicators. Science *333*, 1888-1891.

Zurek, N., Sparks, L., and Voeltz, G. (2011). Reticulon short hairpin transmembrane domains are used to shape ER tubules. Traffic *12*, 28-41.

Zweifach, A., and Lewis, R.S. (1995). Rapid inactivation of depletion-activated calcium current (ICRAC) due to local calcium feedback. J Gen Physiol *105*, 209-226.